3D printing of patient specific bioresorbable cardiovascular stents
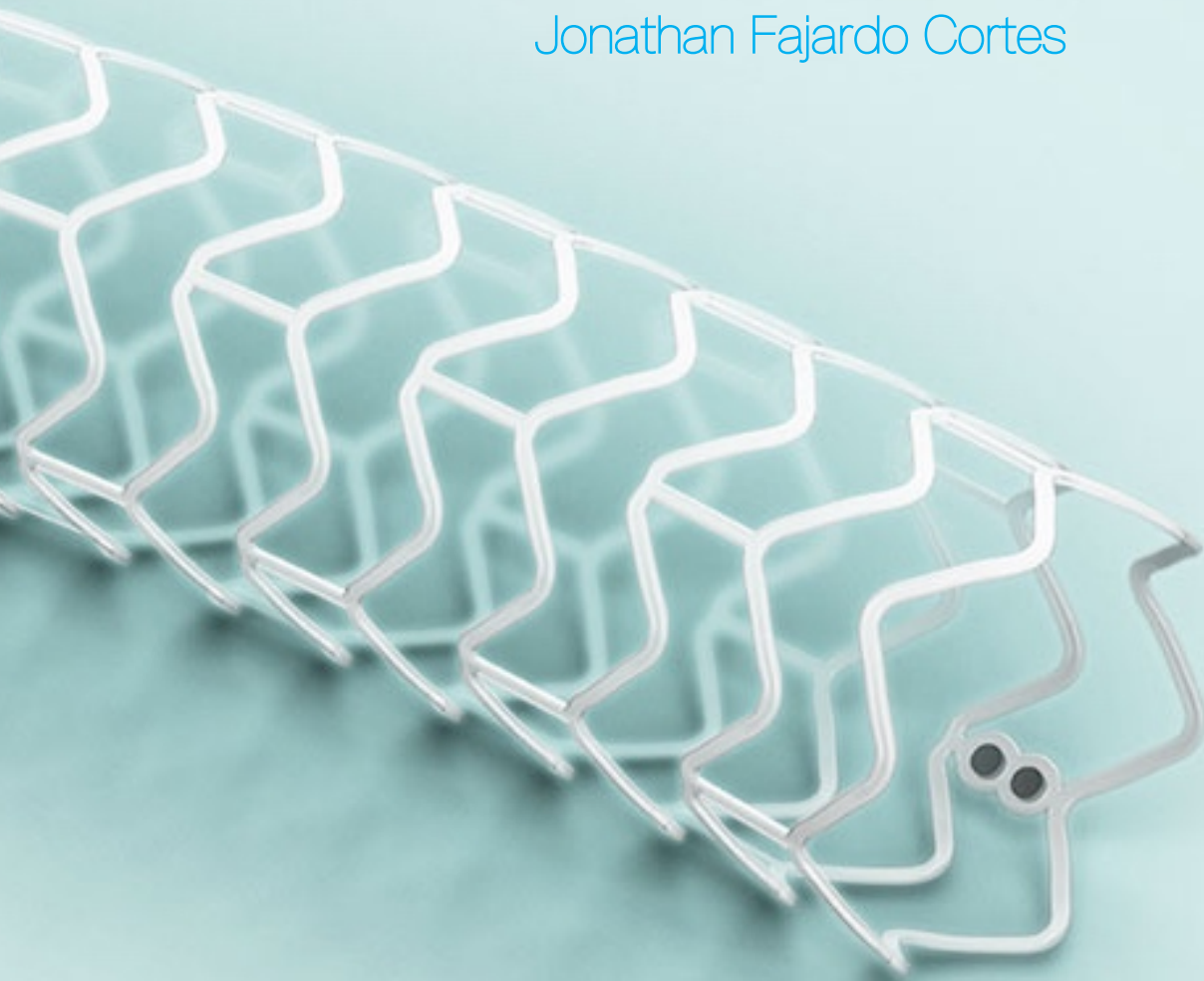
_____

Jonathan Fajardo Cortes

© 2017 Jonathan Fajardo Cortes

3D Printing of patient specific bioresorbable cardiovascular stents

Master Thesis

By

Jonathan Fajardo Cortes

No. 4471067

in partial fulfilment of the requirements for the degree of

Master of Science
in Biomedical Engineering

at the Delft University of Technology,
to be defended publicly on Thursday August 31, 2017 at 11:30 AM.

Supervisors:	Dr. ir. Iulian Apachitei,	TU Delft
	Dr. Amir Zadpoor,	TU Delft
	Bas van Leeuwen MSc PDEng	Corbion
Thesis committee:	Dr. Amir Zadpoor,	TU Delft
	Dr. ir. Iulian Apachitei,	TU Delft
	Dr. ir. Dick Plettenburg	TU Delft
	Bas van Leeuwen MSc PDEng	Corbion

An electronic version of this thesis is available at http://repository.tudelft.nl/.

TUDelft

Corbion

iii

Acknowledgements

Jonathan Fajardo Cortes
Delft, August 2017

Acronyms

3D Printing	Three-dimensional printing
BEC	Backscattered electron composition image
BET	Backscattered electron topographic image
BES	Backscattered electron shadow image
BRS	Bioresorbable stent
CL	Connecting link
DC	Diagonal crest
DES	Drug eluting stent
DI Water	Deionized water
FDM	Fused deposition modeling
FTIR	Fourier transform infrared spectroscopy
GPC	Gel permeation chromatography
HC	Horizontal crest
HFIP	Hexafluoro-2-propanol
HPLC	High-performance liquid chromatography
ID	Inner diameter
Mw	Weight-average molecular weight
Mn	Number-average molecular weight
NC-PLA	Non-clinical grade polylactic acid
OD	Outer diameter
PAE	Poly anhydride ester
PCL	Poly caprolactone
PDI	Polydispersity
PLA	Poly lactic acid
SEM	Scanning electron microscopy
SLA	Stereolithography
THF	Tetrahydrofuran

Glossary

Acute recoil: Recoil experienced by the cardiovascular stent after deployment and removal of the catheter.

Angina: Chest pain as a result of insufficient blood supply to the heart.

Discharge: Percentage of material which is extruded at the nozzle tip of the Freeformer.

Eccentricity index: Ratio between the horizontal and vertical diameter dimensions of the lesioned vessel. Represents how symmetric the supported vessel is.

Extrusion-based printing: 3D printing technique characterized for the extrusion of material through a heated nozzle.

Extrusion width: Width of the extruded filament at the nozzle tip.

Extrusion multiplier: Scalability setting for amount of material to be extruded in FDM printers

Photopolymerization-based printing: 3D printing technique characterized for the use of a photoreactive material which cures when exposed to UV lights or lasers.

Lumen area: Inside surface of the vessel wall.

Nozzle temperature: Temperature needed to bring the material to a molten state at the nozzle during printing.

Primary layer height: Height of the first layer of the sample being extruded. Important for correct bed adhesion.

Printing speed: Speed at which the nozzle moves during the extrusion stage.

Restenosis: Re-narrowing of the vessel due to stent collapse.

Retraction distance: Distance which the filament retracts to avoid extrusion when switching printing areas.

Target lesion vascularization: Vascularization of the vessel wall in the proximity of the implanted stent.

X/Y speed: Speed at which the nozzle moves when going through gaps in between printing areas.

Contents

Abstract

Cardiovascular diseases, in particular atherosclerosis, is currently the leading cause of death worldwide with increasing numbers due to an aging population. Recently, the first bioresorbable stent (BRS), Absorb GT1 (Abbott, USA) was approved by the FDA, consequently sparking enthusiasm in BRSs and degradable polymeric biomaterials. Polymeric BRSs have been shown to be comparable to DES with the added advantage of naturally breaking down in the body within 2 years. Unfortunately, market available stents continue to offer a limited range of geometries and sizes which might not adapt to a patient's unique lesion and vessel. Relatively a new field, additive manufacturing (AM) has been able to provide biocompatible patient specific devices for dental and orthopedic applications, resulting in a less costly and speedy recovery. However, limited developments and research exist within stents and cardiovascular applications. Thanks to the extensive research in polymeric biomaterials and their compatibility of some with AM techniques, printing of 4 mm cardiovascular stents is introduced with an Ultimaker 2+, Freeformer and Form 1+ to provide viability and printing parameter information for the printing of cardiovascular stents with PLA and PCL based biomaterials. Establishment of structural, morphological, mechanical, chemical and biodegradability characteristics with regard to material and AM technique, ideally provides a starting point for further development in the field.

1

Introduction

1.1. Atherosclerosis and stenting

Cardiovascular diseases accounted for 31% of fatalities in 2012, positioning as the leading cause of death worldwide. Around 80% of these deaths are due to coronary artery disease and stroke, mainly as a cause of atherosclerosis in the arteries of the heart [1]. During atherosclerosis (Figure 1), the artery wall undergoes thickening due to the buildup of plaque from white blood cells and other substances found in the blood. As a result of failing to detect the plaque buildup in the early stage, the plaque will eventually harden and narrow the arteries, limiting the amount of blood and therefore oxygen that needs to be distributed through the body.

Coronary artery stenting is still the gold standard for the treatment of coronary artery disease since its introduction in the 1980s [2]. Even though the first stents were purely metallic, various clinical studies and advances in design and materials of stents have geared the market into drug eluting stents (DES) since the early 2000s. Currently, a new shift is expected into bioresorbable stents (BRS) after the first market approval of Absorb GT1 by Abbott (USA) in 2011, followed by FDA approval in mid-2016. A current interest in BRS has been observed, due to the added advantage of a non-permanent foreign object remaining in the body as compared to DES. Moreover, they are believed to reduce current stent complications such as re-narrowing of the vessel, known as restenosis.
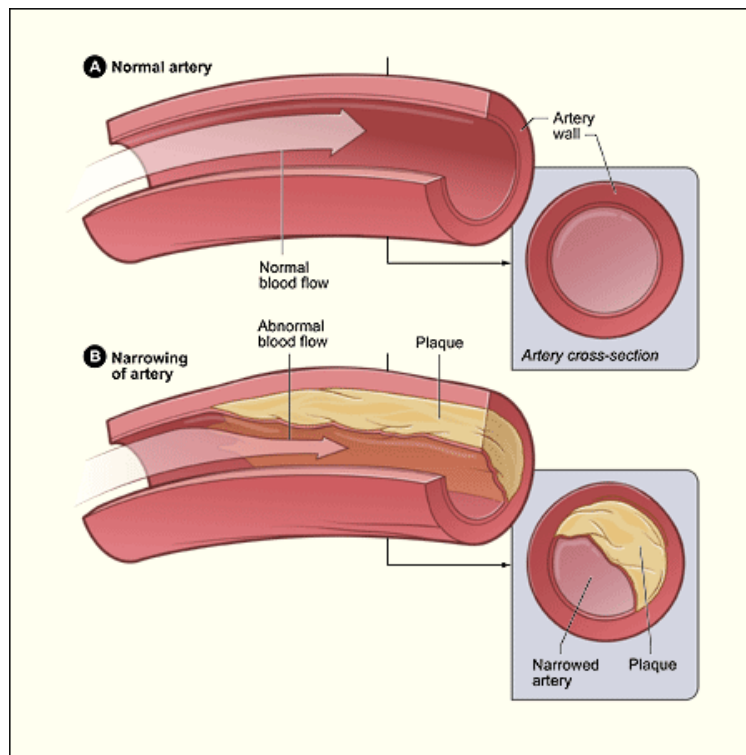
Figure 1 - (a) Normal artery; (b) Artery with plaque buildup and reduced blood flow [3].
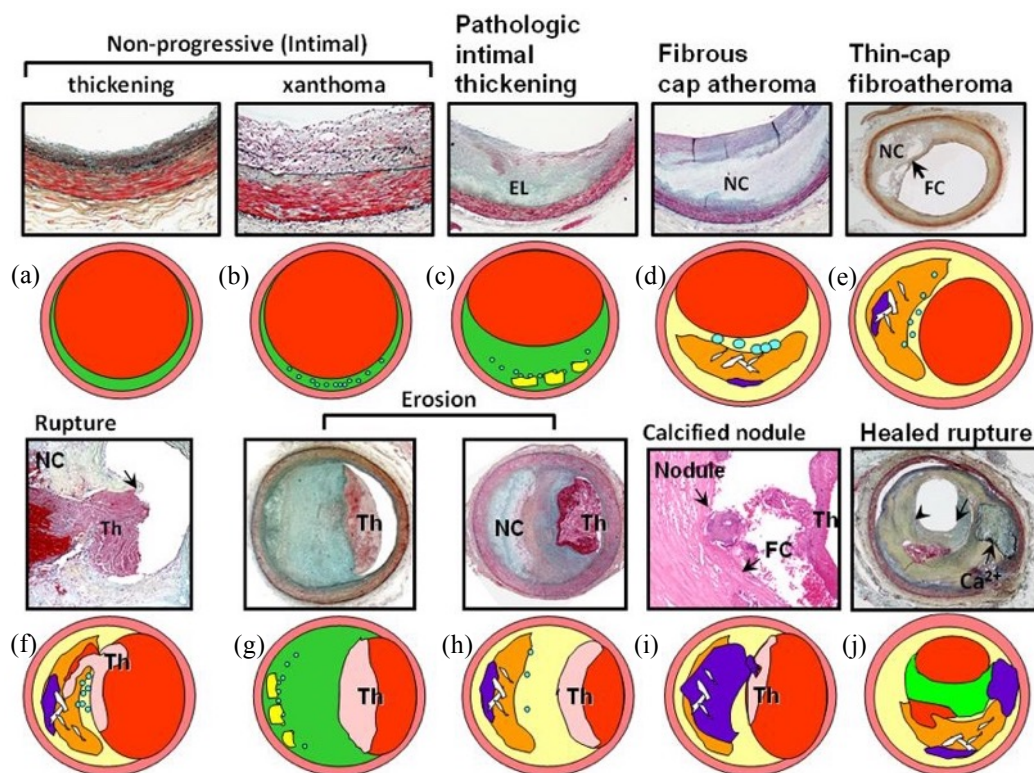
Figure 2 - Different type of plaque formations in atherosclerosis, (a, b) Type II, (c) Type III, (d, e) Type IV, (f-i) Type V, (j) Type VI [4]

Studies [5-7] have shown that different types of plaque exist depending on their location as well as their development timeline. These can range from Type I-III (Figure 2.a-d) which might not result in added problems or symptoms, to Type IV-VI (Figure 2.e-j) which can incorporate thick layers of fibrous and/or calcified connective tissue or even hematomas and thrombus, making them life threatening. Ultimately this

poses a problem due to the limited availability of geometries that cardiovascular stents currently available in the market can offer, resulting in a non-ideal treatment of the injury.

1.2. Bioresorbable stents

Since the introduction of bare metal stents in the 1980's, cardiovascular stents have evolved in various design aspects from including drug releasing polymers such as in DES, to completely bioresorbable polymers such as in BRS. Currently, BRS have gained an increased momentum due to the ability to provide a platform for recovery of the vessel which can resorb over time. Due to their recent development stage, a notable amount of studies have concluded mixed results in terms of superiority [8, 9]. In general BRS have been found to be comparable to DES in regard to eccentricity index, lumen area [10], acute recoil [11] and target lesion vascularization [12]. However, besides the degradability aspects, some studies have been able to show advantages in the early restoration of the function of the vessel [13], a better post-procedure area [11], lower angina [14], and a bigger healed area [15].

1.3. Bioresorbable polymers

Developments in BRS have been greatly linked with developments in biomaterials which can provide a degradable platform for the stent. Absorb GT1 plus most of the other BRS in trials currently use poly (lactic acid) (PLA) as their platform material. However, materials such as poly caprolactone (PCL), tyrosine-based poly-carbonates (TBC) and poly (anhydride-esters) (PAE) have also been explored [16, 17]. As it will be observed in chapter 1.4, PLA and PCL offer a higher compatibility with additive manufacturing techniques, reason why no further focus is provided into TBC and PAE. It is important to note that besides PLA, all other biomaterials mentioned are still in current research stages and/or clinical trials proving the BRS functionality. PLA is currently the material of choice for biomedical applications thanks to its biodegradable and bioactive properties, high affinity for *in vivo* applications, proven track record of excellent clinical outcomes and a strong regulatory history [18]. However, PLA is a brittle material with low elongation and impact strength. Mechanical properties such as tensile and flexural strength can be improved by increasing the molecular weight and annealing the material [19]. Furthermore, improvements in ductility and reduced glass transition temperatures are achieved by making co-polymers, such as adding caprolactone. Thanks to the ability to modify the crystallinity and molecular weight of PLA, degradation rates can be controlled and therefore drug release rates can be tuned for required drug delivery, such as during vessel healing with BRS. It is important to note that degradation rates differ between PLA left in the environment, which occurs due to microorganisms, and PLA inside the body, which breaks as a result of enzymes. These degradation times ultimately are affected by the type of oligomer present at each environment, for example D-lactic acid is hardly degraded by the body enzymes, therefore increasing degradation times [20]. Thanks to these varied mechanical and chemical properties, PLA and its various polylactides are seen as a good candidate for BRS.

Moreover, PCL enjoys of a high biocompatibility and permeability, which makes it a common material of choice for drug encapsulation and long-term delivery [21]. In contrast to PLA, PCL undergoes bio resorption, a longer process which allows it to be completely excreted from the human body. However, where shorter degradation times are needed, such as for stent platforms, this ultimately poses a problem. Nevertheless, PCL is commonly copolymerized with PLA to form PLCL, due to its high elongation break and ability to toughen the PLA. Such copolymers come with disadvantages such as a lower tensile strength and E modulus [22]. These drawbacks can explain why only the stent 'Acute BRS' (Orbus Neich, Wanchai, Hong Kong) is using PLCL as its platform material.

1.4. Additive manufacturing in bioresorbable stents

Throughout the years, different changes in both fabrication and design have occurred with a goal in improving the stent properties and creating the ideal stent. Current fabrication of BRS such as Absorb GT1 and DeSolve, consists of the extrusion of PLA which is then laser cut and post processed to comply with medical standards [23]. Such process is expensive, time consuming and results with limited sizes and geometries for cardiovascular stent applications. To advance further into an ideal BRS, AM is a possible candidate thanks to the possibility of printing patient specific devices which might include complex geometries. However, up to date no ideal stent exists, as the combination of the stent properties proves most of the time inversely related among each other. It is therefore important to take into account during a design and fabrication transition, properties such as radial strength, flexibility, surface roughness, low profile, elastic recoil, radiopacity, drug release and degradation rate.

With the various amount of AM methods currently in market or in development, an implementation of AM in BRS manufacturing should first explore what is currently available, what is compatible with the current BRS biomaterials and which limitations need to be overcome to be able to advance the field even further. It is important to note the recent increase of publications and development of AM technology which has resulted in various classifications, terms and confusion within the field. Therefore, ASTM classification should be considered throughout this thesis.

Among BRS biomaterials, PLA has been highly studied [24-26], experiencing the highest expansion and usability within AM technologies, specifically with extrusion-based processes. PLA can be found in both filament and pellet forms, which allow compatibility with various extrusion-based methods, as well as recently in resin form [27] within the research community. The widespread of PLA has been thanks to its low glass transition temperature and flow characteristics which allow for an easily manageable material. This in turns adds biodegradability and high strength-to-weight ratio properties in the prints. As a result, most developments within AM have been performed with industrial grade material, and only recently developments in the biomedical field have emerged. Various studies in the last year have therefore used AM and PLA for applications such as in auricular implants [28], tissue scaffolds [29-34], dental [35, 36] and cryogenics [37]. Therefore, an advance of technology into the clinical practice will require further research with clinical grade materials.

Unlike PLA, PCL research and developments within AM have been a result of the focus on biomedical applications, primarily within bone and osteochondral defects thanks to their high strength and lower degradation rate (over 3 years). Among the various applications, PCL and its composites have been used with extrusion-based methods to fabricate porous scaffolds for bone regeneration [30, 38-43], ear [44] and nasal [45] reconstruction, wound dressings [46] and drug delivery [47]. Within photopolymerization-based methods, tissue scaffolds [48] and airway splints [49] have been reported. A few tissue scaffolds have also been reported with selective laser sintering [50, 51].

Two AM methods, extrusion- and photopolymerization- based, have been studied for their application of biomedical devices with materials compatible in BRS. Extrusion-based methods have gained momentum thanks to the extended research, easiness of use, low cost of technology and materials, and their availability and widespread compatibility. However, drawbacks in the technology regarding accuracy, speed and material density are often encountered [52]. Higher accuracies often come with longer printing times, which are mostly limited by the nozzle diameter. Moreover, due to the layer by layer material placement, anisotropy in the z-direction results in lower strengths. Purity and composition of the material also affects the easiness in its flow

through the nozzle. Material impurities can hinder a homogeneous construct, affect the properties and even cause clogging, resulting in having to restart the printing process. Finally, the longer times the material remains in molten state are also unfavorable for degradable materials due to the acceleration of their degradation rates experienced at high temperatures. On the other hand, photopolymerization-based methods are preferred over other AM methods due to their ability to work with smaller dimensions at a higher accuracy. Hence, transducing in a higher control over the surface finish and smoothness, advantages which are sought for compliance with the small dimensions of cardiovascular stents. Furthermore, some methods can allow for higher printing speeds. Also materials such as PLA which experience accelerated degradation at higher temperatures, can benefit from such methods as they are only subjected to one heat cycle as opposed to filament-based extrusion methods, where production of filaments plus extrusion adds up to two cycles. Unfortunately, the range of materials for such technologies are still limited as there is a need for biocompatible acrylates or epoxies end-groups to initiate the crosslinking of the polymers [52].

Despite current limitations, Park et al. [53] developed a PCL stent coated with Sirolimus and a PLGA/PEG mixture, with strut size of 300 μm and connecting links of 1300 μm. Instead of printing on a flat bed, the polymer was extruded in a rotating cylinder. *In vivo* animal models proved their efficiency in reducing neointima, inflammation and further complications. Recently, Misra et al. [54] developed a 4 mm diameter and 40 mm length BRS stent. They incorporated graphene oxide (GO) nanoparticles into a previously developed mixture of PCL and PLLA to create the base stent polymer. The reason for the GO lies onto the increase of the tensile strength and young modulus provided to the material. The polymer was then first transformed into 2 mm diameter filaments and then extruded flat through fused deposition modeling (FDM) on a bed surface, followed by folding. Finally, they were able to incorporate two different drugs within the polymer with individual control on their release rates. Moreover, a study in 2016 by Van Lith et al. [55], used a citrate-based polymer as the base material for a stent even though it hasn't been previously used for this applications. Van Lith et al. used micro-continuous liquid interface (microClip), which corresponds to a photopolymerization-based method, to develop the first comparable-BRS to knowledge with 3D printing technology. Photopolymerization methods require a thermosetting resin polymer, which they achieve from the incorporation of methacrylate groups. The study also provides a stent with a smooth surface finish and a continuous layer by layer construction, which can allow for constructions under 20 min. Struts where 150 μm width and 500 μm thick. They could achieve a maximal radial strength of 1.03 N at 25% compression, which complies with the minimum of 1 N. Finally, they obtained a degradation of 25% in the first six months, with a non-ideal decrease of 25% in radial strength. However, further degradation tests where not performed. In short, the results by Park et al., Misra et al. and Van Lith et al. provide promising results for the continuation of extrusion- and photopolymerization-based methods in BRS manufacturing.

Overall, there is an urgent need in new manufacturing and patient specific methods due to the current time-demanding stent manufacturing process, resulting in low cost efficiency. In addition, cases where revisions are needed due to recurring angina or malfunctioning of the stent [56], result in added costs. Due to the importance cardiovascular stents play in world health, it is important to make these affordable to the public while keeping the high quality standards a medical device requires. The future of stent manufacturing with extrusion-based methods and photopolymerization-based methods looks promising, despite the current advantages and drawbacks which are yet to be tested. Information regarding the ability to implement AM manufacturing in various areas such as design, morphology, geometry, dimensions, degradability and materials of the stents is still a research gap to be filled. The use of AM for the manufacturing of BRS is currently in a young unexplored stage, which allows for diverse development and research given the current availability of biodegradable materials and AM techniques. It is expected that the urgent need of a patient specific device which can target the specific lesion geometry and type in the vessel could soon be tackled with the

implementation of AM in day-to-day stent manufacturing process. As a result we could expect a completely turn around in the whole stenting intervention process (Figure 3).
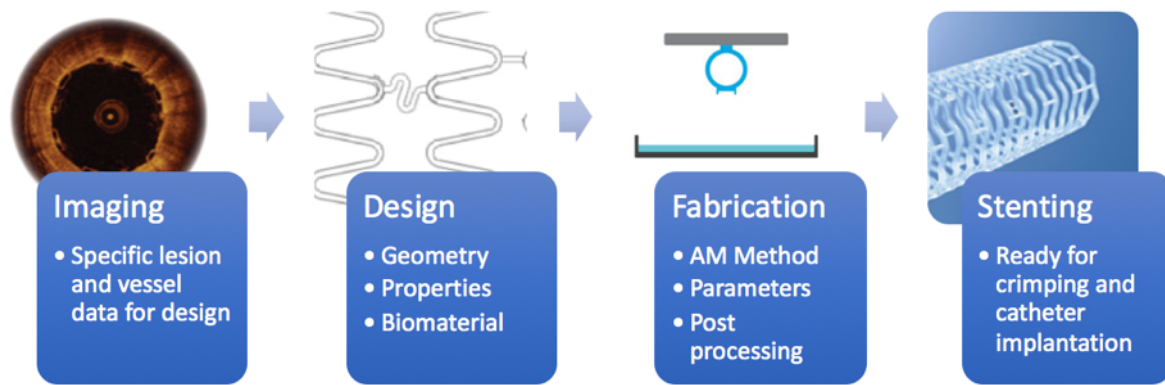

Figure 3 - Future of an on-the-spot patient specific stenting intervention process. First, with the development of new imaging technologies, specific vessel and lesion parameters can be obtained. Second, with the data recollected, specific design modifications for the stent can be implemented for a lesion specific device, furthermore assuming various biomaterials are successfully implemented with AM, an ideal biomaterial can also be chosen based on the first step. Third, through an AM technology of choice, the stent can then be fabricated on the spot, with previously tested parameters. Finally, the stent is ready for delivery into the patient.

1.5. Significance of study

1.5.1. Problem statement

Even though bioresorbable stents have gained popularity due to their ability to be removed by the body in a timeframe of two years, current manufacturing processes are time consuming and expensive. Furthermore, a limited amount of cardiovascular stent options currently exist in the market, hindering an adequate coupling between the stent and the plaque's geometry at the lesioned vessel. Therefore, a huge need for patient specific cardiovascular stents is needed, to which AM provides suitable advantages as a future solution. However, there is still a need for further studies analyzing the suitability of current AM techniques for printing at cardiovascular stents dimensions and geometries, as well as the printability of BRS-compatible biomaterials.

1.5.2. Research goals

To be able to provide novel information on the subject, along the project three AM techniques will be investigated on their ability to print cardiovascular stents and the further effects of printing in the biomaterials properties. Therefore, this thesis will:

- Investigate the printability of stents' dimensions and geometry, and if possible obtain optimal printing settings for every investigated AM technique.
- Quantify printing accuracy and repeatability in stent dimensions and properties within the stent as well as with other stents.
- Provide an insight on the effects of printing in the biomaterials with respect to biodegradation and its chemical properties.

1.5.3. Project outcomes

The novelty of this project expects to provide the initial information needed for a future adoption of AM technologies in the stenting process. Hence, the outcomes of the project will:

- Allow advances in the development of high standard, cost effective and fast patient specific bioresorbable cardiovascular stents.
- Lead to further investigation in biomaterials and its application with AM techniques for the printing of bioresorbable stents.
- Provide challenges and further improvements needed in AM technologies for a better application in cardiovascular stent printing.
- Lead to the development of a new 3D printer which considers the morphological, mechanical and chemical needs of cardiovascular stents.

1.5.4. Research questions

- Is the printing of bioresorbable stents possible with current available AM technologies and biomaterials?
- Do current 3D printed bioresorbable stents offer adequate morphologies, mechanical and chemical properties for clinical applications?
- How do the various AM techniques affect the biodegradability and chemical properties of the biomaterials after printing?

2

Materials and methods

Despite developments and widespread of AM technologies, 3D printing remains a rather new field where slight changes in printer parameters require new tuning data for an adequate printing. In addition, the recent approval of the first BRS in 2016 and the beginning for research in 3D printing of BRS (see Section 1.4) add to the current state-of-the-art. It is therefore known, that the ability to print cardiovascular stents at micrometer dimensions, currently push the boundaries of 3D printing technologies were further research is needed.

2.1. Biomaterials and 3D printers

During the following experiments, PLA- and PCL- based biomaterials, and extrusion- and photopolymerization- based AM technologies were used for the printing of BRS. Transparent filaments of non-clinical grade PLA (NC PLA) were purchased from Ultimaker (Geldermalsen, The Netherlands) with a diameter of 2.85 ± 0.10 mm. NC PLA was used as the reference point for the printer settings and the printing of the rest of the materials. Non-clinical grade materials correspond to materials which can contain traces or contamination of other materials and therefore might not sustain the required results needed in a clinical environment. Clinical grade PLA (PL18) and PCL (PC12), with an inherent viscosity of 1.8 dl/g and 1.2 dl/g respectively, were provided by Corbion Purac (Gorinchem, The Netherlands) in pellet form. Filaments were then produced for each by FET (Leeds, UK) with a diameter of 2.85 ± 0.10 mm. Storage under nitrogen in

plastic and aluminum packaging was needed to prevent material degradation. Distinction between materials which are clinical grade, lies in the purity and the rigorous standards to which the materials go through during fabrication. PLA resin (eResin-PLA) was purchased from Shenzhen Esun Industrial Co. Ltd (Shenzhen, China). Non-biocompatible standard clear resin (methacrylate resin) for the Form 1+ printer was purchased from Formlabs (Somerville, Massachusetts, USA). The resin is proprietarily composed of methacrylated oligomers and monomers, and photoinitiators [57]. PLA-based biomaterials were selected due to the extensive research in biocompatibility and biodegradability with the added aspect that is the material of choice for current BRS such as Absorb GT1 and DeSolve. Furthermore, due to the easiness to handle PLA in filament or pellet form, it can be compatible in various extrusion-based AM methods. On the other hand, PCL-based biomaterials could allow for a higher flexibility and lifetime of the stent thanks to their higher flexibility and elongation over PLA.

Three different 3D printers (Figure 4) were used for experimental comparison. FDM printer Ultimaker 2+ (Ultimaker, Geldermalsen, The Netherlands) and SLA printer Form 1+ (Formlabs, Somerville, Massachusetts, USA) were available at the TU Delft (Delft, The Netherlands). Extrusion-based Freeformer printer (Arburg, Germany) experiments, were carried at CHILL (Geleen, The Netherlands). Extrusion-based technologies including FDM (Figure 5.a), were selected mainly for its current compatibility with PLA and PCL in a non-clinical setting, providing an added advantage when working with the clinical-grade counterparts of these biomaterials. Moreover, for their easiness of use, availability and cost effective technologies. However, it is known that extrusion-based methods can provide disadvantages with overhangs and shrinking of the material, aspects that can affect the geometry and design of the cardiovascular stents. Furthermore, the wall thickness is limited by the nozzle diameter which falls in the limits of strut diameters. To compare degradability as a result of processing cycles, the Freeformer used pellets directly while the Ultimaker 2+ used filaments. Finally, SLA (Figure 5.b) photopolymerization-based method was selected for its ability to provide a higher printing quality and accuracy which is a decisive factor for the printing of smooth surfaces and small dimensions such as in BRS. However, it is known that current available resins are still not biocompatible due to their crosslinker products. After the stents were printed, pictures were taken with a stereoscope (SZX9, Olympus, Tokyo, Japan) at a magnification of 30x.
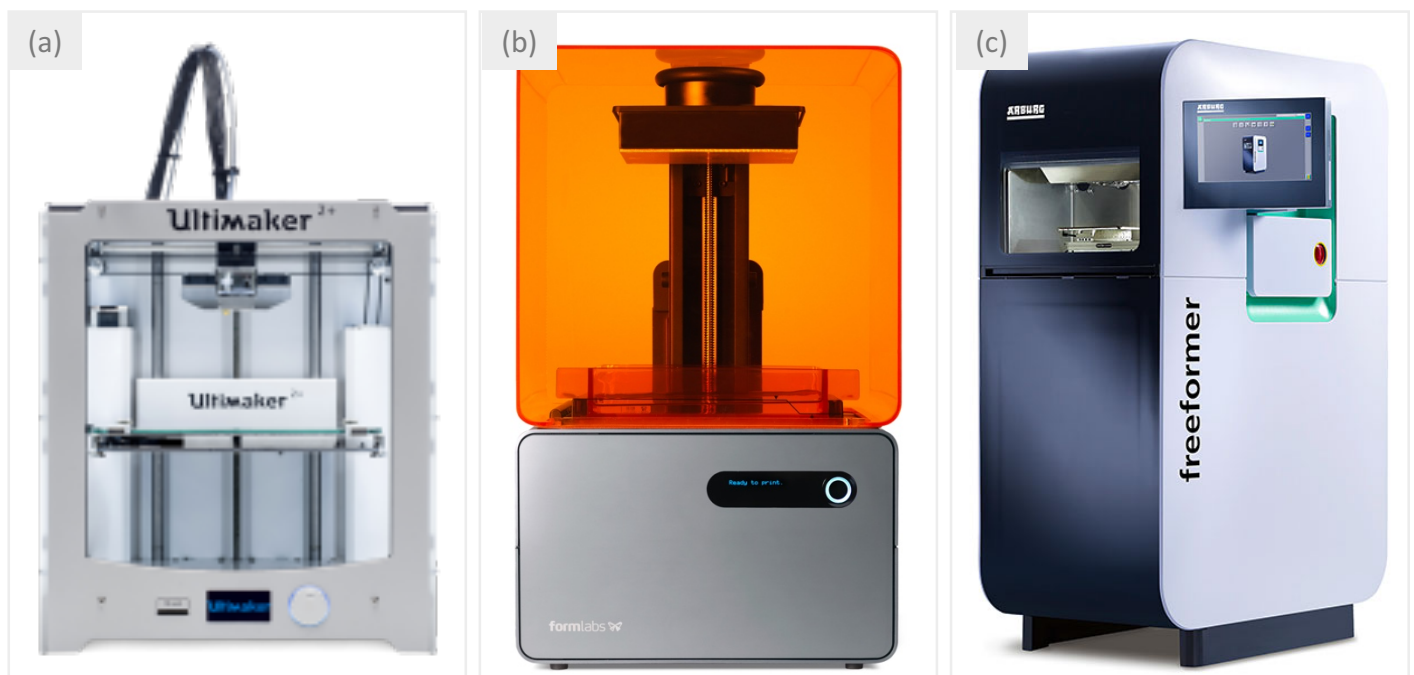

Figure 4 - Printers used for the 3D printing of stents. (a) Ultimaker 2+, (b) Form 1+, (c) Freeformer.
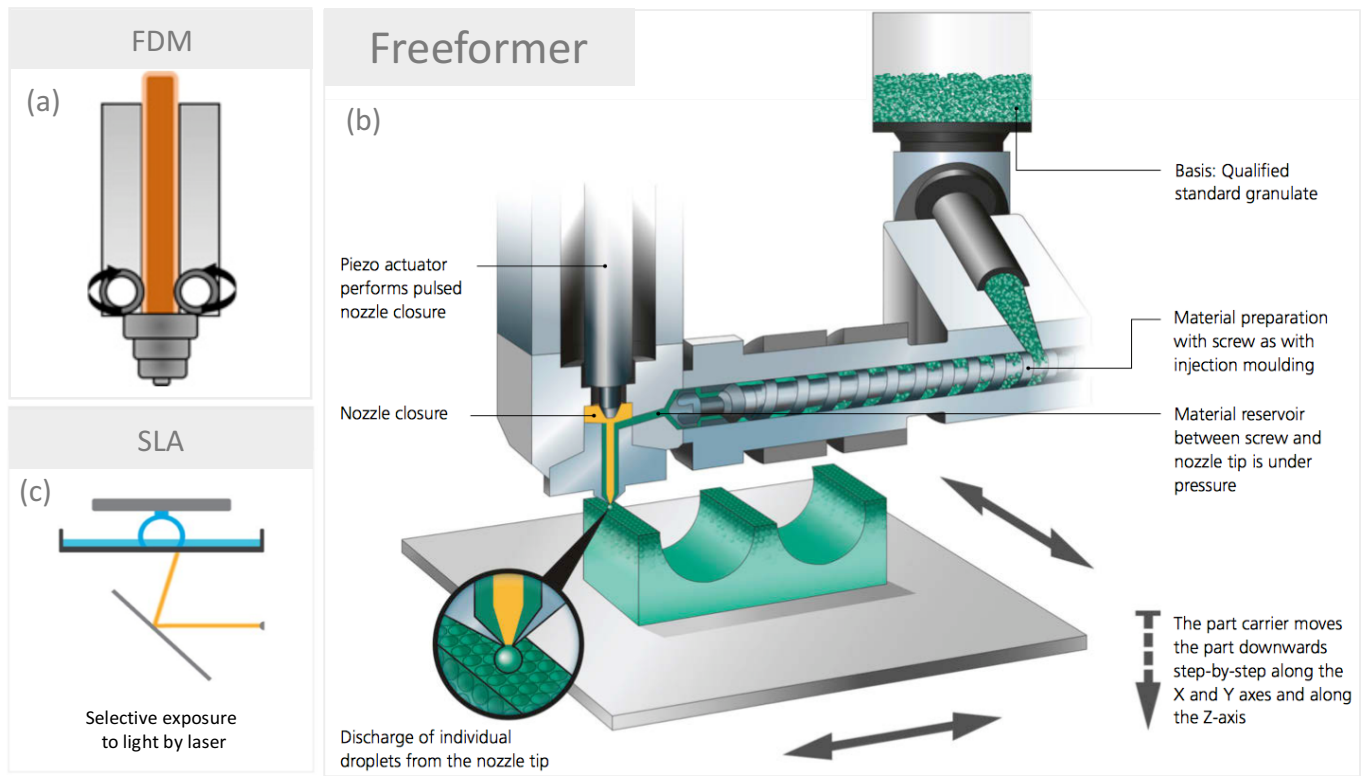
Figure 5 - Techniques used by the various 3D printers. (a) Ultimaker 2+ is an FDM printer which extrudes filament through a heated nozzle tip [58]; (b) Freeformer uses material in pellet form which is warmed up in a screw before being melted in a chamber at the tip and extruded droplet-by-droplet [59]; (c) Form 1+ uses SLA technology in which a laser shines and crosslinks the resin to form the printed sample [60].

2.1.1. Design of stents

Design parameters were chosen from the dimension range provided by Elixir Medical Corp. [23]. The stent design aimed to replicate current bioresorbable stents Absorb GT1 (Abbott, USA) and DeSolve (Elixir Medical Corp, Milipitas, California, USA). Final design (Appendix A) was rendered with Solidworks (Dassault Systèmes, Velizy-Villacoublay, France) with a diameter of 3 mm and strut thickness of 200 μm and width of 200 μm (STL files upon request).

2.1.2. 3D printing of stents
2.1.2.1. Printing with an Ultimaker 2+

Due to the dimensions in the micrometer range not being supported by the Ultimaker 2+, printing was performed with a nozzle of 0.10 mm obtained from 3DSolex (Cepta AS, Oslo, Norway) and Simplify3D (Simplify3D, Blue Ash, Ohio, USA) printing software. Currently, limited data in printing parameters with 0.10 mm nozzles exists. Also 0.10 mm nozzles are not officially software-compatible with Ultimaker printers. As a result, a trial-and-error methodology followed to obtain the ideal printing settings for the 0.10 mm nozzle. Parameters including nozzle temperature, extrusion width, extrusion multiplier, primary layer height, printing speed, X/Y speed and retraction speed were modified. No support material was used due to the dimensions being damaged during detachment.

NC PLA filaments were first used due to the known printing characteristics and compatibility with the Ultimaker 2+. Before printing, the filament spool was first loaded in the printer and kapton tape was placed in the printing bed to aid on the sample release. The design was then uploaded in Simplify3D and the various parameters were one-by-one modified after every test print. Every test print consisted of one stent at a time. Starting from a stent diameter of 8 mm, settings were modified down to a 4 mm stent.
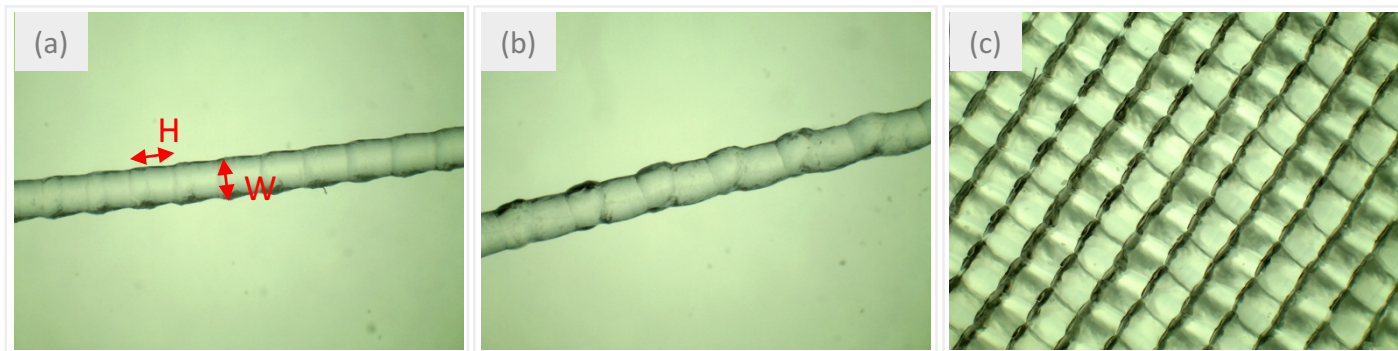
Figure 6 - Overview of the filament from the Freeformer printer. (a) Single droplets in a homogeneous filament; (b) non-homogeneous filament; (c) ideal single droplet pattern of printing with a Freeformer.

After printing settings were identified regarding repeatability of a complete printed stent, a shorter calibration regarding the nozzle temperature was performed with the PL18 and PC12 filaments. Before the printing of every stent, a flush of material was performed in the nozzle to prevent old and degraded material. After printing, every stent was flushed and stored in glass vials under nitrogen to prevent further degradation.

2.1.2.2.   Printing with the Freeformer

In contrast to FDM printers such as the Ultimaker 2+, the Freeformer bases its technology in a combination of injection molding and extrusion printing. Freeformer printers have the advantage over filament-based printers, on being able to use the material in pellet form. Pellets are commonly the first form which a material obtains after production. They are ultimately preferred over filaments, as the final printed material only experiences one heat cycle as opposed to two. Within the printer (Figure 5.c), the pellets go through a slow heating process in a screw, and deposited in a small heating chamber. There the material is melted and then extruded droplet-by-droplet with the help of a piezo actuator.

During this experiment, the Freeformer and its printing chamber were first pre-heated for an hour, point at which the printer did not show any further temperature fluctuations. PL18 in pellet form as the main material and polyvinyl alcohol (PVA) as support were then loaded in the printer. The printing chamber temperature was set to 70 °C, and the three-step temperature at 215 °C, 205 °C and 180 °C for PL18. Material was then flushed from both nozzles for 600s, point at which the printer was able to find the required force for extrusion of the material through the nozzle. Ideal filaments are to be obtained in a range of 280-320 N extrusion force at the nozzle. The extruded filament was then examined under the microscope for a homogenous string of droplets (Figure 6.a). Cases where the filament is not homogenous (Figure 6.b) requires further iterations with a higher temperature and a lower discharge for a lower viscosity in the material. The width (W) and height (H) of the droplet was measured, to obtain the W/H ratio required by the Freeformer software to calculate the printing parameters of the uploaded sample.

A pre-printing test of 5, 2x2 cm blocks with W/H-0.04, W/H-0.02. W/H, W/H+0.02 and W/H+0.04 ratios was performed. The best printing ratio was then selected by microscope observation (Figure 6.c) for a homogenous surface, followed by feeling of the surface if needed. The correct W/H droplet ratio was then input in the Freeformer software and the sample was further uploaded. Further correction of printing speeds was managed in the software.

When printing, a second round of flushing for 120 sec was performed to prevent remains of degraded material and a clogging of the nozzle. Prints were performed with both 0.15 mm and 0.25 nozzles, both with and without support material.

2.1.2.3. Printing with the Form 1+

The selected resin, either the methacrylate or the PLA resin, was first poured in a clean resin tank preventing exposure to direct sunlight and contamination. The build platform was then cleaned with 2-propanol. The STL stent file was first uploaded in the PreForm (Formlabs, Somerville, Massachusetts, USA) software and replicated to 25 samples per print. Printing was performed with a layer thickness resolution of 0.05 mm, a support density of 1.00 and a support point size of 0.60 mm. The build platform was offset to $Z =$ -0.30 mm to aid the print in the adhesion to the platform. After a total printing time of ~45min, the samples were released from the build platform and placed in two baths of 2-propanol for 5 min each, followed by air drying. The samples were then released from their mechanical supports, flushed and placed in glass vials with nitrogen to prevent further degradation.

2.2. Stent structural characterization

Morphology was analyzed before- and after- post processing, followed by investigation of the mechanical and degradation properties. After printing, with the Ultimaker 2+ 0.10 mm nozzle, stent samples from NC-PLA, PL18 and PC12 of 4 mm in diameter were analyzed. Finally, 4 mm diameter printed stents in methacrylate resin and PLA resin with the Form 1+ were also characterized.

2.2.1. Scanning electron microscopy analysis and post processing

Strut thickness and width, stent diameter and surface roughness were analyzed with scanning electron microscopy (SEM) (JSM-IT100, Jeol, Tokyo, Japan). Three stents were investigated simultaneously with electron beam energies ranging from 5-20 kV, working distance of 12 mm and chamber pressures between 20-40 Pa in a low vacuum setting. Due to the polymeric nature of the stents, low visibility is experienced with SEM if no metallic coating is used, therefore the low vacuum mode was used. All three imaging modes, backscattered electron composition image (BEC), backscattered electron topographic image (BET) and backscattered electron shadow image (BES) were used to obtain the best images. Prior to imaging, the stents were cleaned in 2-propanol and deionized water (DI water) for 30 sec, followed by air drying. Measurement of strut width (Figure 7) consisted in the division of the stent in three areas, consisting of the distal, central and proximal area of the stent, where proximal area corresponded to the ring closest to the printer bed after printing. At each area, three measurements per horizontal crest (HC), diagonal crest (DC) and connecting link (CL) were recorded (Figure 8). Furthermore, stent outer- (OD) and inner- diameter (ID) and stent thickness (Figure 8) were only measured at both the proximal- and distal end of the stent from a front view, which avoided the need to damage the stent by separating it in half for a central measurement. The SEM analysis performed before- and after post processing of the stents reveal how the surface and dimensions of the stent were affected. During post processing, each stent except the methacrylate, was placed in a mixture 10:1 of acetone and chloroform for 30 sec, followed by a double submersion in DI water for 30 sec and air drying. Methacrylate samples were placed in acetone for 1.5 minutes instead, followed by a double rinsing in DI water for 30 sec and air drying, as they are not soluble in chloroform.
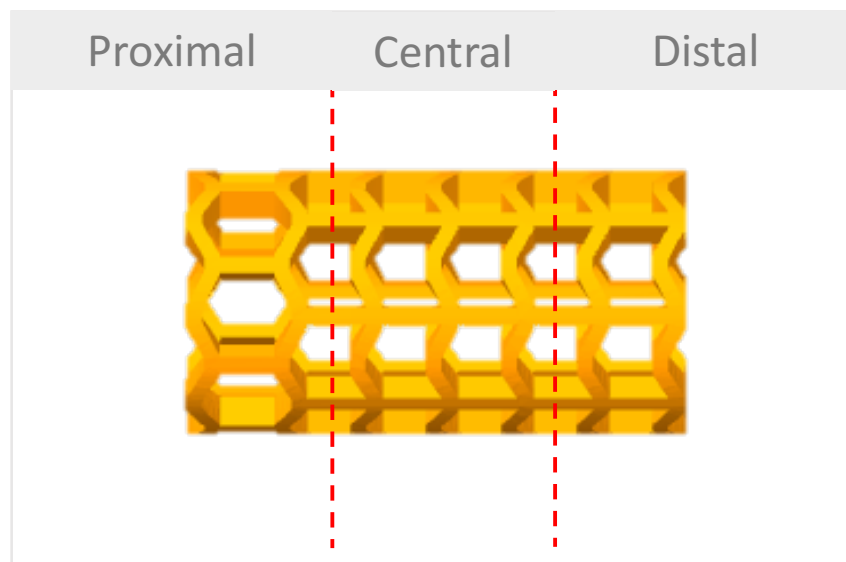
Figure 7 - Division used during the SEM analysis of the BRS. The BRS was divided in three areas, proximal, central and distal. With the proximal area corresponding to the ring closest to the printer bed. For strut width and diameter recordings, only the proximal and distal area were taken into consideration to avoid stent damage.
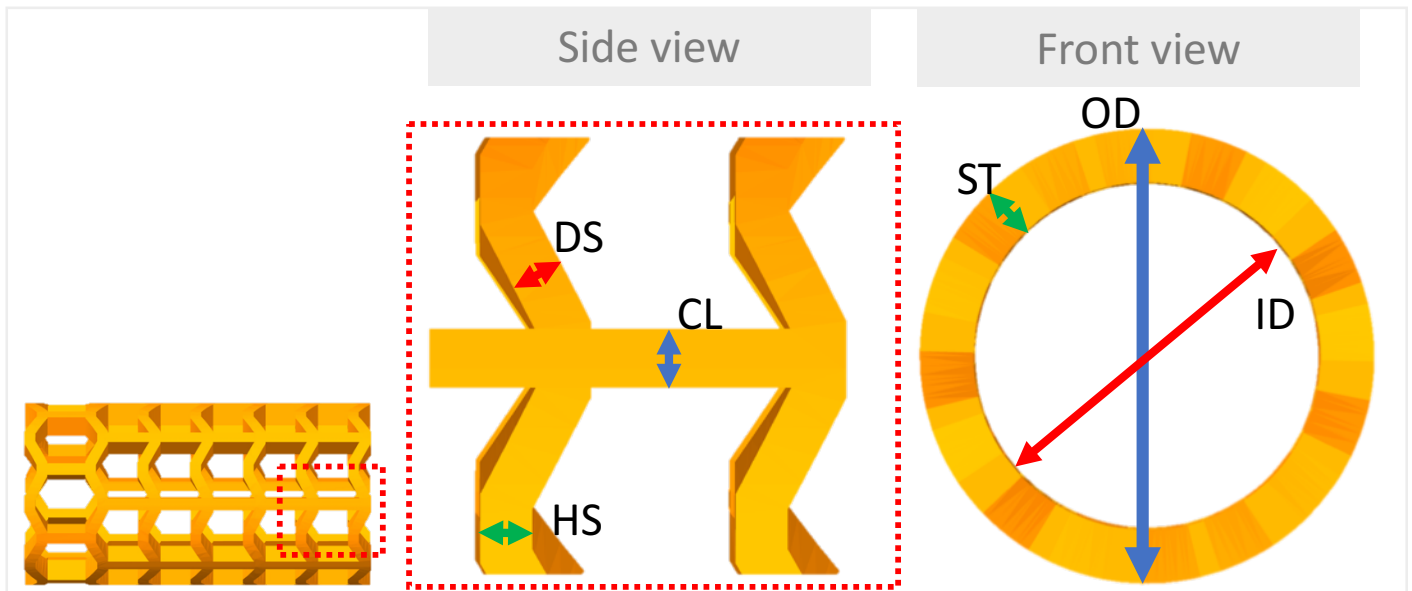
Figure 8 - Representation of the measurements recorded during the SEM analysis of the BRS. From a side view the strut widths were measured from three different structures, the diagonal strut (DS), the horizontal strut (HS) and the connecting link (CL). From a front view the sent strut thickness (ST), inner diameter (ID) and outer diameter (OD) were recorded.

2.2.2. Mechanical testing

Compression tests (Figure 9) were performed to study the ability of the printed stents to withstand the loading force from the damaged vessel, as well as the longitudinal deformation during expansion. The printed stent was placed both horizontally and vertically (Figure 9.a) in a tensile machine (Lloyd LR5K, Ametek, Berwyn, Pennsylvania, USA) with a 5 N load cell, and subjected to a constant load in a single direction. Radial strength was correlated to compression in a single direction. Compression was performed for 5 cycles at a rate of 1 mm/min up to a maximum of 25% compression (Figure 9.b) of the stent diameter. The cycles were used to investigate both the radial force and the recovery capability of the stent. Longitudinal deformation was evaluated by a compression of 1 mm or until break.

Figure 9 - Mechanical testing setup for radial force measurement. (a) Stent before compression. (b) Stent at 25% compression, from a load in the −Y direction.

2.2.3. Biodegradation analysis

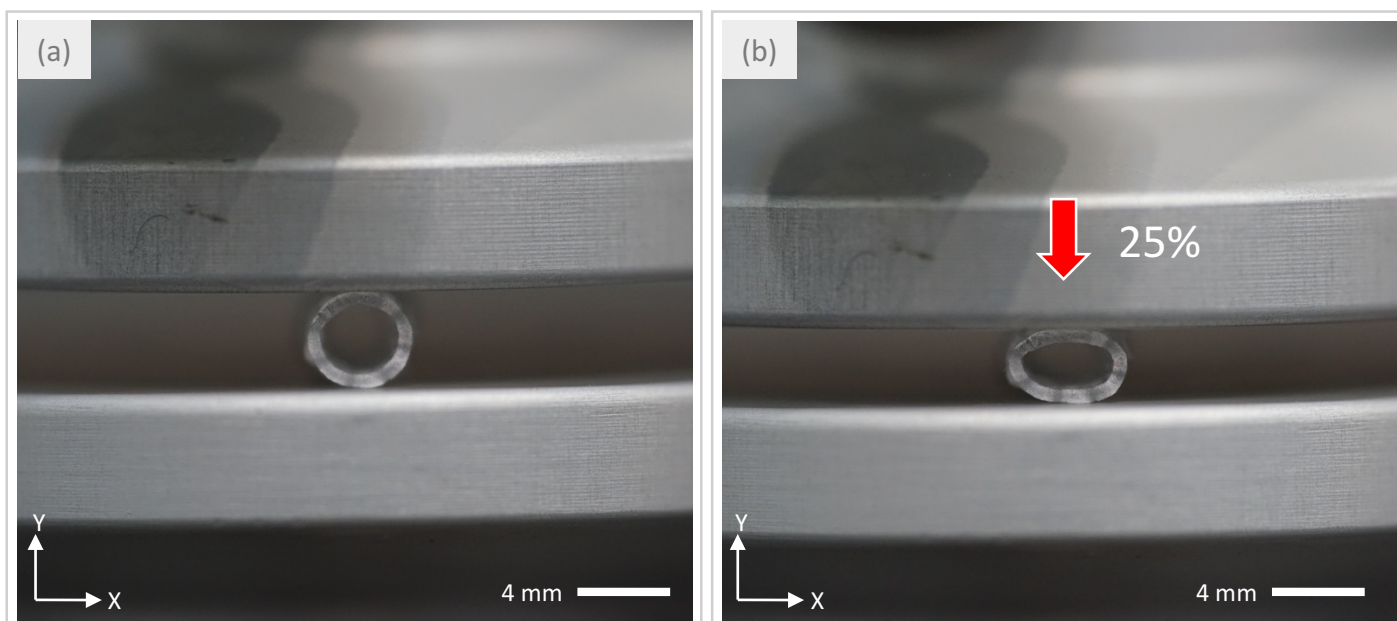*In vitro* biodegradation studies were performed to acquire data on the stents degradation lifetime and their suitability for future *in vivo* applications. All printed stents were first cleaned in 2-propanol and DI water for 30s followed by air drying. Their weight before degradation was recorded. They were then placed in single glass vials with 1.5 ml of phosphate-buffered saline (PBS) and incubated at 37°C. Information was recorded at time points of 5, 10, 15, 20 and 25 days. At each time point the stents were air dried and weighted.

2.3. Stent chemical characterization

Chemical characterization was performed both before and after 3D printing. NC PLA in filament form, PL18 and PC12 in pellet and filament form, the methacrylate resin and the PLA resin were used for characterization before printing. After printing, with the Ultimaker 2+ 0.10 mm nozzle, stent samples from NC PLA, PL18 and PC12 of 4 cm in diameter were analyzed. From the Freeformer, printed PL18 material with 0.15 mm and 0.25 mm nozzles was used. Finally, 4 cm diameter printed stents in methacrylate resin and PLA resin with SLA were also characterized.

2.3.1. Gel permeation chromatography analysis

Changes in the weight-average molecular weight (Mw), number-average molecular weight (Mn) and polydispersity (PDI) as a result of printing were analyzed with gel permeation chromatography (GPC). For NC PLA stents, 100±10 mg of printed samples were placed with 2 ml of tetrahydrofuran stab./BHT (Biosolve Chimie SARL, Dieuze, France) (THF) in glass vials. For PL18 and PC12 stents, 15 mg of printed samples were placed with 2 ml of chloroform in glass vials. Samples of methacrylate and PLA resin where not tested for GPC due to the lack in compatibility of the solvents available. All samples were left overnight to dissolve into a homogeneous mixture. The samples were then placed in the high-performance liquid chromatography (HPLC) value system (1100 series, Agilent Technologies, Santa Clara, California, USA) for further analysis.

16

2.3.2. Inherent viscosity analysis

Degradation of the polymer as a result of 3D printing was further analyzed by measuring its inherent viscosity (IV). A total of 250±10 mg of printed samples were added in a 50 ml volumetric flask with 25 ml of chloroform and placed in a vibrating platform until completely dissolved. The flask was then filled with 25 ml extra of chloroform and shake for a complete mixture. Before measurement, the test setup consisting of a Ubbelohde viscometer (52303/Oc, SI Analytics, Mainz, Germany) was flushed three times with chloroform, followed by a measurement of deviation with a required reading of < 1. The glass viscometer was then flushed three times with chloroform and then once with the prepared mixture (process required after every test run). The mixture, was added up to the glass flask reference points, corresponding to about 15 ml. Measured weight was then input in the IV software (AVS 370, SI Analytics, Mainz, Germany) to begin the measurement. Samples of methacrylate and PLA resin were not tested for IV due to the natural liquid form they are encountered in. IV changes will therefore prove inaccurate as these changes are therefore caused not only by degradation but also by the crosslinking of the polymers.

2.3.3. Differential scanning calorimetry analysis

Further information on the degradation caused by 3D printing was obtained by the analysis of the polymer's melting point with differential scanning calorimetry (DSC). A decrease in melting temperature is therefore interpreted as degradation experienced in the polymer. A total of 6-12 mg of printed material was weighted, recorded and capped in between a 50 µl metal dish (B014-3017, Perkin Elmer, Waltham, Massachusetts, USA) and its cap (B014-3004, Perkin Elmer, USA). The sample was then placed in the DSC 4000 (Perkin Elmer, Waltham, Massachusetts, USA) with a temperature fluctuation between 0 °C and 250 °C under normal air conditions, and analyzed with the software Pyris Series DSC 4000 (Perkin Elmer, Waltham, Massachusetts, USA). Heating rate was 10 °C /min. The onset, peak and end melting temperatures were recorded. Samples of methacrylate and PLA resin where not tested as melting was not possible due to the crosslinking of the polymer.

2.3.4. Fourier transform infrared spectroscopy analysis

To be able to observe if the different 3D printing techniques produced any changes in the chemistry of the materials after being printed, Fourier transform infrared spectroscopy (FTIR) was used. Before measurement, the lens of the FTIR (FT/IR-4200, Jasco, Tokyo, Japan) was cleaned with ethanol and dried completely to avoid any incorrect readings. Enough material to cover the lens was then placed in the FTIR and pressed with the clamp until a reading between the 40% and 60% intensity was observed in the software (Spectra Measurement, Jasco, Tokyo, Japan). The resulting graph was then recorded with its corresponding peaks. After a complete set of tests per material was performed, the graphs were superimposed to look for changes in the peaks if any.

2.4. Statistical analysis

To evaluate the statistical difference when comparing the mean values in each group of materials (three stents per group, five groups), as well as the structures in each group of materials (three stents per group, five groups) was analyzed with an analysis of variance (ANOVA) general lineal model. The analysis was performed in Minitab 18 (Minitab Ltd, Coventry, United Kingdom) software. Statistically significance was noted with a value of $p < 0.05$, $p < 0.01$ and $p < 0.001$.

$$3$$

Results

3.1. Stent fabrication

3.1.1. Ultimaker 2+ stents

A photo overview of the stent fabricated with the Ultimaker 2+ is presented in Figure 10.a. After various iterations, the printing results for a 4 mm diameter stents are presented in Table 1. Different nozzle temperatures were needed as a result of a changing melting point per material used. It is important to note that even though PC12 melts at a temperature of 60 °C, a temperature of 180 °C was needed for a continuous extrusion from the nozzle, as well as due to printer limitations. Average printing time was 4 min, where about 7.2 mm of material filament was used, accounting for an average stent weight of 15 mg.
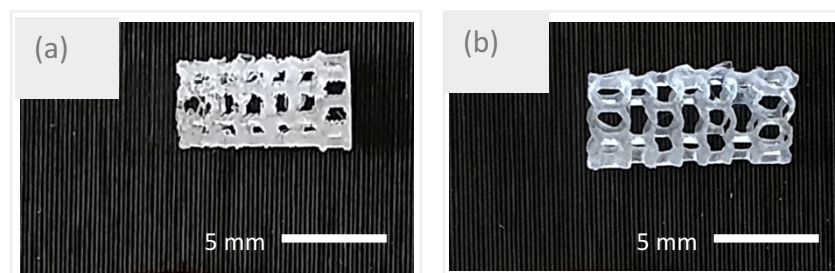

Figure 10 - Overview of 4 mm diameter printed BRS with (a) Ultimaker 2+, (b) Form 1+.

Parameter	Material		
	NC PLA	PL18	PC12
Nozzle temperatures (ºC)	205	190	180
Extrusion width (mm)	0.06	0.06	0.06
Extrusion multiplier	1.15	1	1
Primary layer height (m)	0.11	0.11	0.15
First layer height (%)	150	150	150
Printing speed (mm/min)	3200	3200	1200
X/Y speed	5000	5000	5000
Retraction distance (mm)	4	0	0

A more in detail picture-to-parameter change iteration can be found in Table 2, Appendix B.

Throughout the various iterations, the following parameter findings were obtained (it should be assumed that the expected outcome is a result of changing a single parameter, unless otherwise noted, while keeping the rest constant):

- Reduction in extrusion width results in a conical shrinking. Conical shrinking is caused by the extrusion of less material creating an inadequate base for the printing of the next layers.
- Reduction in printing speed results in more material being deposited, as the nozzle is slowed down but the flow is not. This causes less precision in the final print.
- Reduction in printing speed and X/Y speed results in both less precision and a loose of connections as the material is not moved fast enough in between gaps.
- Reduction in X/Y speed results in less precision but overall a better quality than reducing the printing speed. It allows the nozzle to slow down when switching between struts, which allows longer time for adhesion and a lower pull of material.
- Increase in printing speed and decrease in X/Y speed results in less material being deposited due to the faster nozzle. This allows for finer structures to be printed.
- Reduction in retraction distance allowed for a better extrusion of soft materials, by preventing nozzle clogging and material wear at the feeding gear.

3.1.2. Freeformer printing

Even though adequate printing parameters for PL18 were obtained, printer limitations encountered throughout the iterations, posed specific challenges, revealed in Appendix C, for the printing of stents at the required dimensions. Ultimately, printing of PL18 was achieved with a printing speed of 667 mm/min, a discharge of 50%, a force of 200-210 N and a three-set temperature of 220°C, 210°C and 190°C. Unfortunately, no BRS was able to be printed with the Freeformer printer.

The main Freeformer findings can be summarized as follows:

- As a result of the stent dimensions, the upper plate where the nozzle is located, remains at a close distance to the printing bed. This exerts a constant downwards temperature of the nozzle

into the print, preventing the print from cooling down. Consequently, molted material continues to be printed over molted material without holding onto the printed geometries.

- The material remains too long in the pre-extrusion chamber, resulting in the degradation and burning of the material, followed by the clogging of the nozzle.
- Due to the challenge of the material to cool down, when using support material, it spreads among the whole print. This hinders the correct adhesion in between layers, with an end sample of intercalated layers between base and support material.
- The challenge imposed by the printer software in changing only certain parameters, prevent counterweighting the size of the 0.15 mm nozzle, which is not adequate for the stent dimensions.

3.1.3. Form 1+ stents

Printing of the 4 mm BRS presented in Figure 10.b was obtained with standard Form 1+ parameters. Printing of 25 stents lasted between 50-60 min, with an average weight of 20 mg per stent. Printing iterations consisted in finding the stent inclination angle (θ) with respect to the printing bed (Figure 11.a), for a better release from the support material (Figure 11.b). The most amount of prints were therefore obtained at 40° inclination angle with respect to the bed surface. During the printing, it was observed that contamination and previous crosslinked material resulted in drawbacks when printing one set of stents after the other. After various iterations, mixed crosslinked material was difficult to remove resulting in the need of disposing the used resin and refilling with new one. Furthermore, since the printing took place inside the resin tank, it was difficult to observe if correct adhesion and printing was being performed.
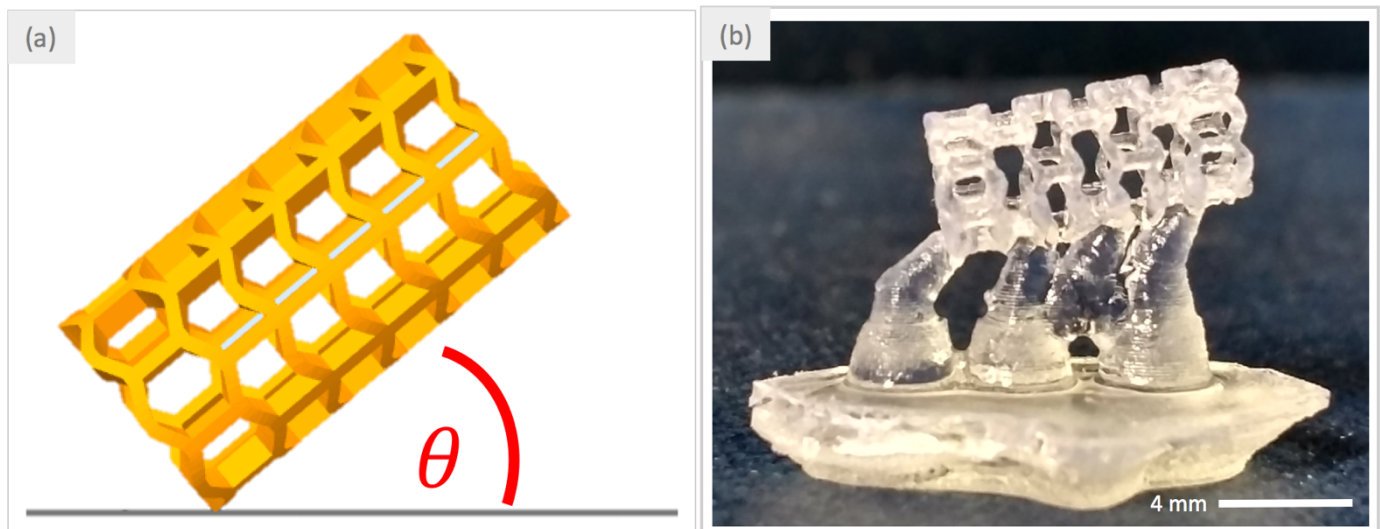

Figure 11 - (a) Representation of the stent inclination with respect to the printing bed. The angle (θ) was variated to obtain the ideal print in the Form 1+. (b) Printed stent before detachment from the support beams.
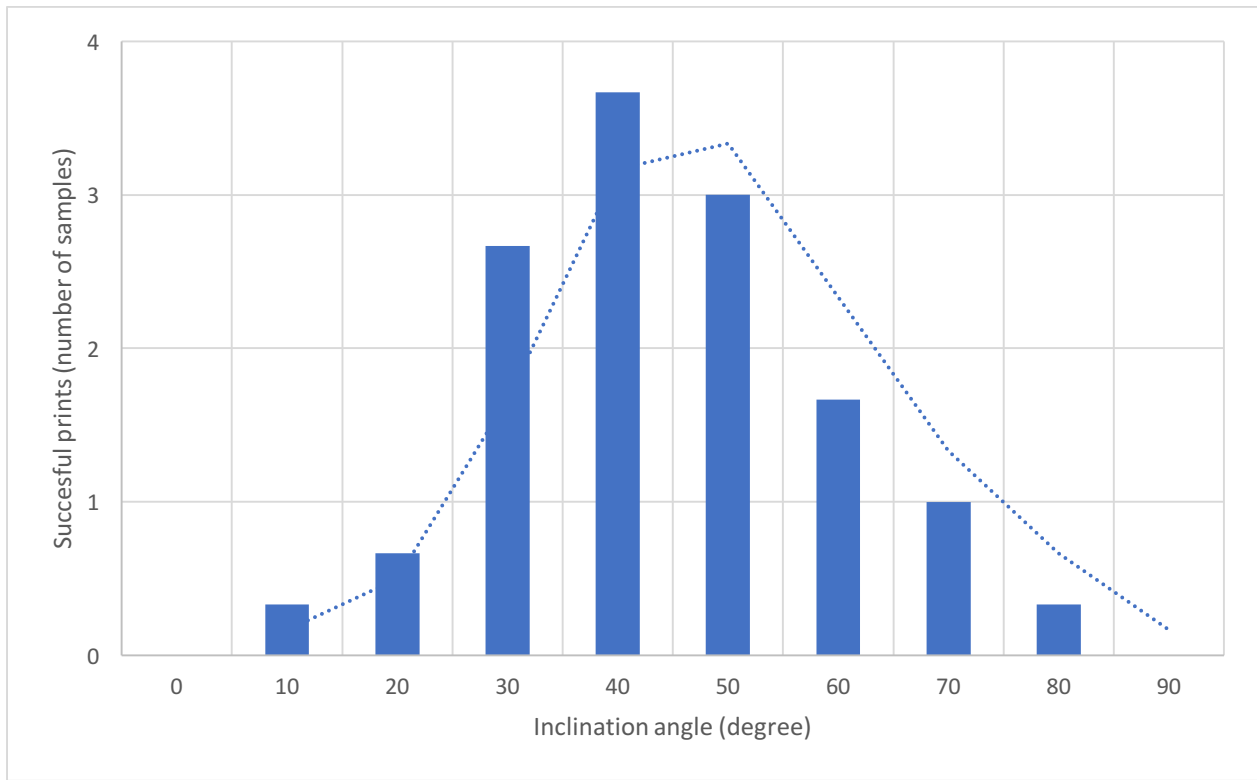
Figure 12 - Average number of printed stents as a factor of the inclination angle of the sample with respect to the bed surface when printing with the Form 1+. A bell curve behavior is observed with a higher success rate around 40°.

3.2. Stent structural characterization

3.2.1. Stent geometrical morphology

The geometrical morphology of the stents was investigated by SEM. A representation of one out of the three areas analyzed per stent is shown in Figure 13, for both a Ultimaker 2+ and Form 1+ printed stent. Preliminary observations show an immediate difference in printing accuracies and surface morphologies between both manufacturing techniques.
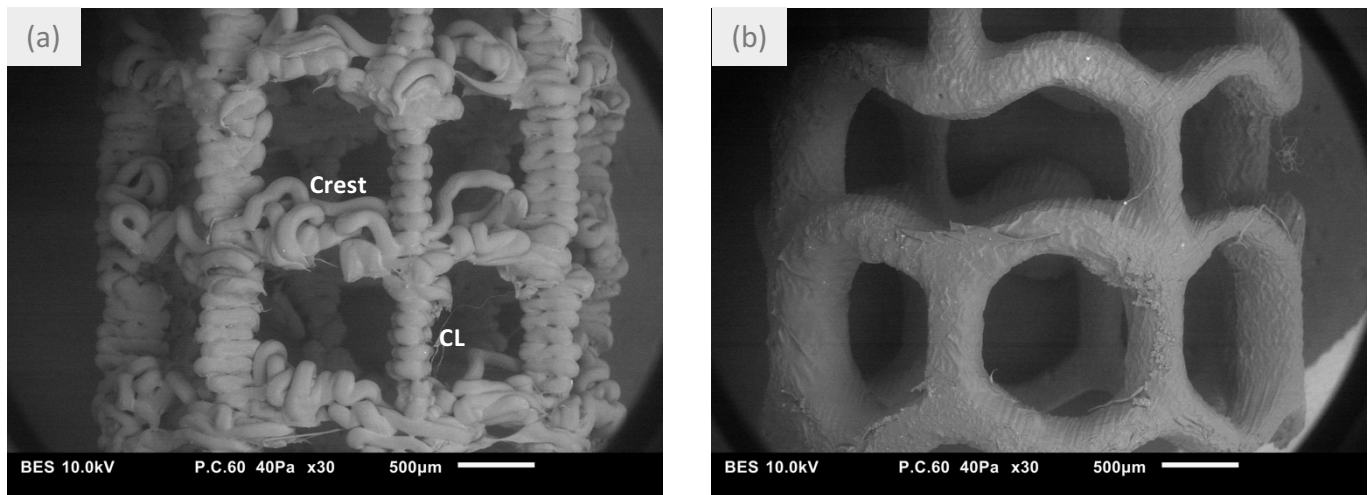

Figure 13 - SEM image comparison of a printed stent with the (a) Ultimaker 2+ and with the (b) Form 1+. Qualitative observation of the images shows the difference in accuracy and surface finish of both techniques. Moreover, (a) presents the layer-by-layer printing which is performed in the Z-direction, for both crests and connecting links (CL).

3.2.1.1.   Strut width and thickness

The measurement of the strut width before post processing revealed the inaccuracy of printing within the stent itself regarding the various techniques. Although changes of more than 25% were commonly observed in stents printed with the Ultimaker 2+, the inaccuracy in the Form 1+ stents was still in the range of 15-20% (Figure 14). Furthermore, the inaccuracy of strut width when compared to other stents within the same material was found the highest in Ultimaker 2+ printed stents. Methacrylate scored the highest standard deviation with 19% difference among the three evaluated stents. In contrast, PLA resin stents showed the greatest homogeneity with only 4% standard deviation within the printed stents.
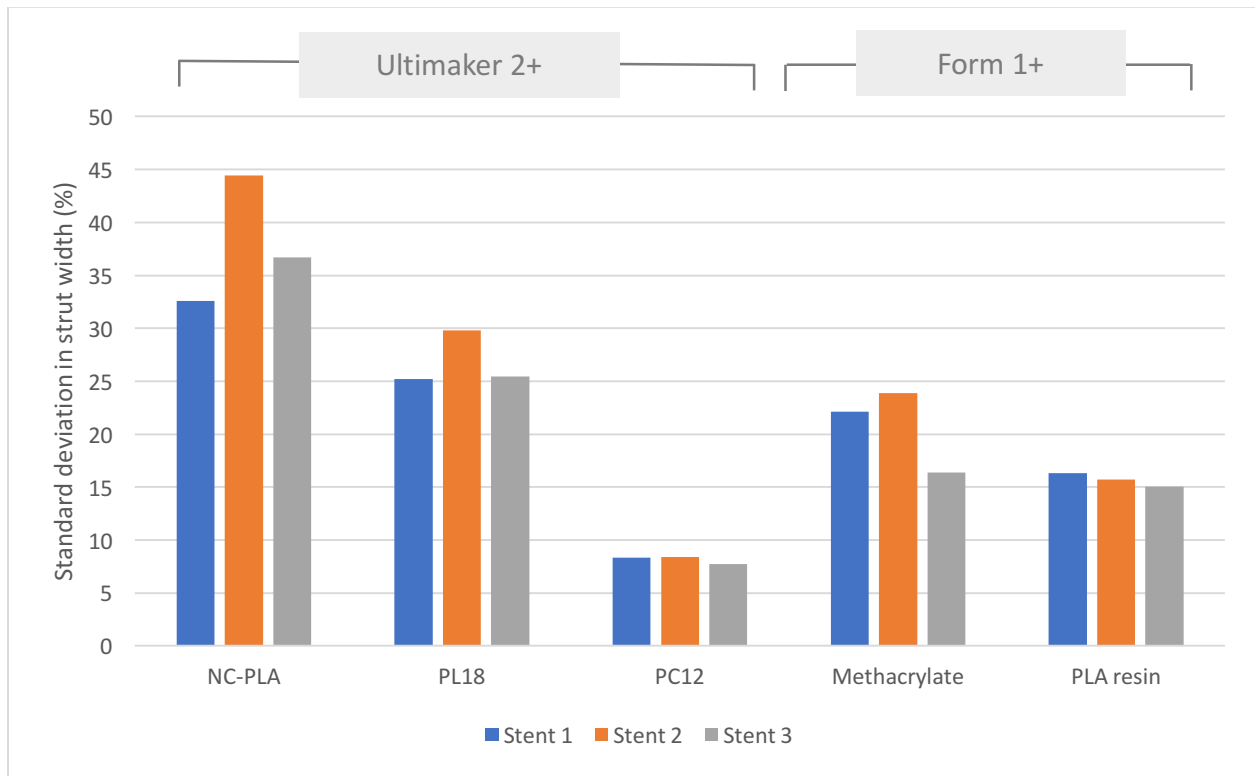

Figure 14 - Percentage of deviation in the width of the struts within a single stent before post processing. Three stents per material are evaluated. Difference in precision are observed not only within a single stent, but also from one stent to the other for every material. NC PLA, PL18, PC12 stents were printed with an Ultimaker 2+. Methacrylate and PLA resin stents were printed with a Form 1+.

A closer look into strut width in the different structures of the stents such as the HC, DC, and CL (Figure 15), provided further information on how the printing direction affected the accuracy of printing. Among all stents, the highest width was commonly found in the HC, followed by the DC and the CL. Moreover, Form 1+ prints showed the highest homogeneity as compared to Ultimaker 2+ prints. The deviation of PC12 prints was the lowest with 8%, while NC PLA position with 40% deviation as the most inaccurate. It is interesting to note that among all the structures, the CL remained the most homogeneous across all printed materials with a deviation of about 12%.

Similar to the strut width, it was found that the strut thickness equally differed depending on the area of the printed stent (Figure 16). In general, the highest strut thickness was commonly found in NC-PLA prints, however the highest deviation was found to be PL18 with 41%. As expected, the biggest differences were found in prints with the Ultimaker 2+. In terms of uniformity, Form 1+ prints greatly outperformed with a common deviation about 3 to 4 times smaller than Ultimaker 2+ prints. Finally, it is important to note, that strut thickness in the proximal area of the stent was found to be always greater across all prints.
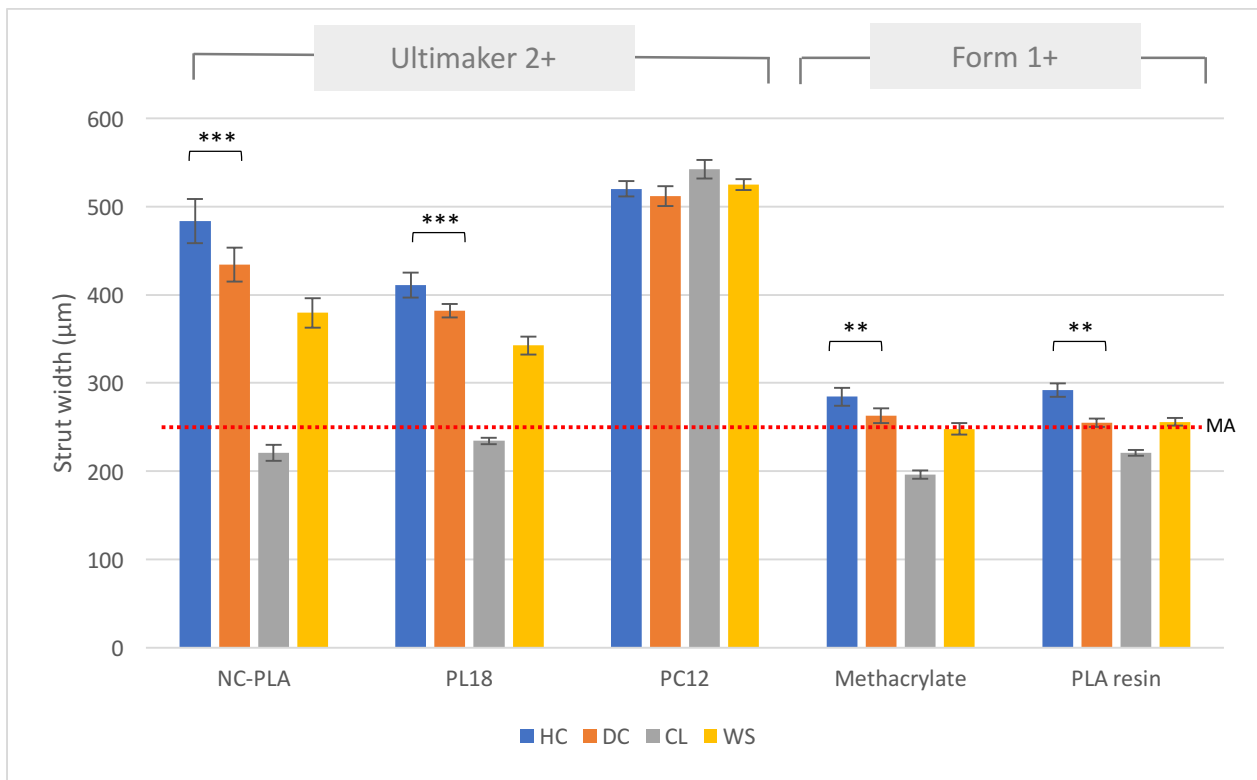
Figure 15 - Average of the strut width per stent structure with respect to the material before post processing. The strut width is calculated for the horizontal crest (HC), diagonal crest (DC), the connecting link (CL) individually. WS corresponds to the total average of HC, DC and CL. Dotted line corresponds to the market-available stent average (MA). NC PLA, PL18, PC12 stents were printed with an Ultimaker 2+. Methacrylate and PLA resin stents were printed with a Form 1+. Three printed stents were used per material. Error bars correspond to standard deviation. Statistical significance with P < 0.05 (*), P < 0.01 (**) and P < 0.001 (***) is presented.
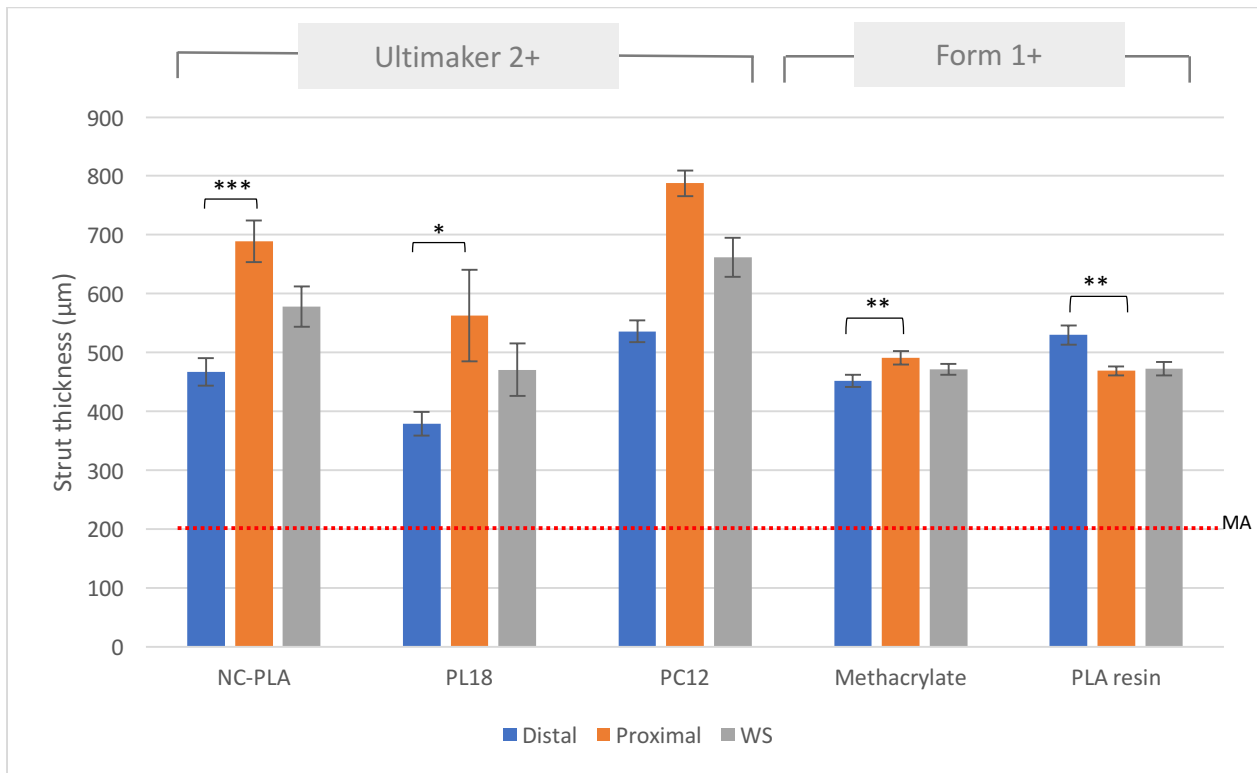
Figure 16 - Average of the strut thickness per stent area with respect to the material before post processing. The strut thickness is calculated for the distal and proximal edge of the stent. Proximal edge corresponds to the printed ring closest to the printer bed. WS corresponds to the total average of the distal and proximal area. Dotted line corresponds to the market-available stent average (MA). NC PLA, PL18, PC12 stents were printed with an Ultimaker 2+. Methacrylate and PLA resin stents were printed with a Form 1+. Three printed stents were used per material. Error bars correspond to standard deviation. Statistical significance with P < 0.05 (*), P < 0.01 (**) and P < 0.001 (***) is presented.

23

The effects of post processing were observed across all materials as both the strut width and thickness decreased (Figure 17). In average a decrease of <5% and 15-20% was seen in strut thickness and width respectively. Finally, it is important to note that the stent designs expected for a stent of 4 mm, a strut thickness of around 115 μm and a width of 230 μm. Despite the Form 1+ showing the highest accuracy among both techniques, the thickness dimensions were almost two folded while the width was more than doubled in most cases.
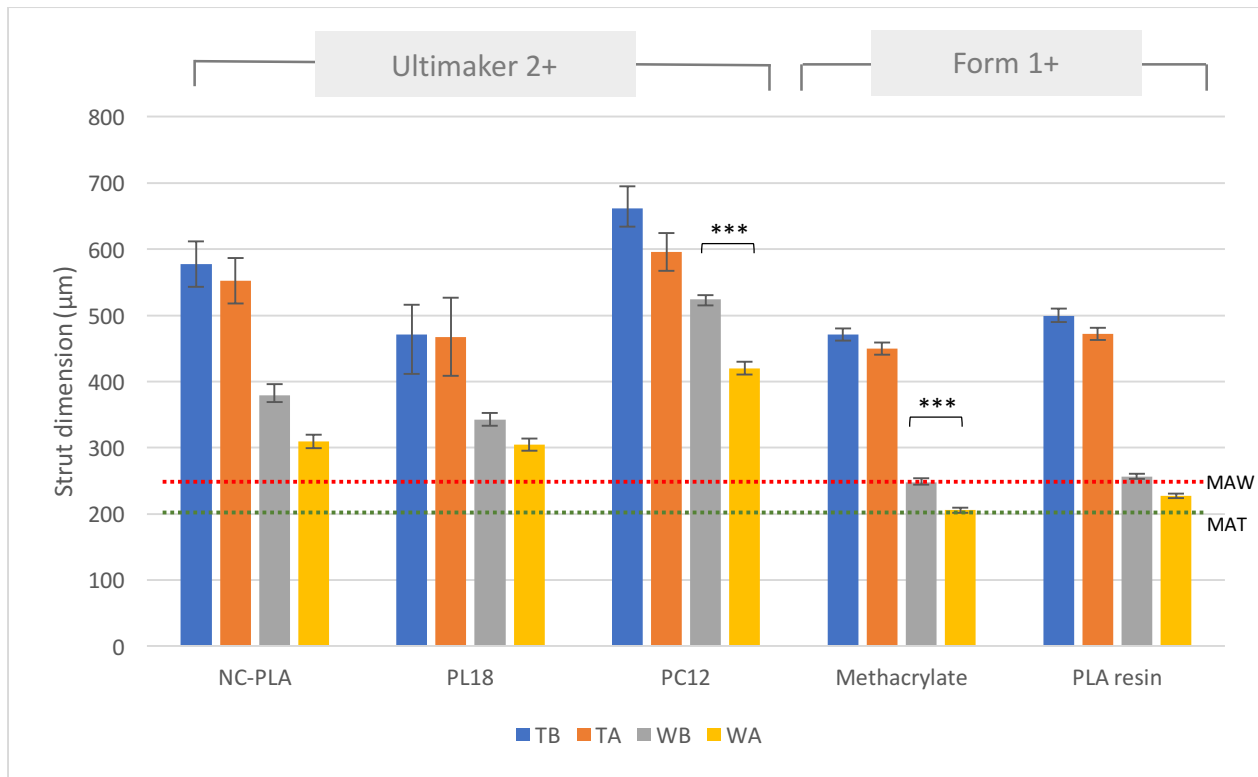

Figure 17 - Comparison of the average strut width and thickness in the stent before and after post processing. Thickness before- (TB), thickness after- (TA), width before- (WB) and width after- (WA) post processing, correspond to the total average of the whole stent strut corresponding dimensions. Dotted line corresponds to the market-available stent average for width (MAW) and thickness (MAT). NC PLA, PL18, PC12 stents were printed with an Ultimaker 2+. Methacrylate and PLA resin stents were printed with a Form 1+. Three printed stents were used per material. Error bars correspond to standard deviation. Statistical significance with P < 0.05 (*), P < 0.01 (**) and P < 0.001 (***) is presented.

3.2.1.2.   Outer diameter

In line with the strut thickness, the OD was expected to be the highest at the proximal edge of the stent (Figure 18). Furthermore, Form 1+ stents showed the highest OD when compared to Ultimaker 2+ stents, nevertheless the deviation among all materials remained <5%. The average difference between the distal and the proximal areas were highest in NC PLA with 20%, while PLA resin had the highest uniformity from edge-to-edge with only a 3% difference.

Observing the changes as a cause of post processing, opposite results from what was expected were found (Figure 19). The OD tends to increase after post processing across all stents at around 5%, with exception of the methacrylate stents which increase almost 10%. It should be highlighted, that different from strut thickness and width, outer diameter does stay closer to the design dimensions with all stents staying at <10% dimensions of 4 mm diameter. Further measurements and a similar behavior was also observed for the diameter ID. These results are presented in Appendix D.
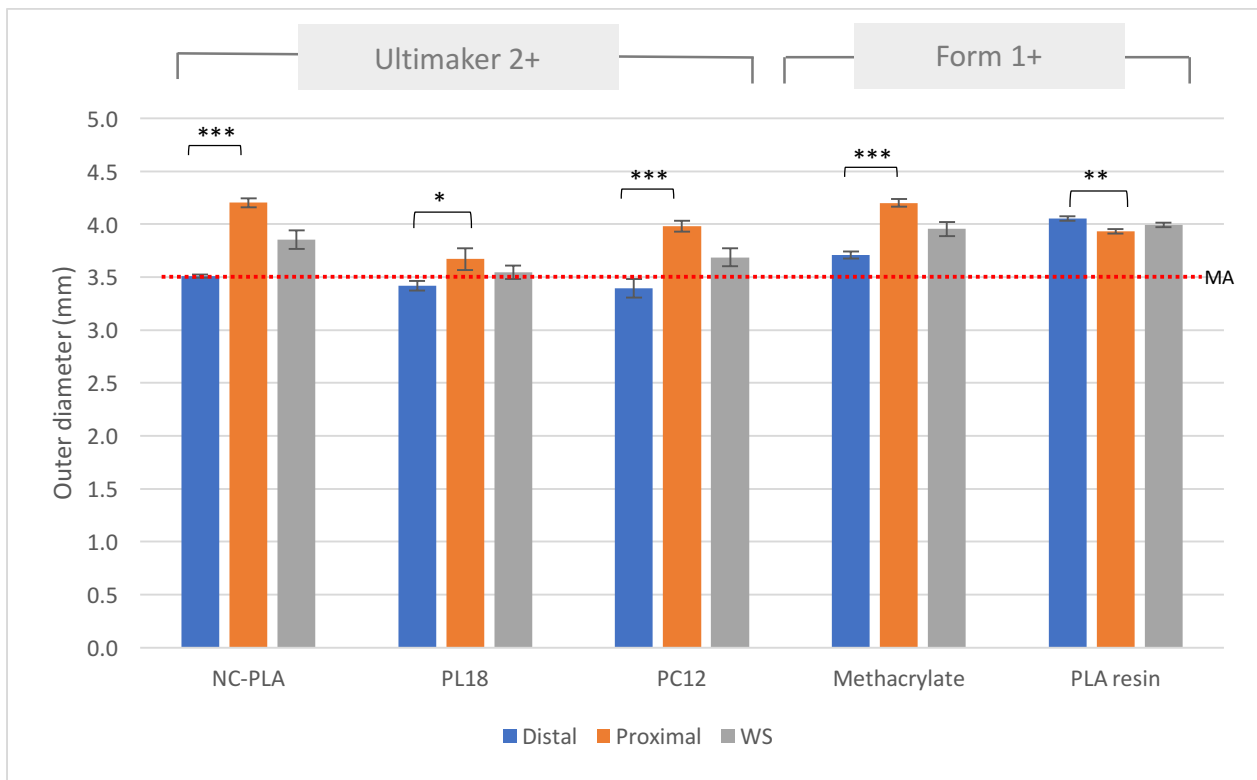
Figure 18 – Total average of the outer diameter in various materials before post processing, at both the distal and proximal edges of the stent. WS corresponds to the total average of the distal and proximal area. Dotted line corresponds to the market-available stent average (MA). NC PLA, PL18, PC12 stents were printed with an Ultimaker 2+. Methacrylate and PLA resin stents were printed with a Form 1+. Three printed stents were used per material. Error bars correspond to standard deviation. Statistical significance with $P < 0.05$ (*), $P < 0.01$ (**) and $P < 0.001$ (***) is presented.

Figure 19 - Comparison of the outer diameter in the stent before and after post processing (PP). Dotted line corresponds to the market-available stent average (MA). NC PLA, PL18, PC12 stents were printed with an Ultimaker 2+. Methacrylate and PLA resin stents were printed with a Form 1+. Three printed stents were used per material. Error bars correspond to standard deviation. Statistical significance with $P < 0.05$ (*), $P < 0.01$ (**) and $P < 0.001$ (***) is presented.

3.2.1.3. Stent surface morphology

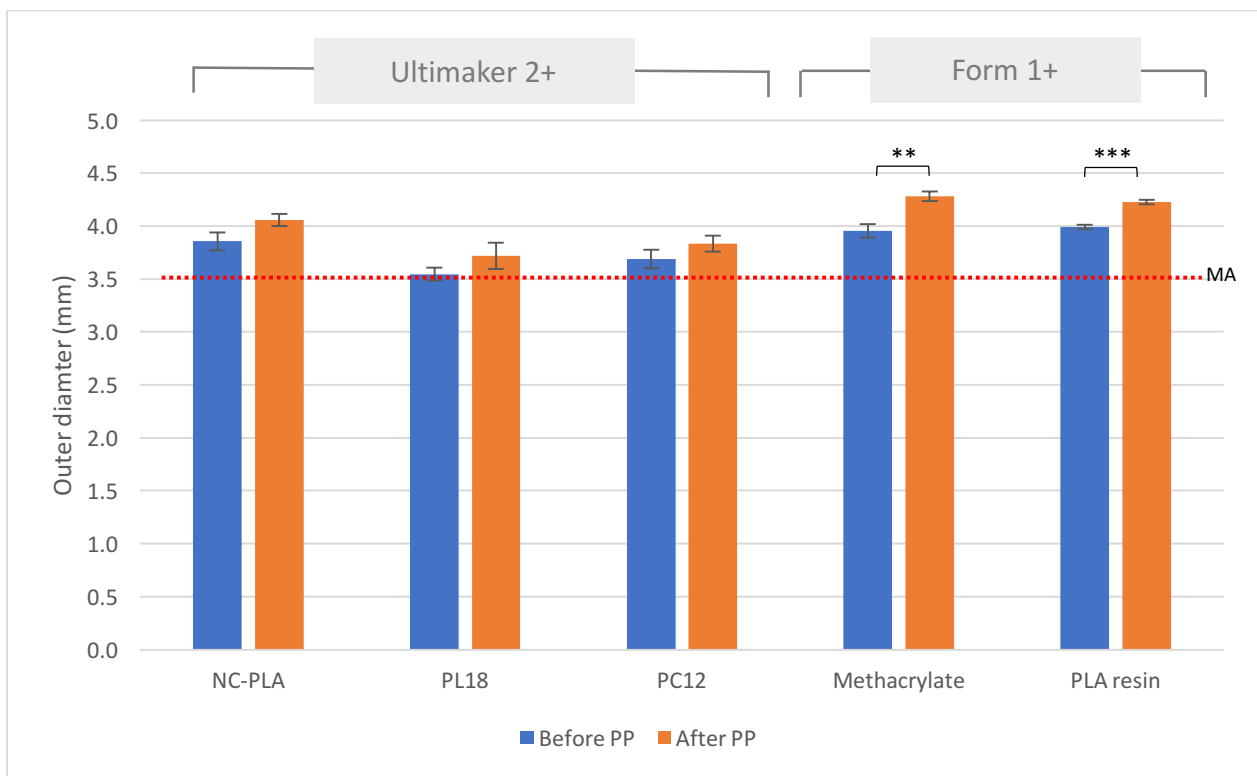Ultimaker 2+ prints showed a rough surface not ideal for stent applications in a macro scale (Figure 20.a-f), however at a closer look, the micro surface does provide a smooth finish. After post processing, the material as-a-whole washed away, which did not prove effective as the imperfections were too large. Furthermore, post processing resulted in the generation of micro porosity and the appearance of spider web structures in NC PLA and PL18 as indicated in Figure 20.d, therefore damaging the previous smooth micro porosity encountered in Figure 20.a. On the other hand, PC12 did provide a smooth surface but as presented in Figure 21.a, there was a loss of structures and general geometry after the samples where post processed. Opposite to Ultimaker 2+ stents, the Form 1+ was able to produce a smoother surface (Figure 21.a-d), although still not ideal for stent applications. A qualitative inspection showed no significant change in the surface of the methacrylate or PLA resin stents as a result of post processing. Also, the particles present in the picture similar to contamination were embedded in the material itself and not on the surface.
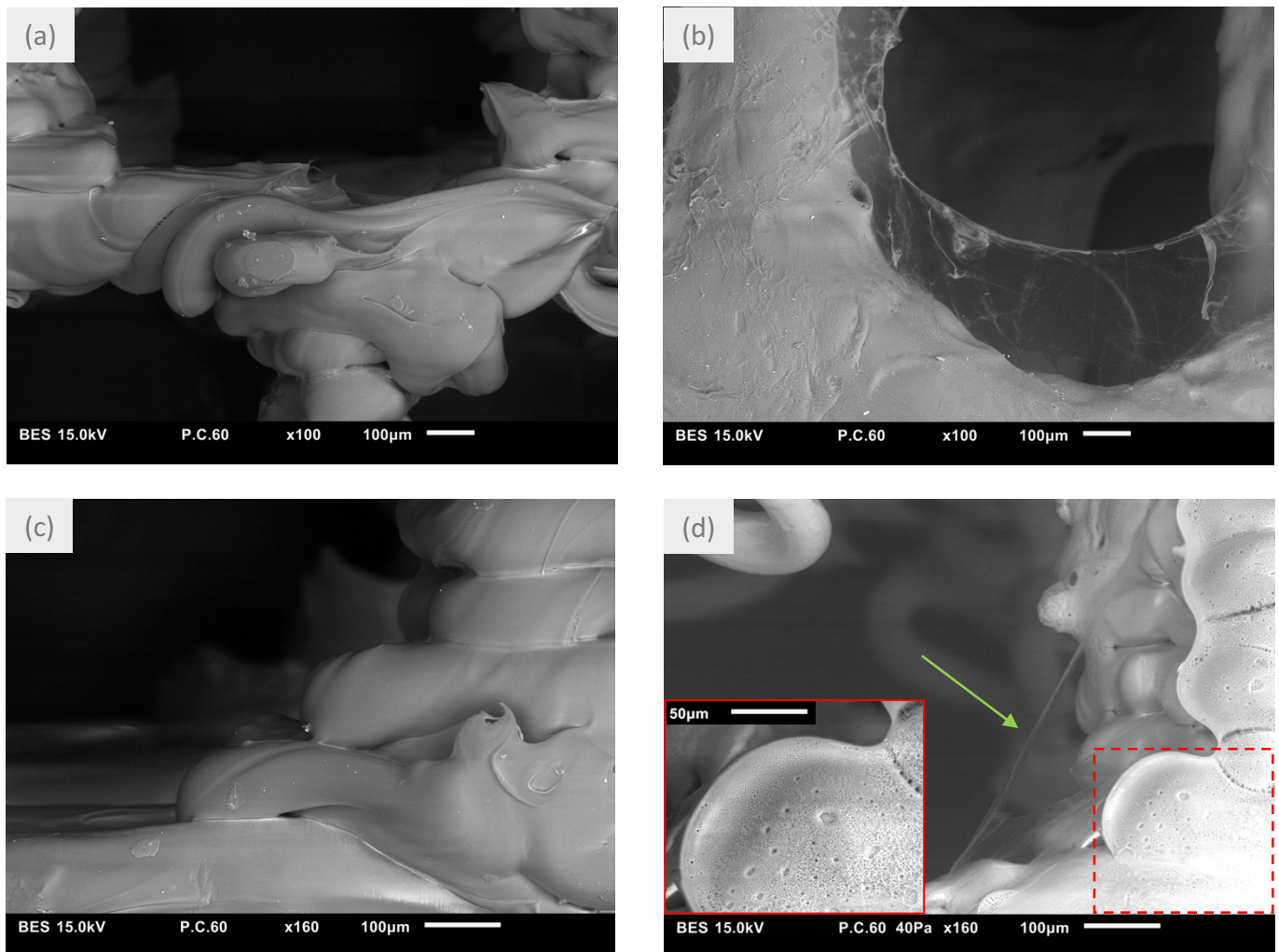
Figure 20 - SEM pictures depicting the surface roughness of a) NC PLA before-, (b) NC PLA after-, (c) PL18 before-, (d) PL18 after- post processing. For (d) the dotted area is zoomed in at 50 μm depicting the porous structure and the green arrow the spider web like structure.
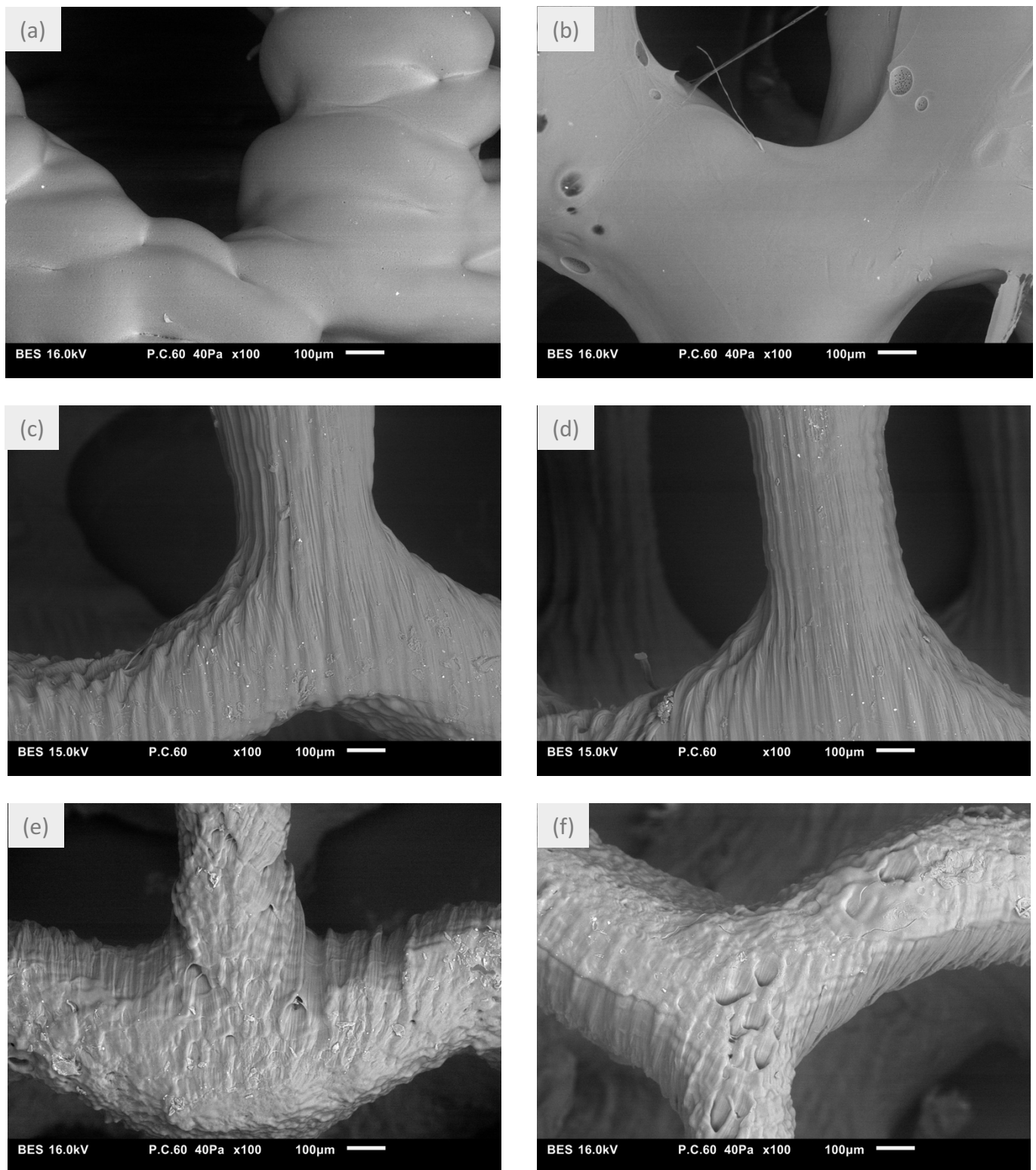
Figure 21 - SEM pictures depicting the surface roughness of (a) PC12 before-, (b) PC12 after-, (c) Methacrylate before-, (d) Methacrylate after-, (e) PLA resin before-, (f) PLA resin after- post processing.

3.2.2. Mechanical properties
3.2.2.1. Radial strength

Despite an ideal setup for radial strength investigation, radial compression in one direction of the stent was investigated. Figure 22 provides information on the first cycle of compression and relaxation of the evaluated tests. At a compression of 25%, the PC12 stent provided the highest radial strength at 4.3 N, in accordance with the minimum standard of 1 N [61], followed close by the methacrylate stent at 3.7 N.

However, further cycles resulted in an average loss of about 19% of the radial strength (Appendix E). Despite NC PLA and PL18 failing to reach the 1 N minimum with 0.95 N, the average loss of radial strength after 5 cycles was of 15%.

Figure 22 - Radial strength and recovery behavior up to a 25% compression of the initial diameter. Radial strength is correlated to a horizontal compression force. Minimum value (MV) used in values for current stents is represented with the dotted line. The compression test was recorded for a full cycle to investigate recovery of the stent after compression. Three stents per material were measured.

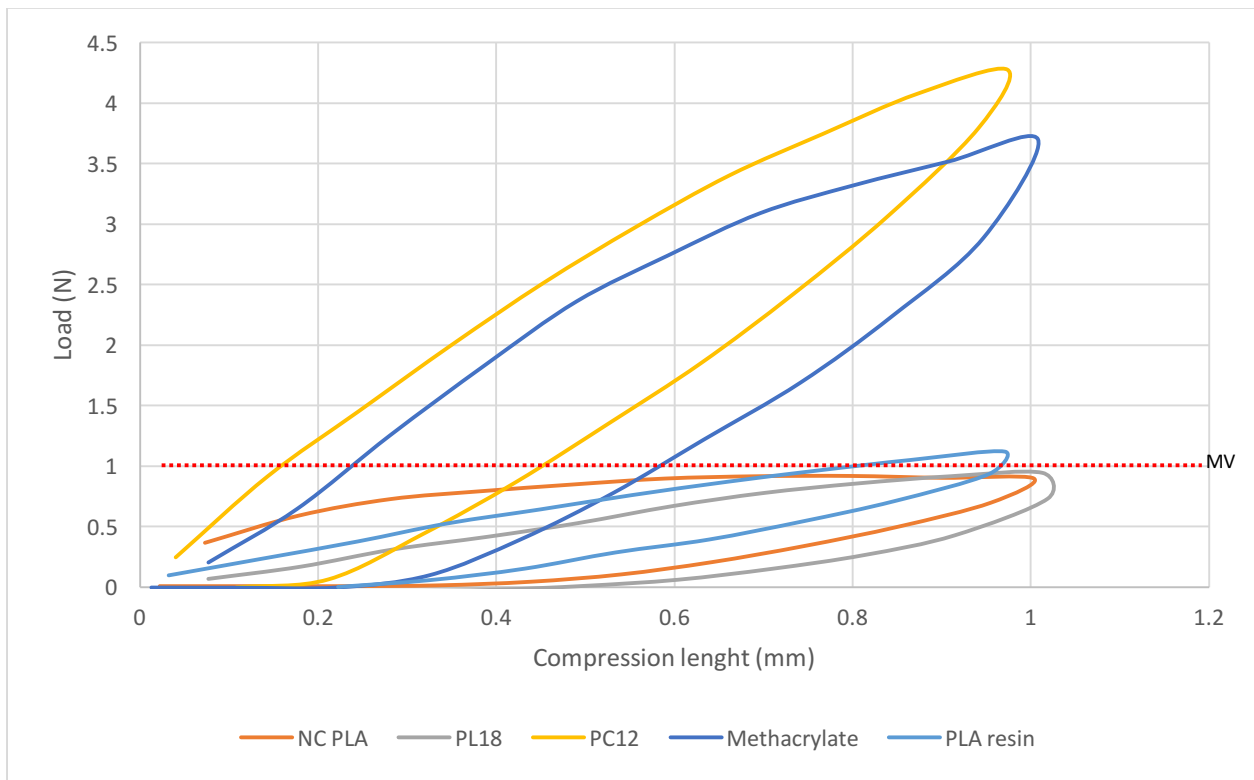### 3.2.2.2. Longitudinal deformation

Figure 23 represents the longitudinal deformation experienced by the stent representing the forces the stent experienced during deployment. Unless break happened, the force was calculated for up to 1 mm compression. Bench tests measures the ability to withstand compression at around 1 N ideal without damage of the stent structure. Results demonstrated that even though NC PLA offered the second highest resistive force just after 0.25 mm longitudinal compression, break of the stent resulted at about 0.6 mm. Results suggest methacrylate to have the highest longitudinal compression at 0.36 mm without experiencing break, while PC12 exceeded the 5 N of resistive force at just about 0.6 mm. Such high longitudinal resistive forces can result in added damage to the vessel's wall.

3.2.3. Biodegradability

Degradation patterns within a month for the materials analyzed are presented in Figure 24. Even though the methacrylate is a non-degradable polymer, measurements were taken to have a reference point in accuracy of the measurements. PL18 has the highest degradation pattern despite the high deviations. NC PLA on the other hand, even though an initial increase in weight was experienced, as a cause of swelling, it tends to follow the PL18 degradation trend. It is important to note that PL18 and NC PLA experienced breaks in the material along the degradation process, likely due to the low attachment between layers. Degradation of PC12 remains almost at zero levels similar to the methacrylate. Despite degradation being experienced regarding the PLA resin, the degradation seems to be hindered with time.
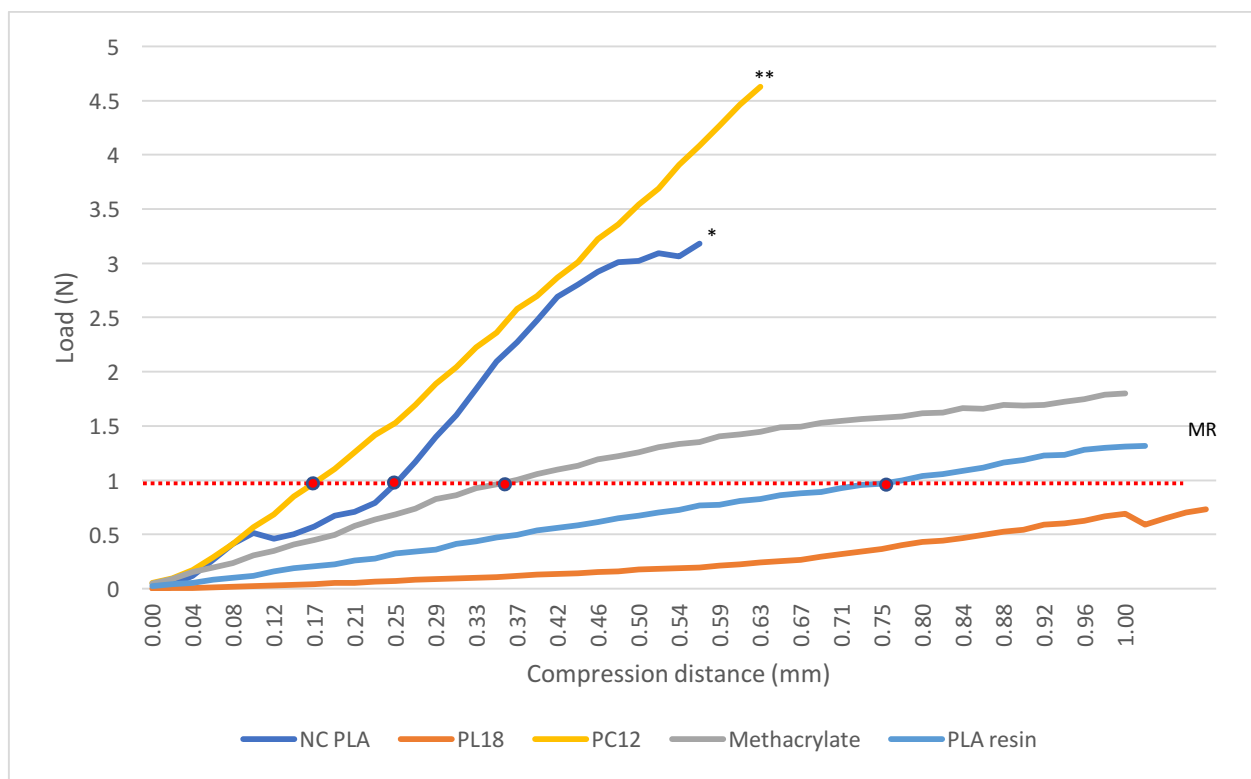
Figure 23 - Longitudinal deformation up to 1 mm of compression of the stent length or until break. Minimal reference(MR) value used in bench tests is represented by the dotted line. (*) Break of the stent. (**) Force exceeded 5N. Three stents per material were measured.

Figure 24 - In vitro changes in weight as a result of biodegradation of the material. NC PLA, PL18, PC12, methacrylate and PLA resin materials were evaluated. Three stents per material were degraded in PBS at 37℃. As a result of the high deviations, changes in weight >1 g were considered significant.

3.3. Stent chemical characterization
3.3.1. Molecular weight

Investigation of the polydispersity index (PDI) can provide information on the degradability experienced by a polymer as the index looks on how heterogeneous a polymer is with respect to its molecule size. The index is commonly calculated as:

$$PDI = \frac{Mw}{Mn}$$

The fact that degradation affects the mass of the molecules can be represented by an increase of PDI. This is because Mn is more sensible to low molecular mass molecules [62]. However, it should be noted that an equivalent decrease in both Mw and Mn, which is considered degradation, can still result in a same PDI ratio. Figure 25 shows the changes in PDI across the various materials and 3D printing techniques used. As previously mention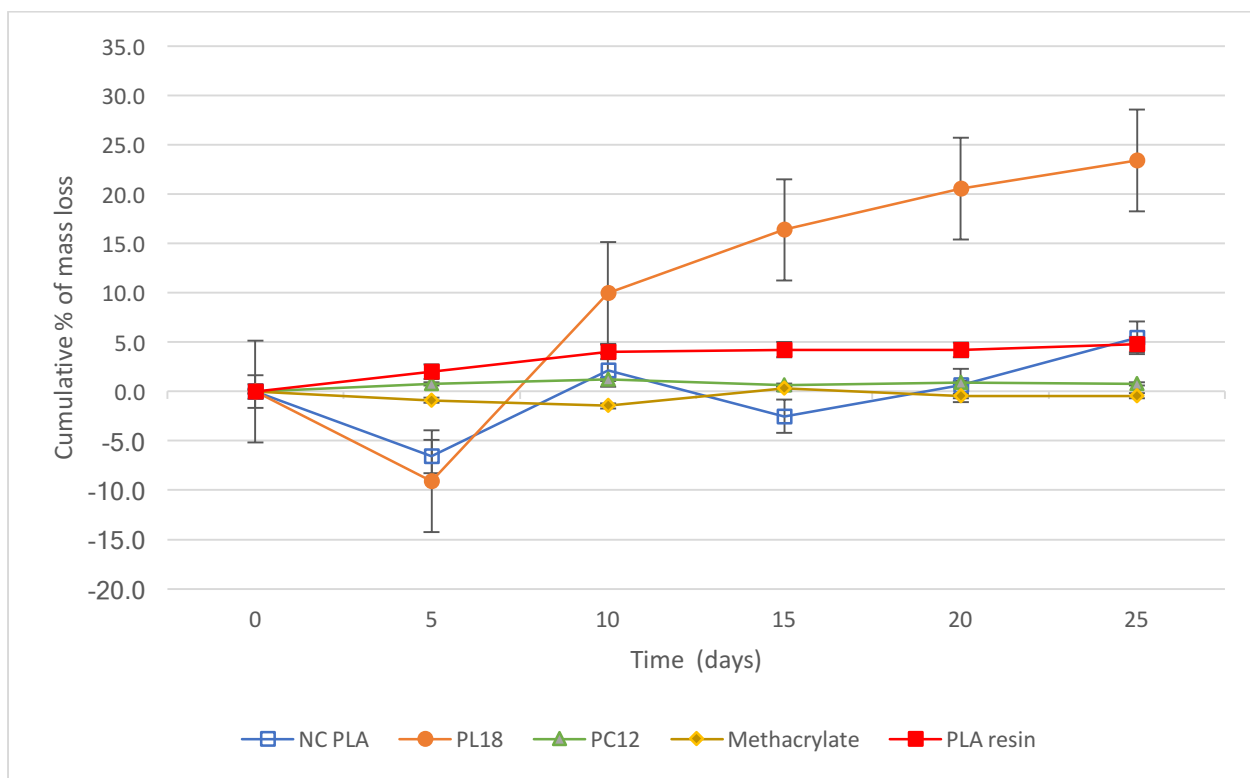ed methacrylate and PLA resin were not tested due to the lack in compatibility of solvents available. Considering standard deviations, the change in PDI is insignificant when going through a heat cycle from filament to printed form in the Ultimaker 2+ across PL18 and PC12. Nevertheless, with NC PLA, there is a decrease in PDI of about 10% after being printed which can be attributed to a higher degradation of its high molecular mass molecules represented by Mw. PDI did increase significantly at about 30% for both prints coming from the Freeformer, as compared to about a 1% increase in PDI from the complete pellet-filament-print cycle in the Ultimaker 2+. This significant change can be attributed to the longer times the material remained in the melted state, and therefore the rapid degradation of low molecular weight molecules. Regarding the complete PDI for PC12, a change of about 4% occurred showing degradation mainly in the heat cycle experienced from pellet-to-filament form. Specific molecular weight and deviation data is presented in Appendix F.
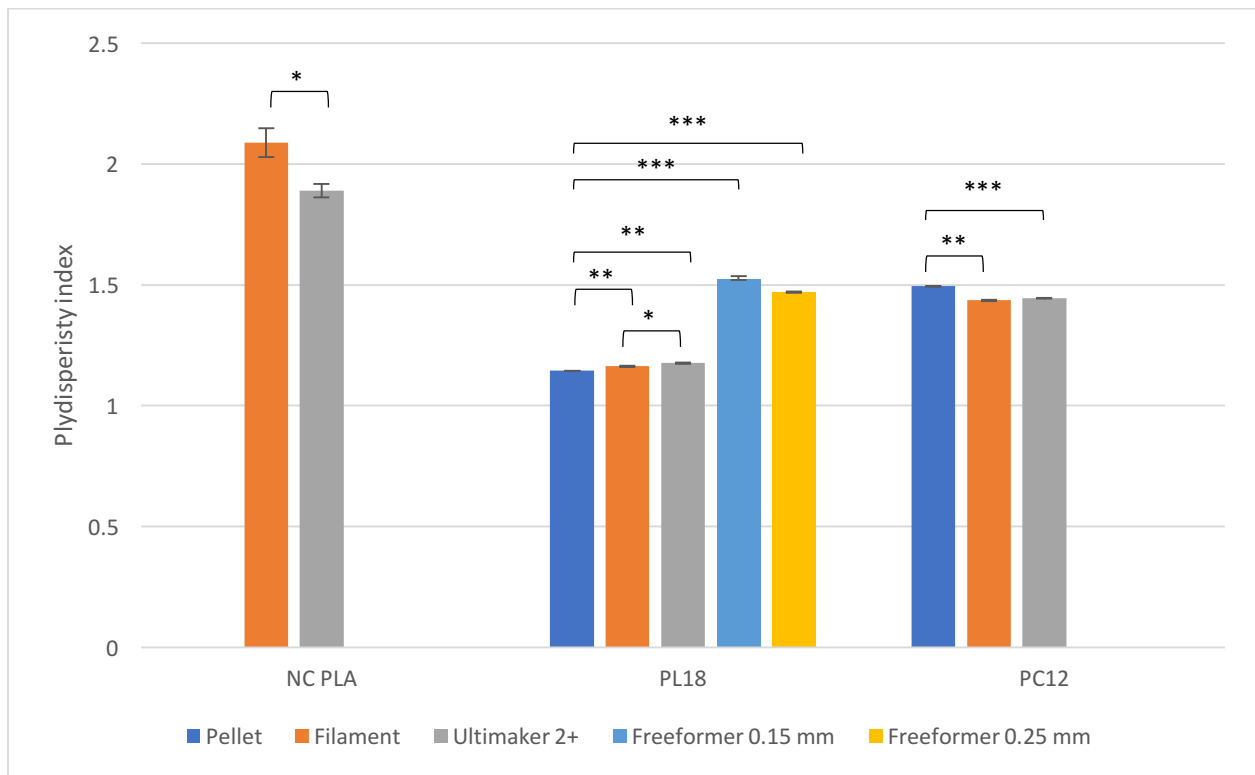

Figure 25 - Changes observed at the molecular level of NC-PLA, PL18 and PC12 at pellet, filament and printed stages of the material. The PDI correlates at >1 to a higher degradation experienced. Three printed stents were used per material. Error bars correspond to standard deviation. Statistical significance with P < 0.05 (*), P < 0.01 (**) and P < 0.001 (***) is presented.

3.3.2. Inherent viscosity

Changes in inherent viscosity also provide an indication of the degradation in polymers, with higher degradation being reflected with lower viscosities (Figure 26). As previously mentioned methacrylate and PLA resin were not tested due to the liquid state they are encountered in. Taking into account standard deviations, the change in IV experienced from filament to printed stent with the Ultimaker 2+ is insignificant <1%. However, with PL18 material, Freeformer prints experience a drop of IV at about 51±5% and 53±5%, for 0.25 mm and 0.15 mm nozzles. This drop in IV as a cause of degradation is more than double the complete drop in IV from pellet to print, situated at around 20% depending on the starting IV, on prints of Ultimaker 2+. Regarding PC12, a decrease in viscosity of around 5% from pellet-to-filament form is observed. As a result of the insignificant change from filament-to-printed form, can be assumed that the total change in IV, as a cause of degradation, stays at around 5%.
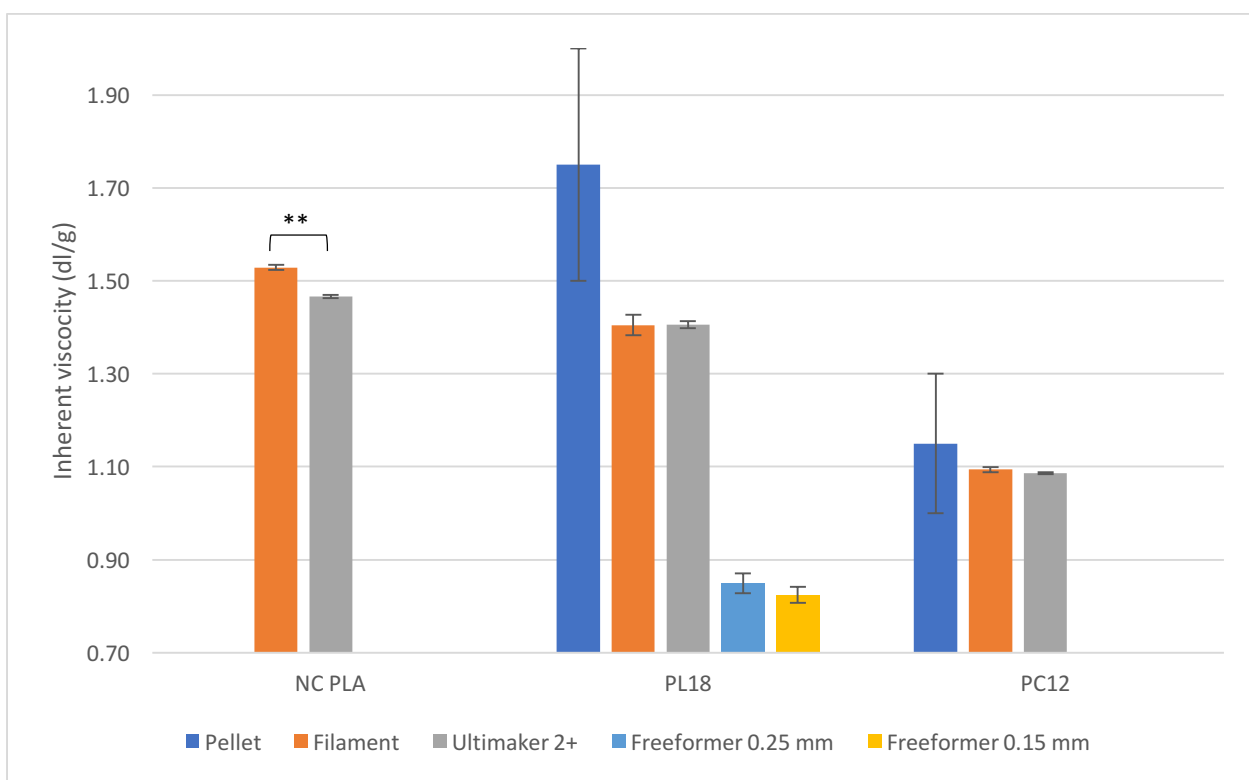

Figure 26 - Changes observed in the inherent viscosity of NC-PLA, PL18 and PC12 at pellet, filament and printed stages of the material. Difference in IV values after printing are observed among the various AM techniques. Three printed stents were used per material. Error bars correspond to standard deviation. Statistical significance with P < 0.05 (*), P < 0.01 (**) and P < 0.001 (***) is presented.

3.3.3. Melting temperature

Decrease in melting temperature, which can also reflect the degradation process was observed across all materials (Figure 27). However, comparing to the IV tests, the percentage changes were almost insignificant, <1% in the degradation experienced by printing with the Ultimaker 2+, from filament to printed stent. Cumulative degradation from pellet to printed form in PL18 with the Ultimaker 2+ corresponded to about 4% decrease in the melting temperature. In contrast, degradation from pellet to printed form caused by the Freeformer, resulted in a melting temperature drop of 6% with the 0.25 mm nozzle and of 8% with the 0.15 mm. Regarding PC12, it is interested to see an insignificant change in melting temperature across all heat cycles, with <1%. It should be highlighted that melting temperature is highly related to the molecular weight and structure [63], however changes in molecular weight might not directly translate in a change in molecular structure and therefore a change in melting temperature. As previously mentioned methacrylate and PLA resin

were not tested due to the crosslinked samples not being able to melt. Glass transition temperatures presented in Appendix G, experience a similar behavior as to melting temperature.
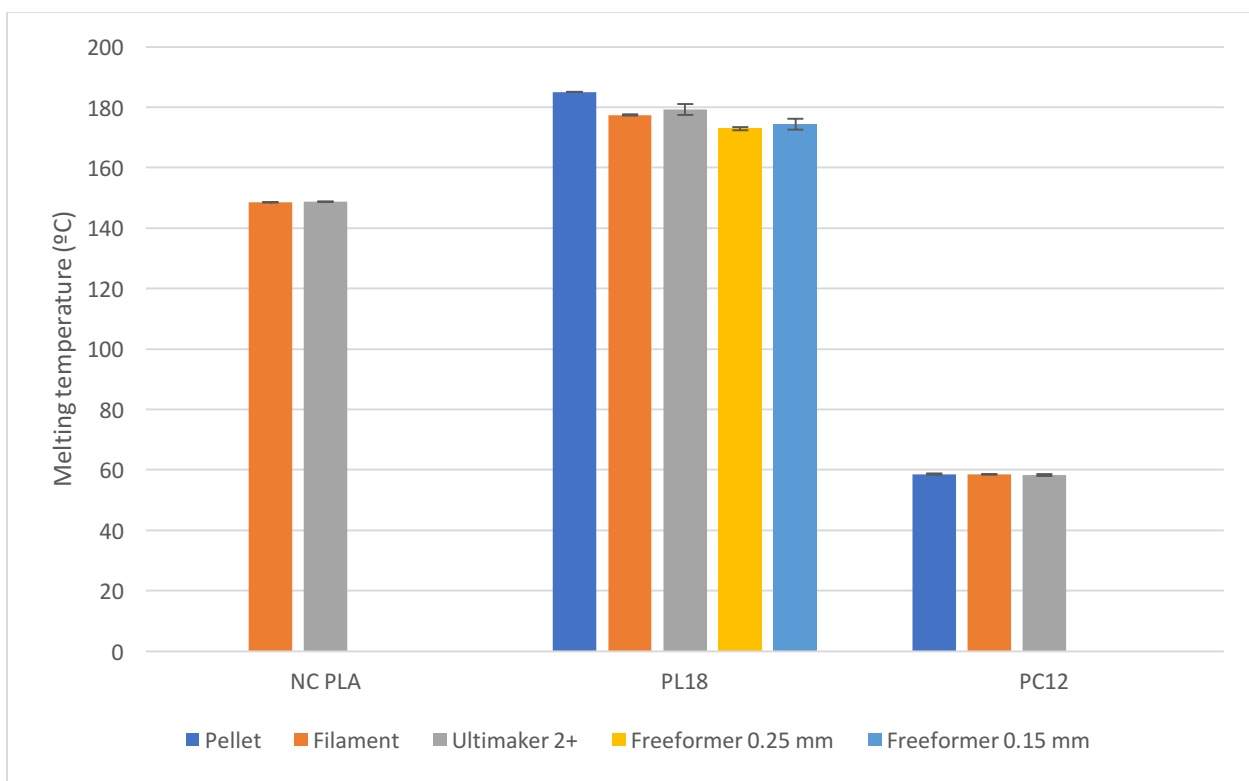
Figure 27 - Changes experienced on all the tested materials in the melting temperature after every heat cycle. Three printed stents were used per material. Error bars correspond to standard deviation.

3.3.4. FTIR analysis

The FTIR analysis proved no changes in the molecular structure and bonding in NC PLA, PL18 and PC12 as a result of the various methods of printing used. Correlation of the different wavenumber peaks observed in the FTIR, resulted in the exact materials being tested, as peaks remain constant across all heat cycles. A typical FTIR corresponding to the PLA resin and presenting peak shifts is presented in Figure 28. In the methacrylate and the PLA resin, changes in peak intensity at 1240 cm^{-1} and peak shifting from 1193 cm^{-1} to 1159 cm^{-1} were observed respectively. Changes in peak intensity are interpreted as creation of more specific bonds, being C-O acetates in the case of the methacrylate resin. Shifts in peak on the other hand are related to polymer structural changes. In the case of PLA resin, the change of peaks is only attributed from a stretch of the C-O bonding [64], commonly referred as a C-C-O asymmetric bonding. This stretching of the linkage however does not result in a change of the chemistry of the material [65]. NC PLA, PL18, PC12 and methacrylate FTIR graphs are presented Appendix H.

Figure 28 - FTIR analysis of PLA in resin form (green) and after printing with Form 1+ (blue), presenting a peak shift from 1193 cm^{-1} to 1159 cm^{-1} (red arrow) due to a C-O bonding stretch.
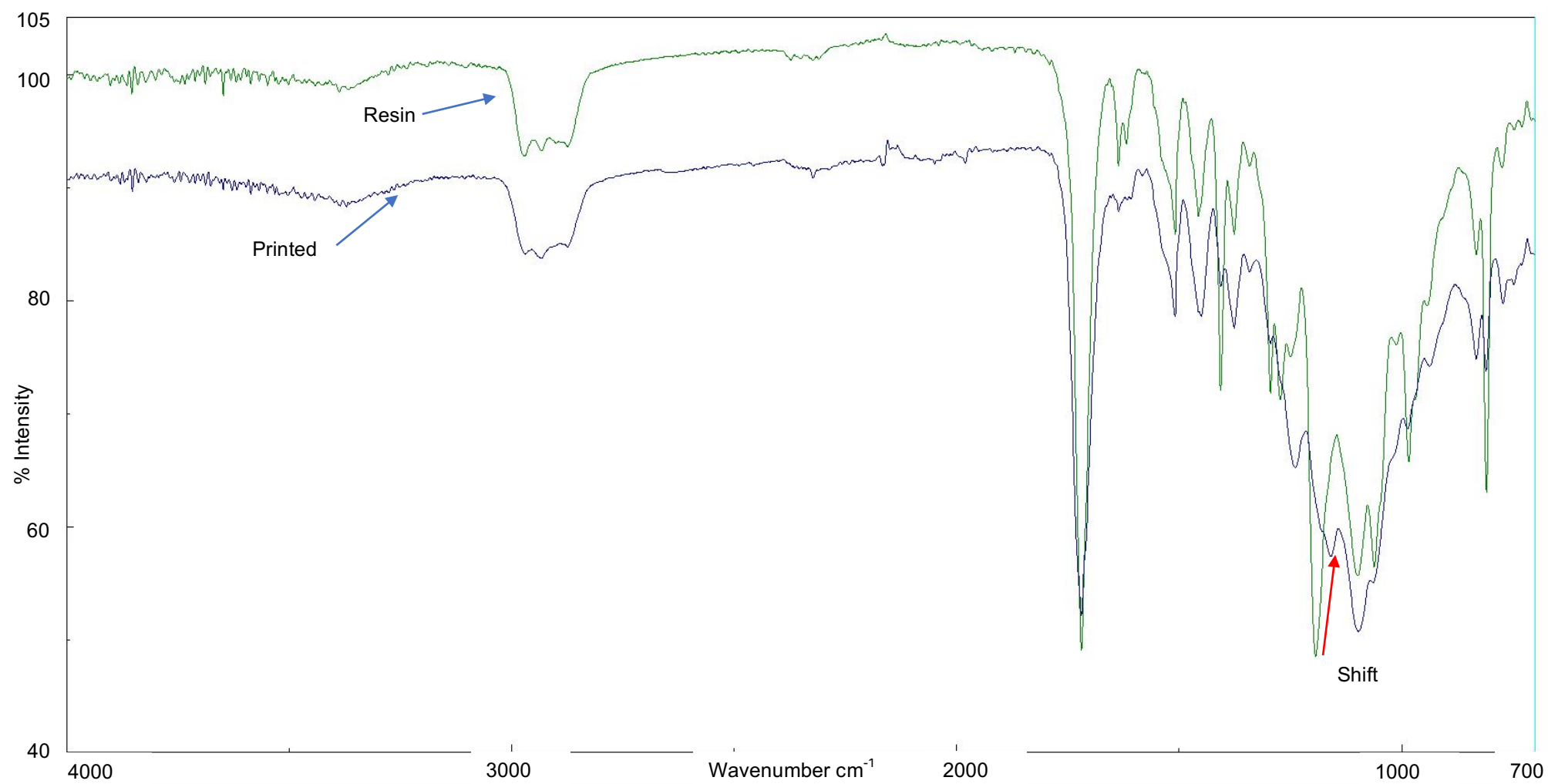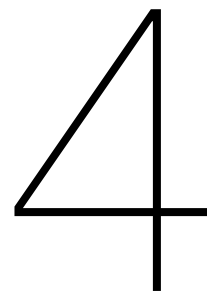
4

Discussion

Atherosclerosis is a complex cardiovascular disease which affects the vessel walls in complicated geometries and dimensions [66]. Despite advances in cardiovascular stents, BRS stents considered state of the art, are still not able to adhere to the patient specific lesion and needs. Taking into advantage the traction AM technologies have generated in the last couple years, this exploratory study aimed to provide the first results on available 3D technologies which are compatible with currently used BRS biomaterials, for the future printing of a patient specific BRS. Printer specific parameters, mechanical and morphological characteristics and chemical analysis regarding degradation and chemistry change of the printed BRS was presented.

The rather new stage of AM technologies still pose various challenges in product design and manufacturing which if tackled could provide improved properties to printing devices such as BRS. Accuracy in FDM and SLA printing is an important factor when printing small dimensions and geometries encountered in BRS. Even though it has been showed that printing at the microscale dimension such as with BRS is almost impossible [52, 67], this study was able to manufacture from a geometrical stand point, a BRS with 4 mm in diameter. However, the fact that printing with a 0.10 mm nozzle and the required dimensions are past the capabilities of the printer, resulted in a high inaccuracy observed within the BRS and with respect to others.

Within the Ultimaker 2+, challenges in the nozzle diameter and extrusion technology were presented (Chapter 3.1.1). Printing dimensions and surface morphology, are therefore limited by the nozzle diameter, which result in the need for nozzles smaller than 0.10 mm. However, due to the friction forces caused by the wear in the nozzle and material properties, these dimensions could result impractical [68-70]. Moreover, it was noticed, that at the micrometer dimensions, choice of a material with high purity was required. The minimum sign of contamination would clog the nozzle. Furthermore, FDM technology currently prints layer-by-layer in the z-direction (Figure 13.a). Such printing affects structures such as connecting links where thin structures have to be printed as single structures (Figure 13.a), also in crests which have to create sinusoidal overhangs without correct supports (Figure 13.a) [52, 71]. Moreover, printing was found to be unachievable when environment temperatures rose over 20 °C and/or high humidity environments were present. This is corroborated by Ho et al. [72] and Halidi et al. [73] showing changes in the morphology, mechanical and thermal stability changes as a cause of temperature and humidity. Correct extrusion of the material, adhesion between layers, and functionality of the printer electronics were all hindered at elevated temperatures. Temperature effects were also observed when the printer was placed in a hood for printing under nitrogen. The continuous flow of nitrogen created high temperature fluctuations in the nozzle, preventing correct extrusion. On the other hand, by turning off the nitrogen, the temperature inside the chamber turned on too high making the manageability of the material not possible. Finally, as a result of the printer settings not being compatible with 0.10 mm nozzle, the feeding of material remains at the constant rate of the bigger nozzle. This poses a challenge as the feeding gear wears off the material, making the feeding stop. The remaining filament has then to be extracted and cut off from the filament spool. This results in high wastes of material, as a stent of about 1cm of used filament results in the waste of about 40 cm of worn material. Adding to the waste of material, initial material flushes before ever print, and the printing of various iterations before a correct print is obtained, poses further disadvantages for this technology. Ultimately, the challenges presented above provided drawbacks in the technology's accuracy and precision, resulting in the increased strut sizes (Figure 15-16) and its high standard deviations (Figure 14).

Among the three 3D printers investigated, the Freeformer unfortunately posed the greatest challenges from the point of view of being able to print a full cardiovascular stent. However, due to the limited amount of time available to work with the printer, it is not possible to provide an accurate discussion on the usability and possible benefits of the technique. Within the Freeformer, similar to the Ultimaker 2+, nozzle diameters result in one of the biggest drawbacks when printing at the micrometer scale, added to the unstable layer printing and adhesion in the z-direction. As presented in Chapter 3.1.2, the small scale of the prints is further affected by the constant heat due to the proximity of the bed with the top extrusion plate. Hence, a correct and fast cooling needed to retain the printed geometries is hindered, resulting in a printed blub of material (Appendix C, Figure 30). Such challenge also affects the possibility of an adequate use of support material. The fact that the support material after printing, remains in the molten state and spreads across the whole print, results in inadequate layer adhesion caused by the layer of support material in between the normal sample layers (Appendix C, Figure 31). During printing (Appendix C, Figure 32) and later corroborated by the DSC, GPC and IV analysis (Figure 25-27), it was noticed that the extended time the material remained molted in the pre-extrusion chamber resulted in degradation of the material. This was initially noted by a change of color (Appendix C, Figure 32). The minimal amounts of material needed to print a single stent, translates in a challenge for the printer, as the material remains longer than usual in the molten state at the reservoir (Figure 5.b). Ideally with bigger dimensions, the material remains shorter times in the molten state providing lower total degradations from the single heat cycle. Finally, due to the uniqueness of the printer, work with its parameters is limited to the official software.

Challenges within the Form 1+ printer were mostly as a result of material availability and post processing. Even though recent studies [74-77] have been successful in demonstrating the development of biocompatible resins, such as with gelatin based crosslinkers [78], current offer of materials is still limited. Moreover, biodegradable materials such as the PLA resin obtained, still consists of a mixture of toxic photo-crosslinkers, making it non-biocompatible in cardiovascular stents and medical applications. Unlike the Ultimaker 2+, stents with a Form 1+ also require an added support (Figure 11.b) for correct adhesion to the bed and printing of spread structures such as with the rings of the stent. Removal of such structures proved to be a challenge, as interconnection with the struts was not ideal for release adding to the dimension of the stents. To prevent damage, remains of support material were commonly found in the attachment areas. Moreover, the sensitivity of the printer to contaminations added to the printing taking place inside the resin tank, prevents the user to know if the samples are being successfully printed through the process. This can ultimately translate in time costs by prints not attaching correctly, or material waste due to contamination affecting an area of the print.

Within the Ultimaker 2+ and the Form 1+ printer accuracy was evaluated with respect to values obtained for the strut width and thickness among the various prints. It is important to note that the stent STL designs expected for a stent of 4 mm, a strut thickness of around 115 μm and a width of 230 μm. This study proved successful in prints down to 4 mm in diameter for both Ultimaker 2+ and Form 1+ stents (Figure 18). However, all printed stents failed to cope with the strut thickness and width, specially Ultimaker 2+ stents (Figure 15-16). Moreover, the repeatability of stents dimensions presented (Figure 14), was not constant from print-to-print. Nevertheless, strut widths for the SLA prints resulted close in accordance to current market available dimensions of 250 μm [17, 79]. Unfortunately, market available strut thickness of about 200 μm [16] was not met for any of the stents. Accuracy from design to print across all stents regarding diameter, suggests the possibility of future studies to fine tune printing parameters and focus in the range of 2.5 mm to 3.5 mm which is the current market standard [80].

Post processing of the stents provided unexpected results regarding a decrease in strut thickness and width (Figure 17) with an overall increase in both inner (Appendix D, Figure 34) and outer diameter (Figure 19). This increase in dimensions is explained by Sharp et al. [81] and Milovanović et al. [82] as a cause of the swelling of the material. This phenomenon is related mainly to the crystalline and amorphous regions in the polymers where case II diffusion takes place [83]. Such diffusion is characterized by an initial hydrolytic cleavage of the chains in the amorphous region of the polymer, up to the border chains of the crystalline regions. This initial absorption of the solvent or solution results in the swelling of the material. Moreover, this swelling was also found to be the first step in the degradation process observed by PLA and PCL (Figure 24). PLA and PCL experience bulk erosion through hydrolytic degradation [84], by an initial penetration in the bulk material through the amorphous regions. It is then followed by a decrease in molecular weight without weight change and finally a decrease in weight by the formation of oligomers and monomers. The easiness of solvents to penetrate amorphous regions first over crystalline regions explains then the porosity observed as a cause of chloroform used during post processing.

Mechanical strengths (Figure 22) were comparable to the minimum standard of 1N for all stents except PL18 and NC PLA, and PLA barely exceeding the minimum with 1.15N. Furthermore, van Lith et al. [55] and Gore Medical [61] corroborate current mechanical compression values between 1-3N for market available stents. Currently, Absorb GT1 has a radial strength of about 3N at 24 months implantation [80]. Contrary to the results, it was found [85] that PLA materials should have experienced a higher mechanical strength as compared to the PCL. However, the reason why the radial strength and longitudinal compression of PC12 was higher than expected could be explained as a result of post processing. As observed in Chapter 3.2.1.3, the

intermediate step smoothens the surface but in the case of PC12, it makes the sample lose its geometry, by widening all structures evenly. This spread of material (Figure 21.b) allows for better attachment between layers as well as a higher surface area needed to be compressed, explaining the higher compression forces recorded.

Decrease in total weight as cause of *in vitro* degradation (Figure 24) is supported by various studies [86, 87] where PCL composites are characterized for higher degradation times over PLA. However, as mentioned in Chapter 1.3, depending on the L- or D- lactide, degradation times are affected as D- lactates are not able to be degraded by human enzymes. However, PL18, consists only of the L-lactide with a set low viscosity and lower molecular weights. As a result, degradation times are expected to be shorter [88], which agree with the results in this study. The fact that previous studies [89, 90] have shown that PCL composites can easily take over 2-3 years for degradation explains the almost zero degradation rate observed by the PC12 in this study. Therefore, more extensive studies are needed to provide adequate information on degradation of PCL cardiovascular stents. PLA resin, even though is considered a semi-crystalline polymer, the smaller chains which conform resins, form complicated and tighter networks when crosslinked [91-93], this in turn provides areas which are more complicated to reach for degradation to take place. This results in lower degradation rates, similar as obtained in this study.

Thermal degradation has been showed to result in changes of molecular weight, inherent viscosity, melting point and glass transition temperature [94, 95]. The results provided seem to agree with a related decrease in values as a cause of degradation. Nevertheless, it was noticed that the melting temperature (Figure 27) changes were at a lower rate when compared to changes in molecular weight (Figure 25) and inherent viscosity (Figure 26). As found by Brown et al. [63], the melting temperatures greatly depend on the structure and symmetry of the molecules in the material. This seems to explain that while there was a decrease in the molecular weight which affects the inherent viscosity, the symmetry was still able to be maintained and therefore hold a lower decrease rate in melting temperatures. Furthermore, data resulting in a decrease of glass transition (Appendix G, Figure 36) due to thermal degradation was presented in accordance with previous studies [96, 97]. However, an increase in glass transition was found from filament-to-printed form with PL18. Such results can be argued by Sousa et al. [98] and Wondraczek et al. [99] were sudden increases in glass transition temperature can be attributed to configurational changes, corresponding to the order of the molecules, during a decrease in monomer concentration.

Chemical composition and molecular structure was shown not to be affected by the different additive manufacturing techniques. For NC PLA, PL18 and PC 12, besides mechanical changes [100] and degradation, heating right above the glass transition temperature and around the melting point has not been proved to change the chemical compounds in the material. Regarding the methacrylate and PLA resin, studies [101, 102] have shown that crosslinking does not necessarily induce changes in the chemical compounds of the material. These studies agree with the results gathered during this study and presented in Chapter 3.3.4. Changes in peaks are therefore attributed to bond formation or stretching of the linkages in the molecules, and therefore methacrylate and the PLA remain similar after crosslinking has taken place.

The study as a whole, was able to demonstrate that the current state of FDM technology is still not ideal for the printing of BRS as a result of accuracy in dimension printing, the printer sample mechanical properties and the surface roughness at the macro scale. The Ultimaker 2+ demonstrated to cause the lowest degradation in the printed material when compared to the Freeformer, which ultimately is an important advantage in the future of BRS manufacturing. However, future experiments which can investigate the degradation as a cause of printing in the Form 1+ is needed. In contrast, it was evident that SLA technology

currently provides the highest accuracy in printing at small scales and the closest to a smooth macro surface. Nevertheless, further studies regarding biomaterial resin products compatibility are needed for the advancement of SLA in the field of BRS manufacturing.

5

Conclusions

The presented results were able to provide initial information on AM usability for the printing of BRS. However further research is still needed to tackle the individual challenges of every 3D printing technique. FDM technology was presented with the use of the Ultimaker 2+. Pushing the printer settings and limitations, it was proved the ability to print with clinical grade biomaterials a 4 mm BRS up to a geometry standpoint with the use of a 0.1 mm nozzle tip. Nevertheless, FDM technology was found not prove ideal for prints with such small dimensions and overhangs were supporting material is not an option. Also were single thin structures have to be printed in the z-direction. Moreover, the Freeformer printer was not capable in printing at the microscale, not only because of the limitation in nozzle diameter, but because of the high temperatures which prevent small scale objects from obtaining the correct geometry during cooling. Even though this extrusion based printer is not ready for BRS production, ideal parameters for the printing of PL18 material were presented. Such information can therefore prove useful for other large scale biomedical applications such as dental or orthopedic, where a clinical biodegradable material could be of benefit. Lastly, the expected high accuracy offered by SLA printers such as the Form 1+, proved effective in the printing of BRS from a geometrical stand point. A direction angle of 40° with respect to the printing bed resulted in the highest amount of prints.

Across all materials and techniques, the accuracy of printing played a big role on the structural morphology of the printed stents. High deviations, commonly above 20%, within the dimensions of the strut width and thickness were observed in a higher degree in stents printed with the Ultimaker 2+ over the Form 1+. Deviations did not only become relevant among the various stent printed, but also within the stent itself. This calls for the need of a higher precision printer and/or parameters which can provide a higher reproducibility in the micrometer scale. Furthermore the printing direction became relevant when printing connecting links as opposed to unsupported areas such as crests, highlighted by the lowest average width as well as the lowest deviation among stents. Differences in strut thickness were also noticeable with respect to the area of the stent, with higher dimensions in the proximal area. This as a result of the attachment of the first to the bed and a better printing at the beginning of the print. Unlike other stent dimensions, the deviations in diameter among the various materials and printers proved to be less than 5%. Post processing effects were observed with higher material losses in strut width than in the strut thickness. It was also interesting to observe an increase in the stent diameter after post processing. Regarding stent surface morphology, all AM techniques failed to provide a smooth surface without evident protrusions even after post processing. However, the Form 1+ provided the closest smooth surface over the Ultimaker 2+. Investigation with atomic force microscopy is still needed for quantification of the surface roughness and further comparison to literature. Finally, post processing was shown to create porosity in the micro surface of NC PLA and PL18 and affect the geometrical structure of PC12.

The study of the mechanical properties showed the printed stents to have close or higher radial strengths than existing standards. Specially methacrylate and PC12 provided high strengths which should be further investigated to conclude if these high values presented can affect other properties such as flexibility or pulsatile fatigue. Moreover recovery of the initial shape after compression should be further studies as high losses in radial strength were observed after the first cycle. On the other hand, regarding longitudinal compressions, Form 1+ prints were observed to outperform Ultimaker 2+ stents.

Among all materials, biodegradation followed the trend as observed in literature. Higher degradations in PL18 and NC PLA were observed, as compared to PC12 which being a PCL is usually characterized for degradation times of 2-3 years. As a result of time constraints, initial biodegradation data was provided for a month. However, further biodegradation analysis is still needed for evaluations past 6 months to 1 year.

FTIR analysis of the stents, provided assurance that the 3D printing techniques investigated do not cause chemical changes in the structure of the biomaterials. Furthermore it became evident that the heat cycles the materials are exposed to, do have a changing impact on the degradation of the material depending on the AM technique used. Investigation of the PDI, allowed us to see that degradation represented by the creation of low molecular weight molecules occurred mainly after the Freeformer printers processed the material from the pellet form. PDI changes in the Freeformer were about 6 times bigger than the ones occurring from the pellet-to-filament heat cycle. Interesting enough, insignificant changes in PDI were observed in the filament-to-print cycle by the Ultimaker 2+ for PL18 and PC12. The analysis of the IV and the melting temperature provided comparable data as the one obtained from the PDI, allowing it to be corroborated. It is therefore safe to mention, that printed stents coming from filament forms experience an almost non-existing degradation, with most of the degradation taking place when the filament was produced from its pellet form. Even though further research is needed, it was seen that printers such as the Freeformer which subject materials to a single heat cycle but are not meant for smaller dimensions such as the ones required, ultimately have a greater impact in the post-print degradation of the material.

6

Recommendations

The current project was able to provide the first results regarding printability of BRS with AM technologies, as well as physical and chemical characteristics as a result of printing. However it is expected that this exploratory work provides the tools needed for more in depth studies regarding specific application of biomaterials to single AM technologies in the printing of BRS. The author believes both extrusion-based and photopolymerization-based techniques still have to be further investigated. Within extrusion-based technologies, nozzle developments as well as better printing algorithms, could provide an open road for smaller prints. On the other hand, within photopolymerization-based technologies a special focus should be given to the creation of biomaterial resins with biocompatible products.

It should be highlighted, that due to project limitations, 3D printing for both the Ultimaker 2+ and the Form 1+ was performed under normal environment conditions. Nevertheless, it is known that the combination of high temperatures and the oxygen found in the environment accelerates degradation. Also changes in environment temperature and humidity affect the printing as highlighted in Chapter 3.1.1. Hence, future studies should provide new set of results under controlled conditions, where printing under nitrogen and monitoring of the temperature and humidity is a must. In addition, research on alternative post processing methods are also beneficial. Current solvents such as chloroform are too strong for stent dimensions, and a single second flush in pure chloroform, can cause a total damage and swelling [103] of the BRS. Finally, it is important to note that the results presented here can also prove useful outside the scope of BRS, such as in applications where printing of bioresorbable materials becomes relevant.

References

[1] O. World Health, Global status report on noncommunicable diseases 2014, World Health Organization2014.

[2] J. Iqbal, J. Gunn, P.W. Serruys, Coronary stents: historical development, current status and future directions, British Medical Bulletin 106(1) (2013) 193-211.

[3] L.a.B.I. National Heart, What is Atherosclerosis? <https://www.nhlbi.nih.gov/health/health-topics/topics/atherosclerosis>, 2016 (accessed 13/02/2017.2017).

[4] A.P. Burke, Lessons from sudden coronary death: a comprehensive morphological classification scheme for atherosclerotic lesions, Atherioscler Thromb Vasc Biol 20 (2000) 1262-1275.

[5] H.C. Stary, A.B. Chandler, R.E. Dinsmore, V. Fuster, S. Glagov, W. Insull, M.E. Rosenfeld, C.J. Schwartz, W.D. Wagner, R.W. Wissler, A Definition of Advanced Types of Atherosclerotic Lesions and a Histological Classification of Atherosclerosis, Circulation 92(5) (1995) 1355.

[6] W. Insull Jr, The Pathology of Atherosclerosis: Plaque Development and Plaque Responses to Medical Treatment, The American Journal of Medicine 122(1, Supplement) (2009) S3-S14.

[7] J.-M. Serfaty, L. Chaabane, A. Tabib, J.-M. Chevallier, A. Briguet, P.C. Douek, Atherosclerotic Plaques: Classification and Characterization with T2-weighted High-Spatial-Resolution MR Imaging—An in Vitro Study, Radiology 219(2) (2001) 403-410.

[8] S. Brugaletta, J. Gomez-Lara, R. Diletti, V. Farooq, R. Jan van Geuns, B. de Bruyne, D. Dudek, H.M. Garcia-Garcia, J.A. Ormiston, P.W. Serruys, Comparison of in vivo eccentricity and symmetry indices between metallic stents and bioresorbable vascular scaffolds: Insights from the ABSORB and SPIRIT trials, Catheterization and Cardiovascular Interventions 79(2) (2012) 219-228.

[9] D. Dalos, C. Gangl, C. Roth, L. Krenn, S. Scherzer, M. Vertesich, I. Lang, G. Maurer, T. Neunteufl, R. Berger, G. Delle-Karth, Mechanical properties of the everolimus-eluting bioresorbable vascular scaffold compared to the metallic everolimus-eluting stent, BMC Cardiovascular Disorders 16 (2016) 104.

[10] A. Mattesini, G.G. Secco, Dall, G. Ara, M. Ghione, J.C. Rama-Merchan, A. Lupi, N. Viceconte, A.C. Lindsay, R. De Silva, N. Foin, T. Naganuma, S. Valente, A. Colombo, C. Di Mario, ABSORB Biodegradable Stents Versus Second-Generation Metal Stents, JACC: Cardiovascular Interventions 7(7) (2014) 741.

[11] P.W. Serruys, B. Chevalier, D. Dudek, A. Cequier, D. Carrié, A. Iniguez, M. Dominici, R.J. van der Schaaf, M. Haude, L. Wasungu, S. Veldhof, L. Peng, P. Staehr, M.J. Grundeken, Y. Ishibashi, H.M. Garcia-Garcia, Y. Onuma, A bioresorbable everolimus-eluting scaffold versus a metallic everolimus-eluting stent for ischaemic heart disease caused by de-novo native coronary artery lesions (ABSORB II): an interim 1-year analysis of clinical and procedural secondary outcomes from a randomised controlled trial, The Lancet 385(9962) (2015) 43-54.

[12] C. Costopoulos, A. Latib, T. Naganuma, T. Miyazaki, K. Sato, F. Figini, A. Sticchi, M. Carlino, A. Chieffo, M. Montorfano, A. Colombo, Comparison of early clinical outcomes between ABSORB bioresorbable vascular scaffold and everolimus-eluting stent implantation in a real-world population, Catheterization and Cardiovascular Interventions 85(1) (2015) E10-E15.

[13] B.D. Gogas, J.J. Benham, S. Hsu, A. Sheehy, D.J. Lefer, T.T. Goodchild, D.J. Polhemus, Y.H. Bouchi, O.Y. Hung, S.-Y. Yoo, U. Joshi, D.P. Giddens, A. Veneziani, A. Quyyumi, R. Rapoza, S.B. King, H. Samady, Vasomotor Function Comparative Assessment at 1 and 2 Years Following Implantation of the Absorb Everolimus-Eluting Bioresorbable Vascular Scaffold and the Xience V Everolimus-Eluting Metallic Stent in Porcine Coronary Arteries, JACC: Cardiovascular Interventions 9(7) (2016) 728.

[14] B. Chevalier, M. Grundeken, R. White, Y. Ishibashi, H.G. Garcia, Y. Onuma, P. Serruys, Difference in the occurence of new or worsening angina between the absorb bioresorbable vascular scaffold and xience metallic stent: a post-hoc analysis of the Absorb II randomized trial, Journal of the American College of Cardiology 65(10, Supplement) (2015) A1707.

[15] M. Sabaté, S. Windecker, A. Iñiguez, L. Okkels-Jensen, A. Cequier, S. Brugaletta, S.H. Hofma, L. Räber, E.H. Christiansen, M. Suttorp, T. Pilgrim, G. Anne van Es, Y. Sotomi, H.M. García-García, Y. Onuma, P.W. Serruys, Everolimus-eluting bioresorbable stent vs. durable polymer everolimus-eluting metallic stent in patients with ST-segment elevation myocardial infarction: results of the randomized ABSORB ST-segment elevation myocardial infarction—TROFI II trial, European Heart Journal 37(3) (2015) 229-240.

[16] E.L. Boland, R. Shine, N. Kelly, C.A. Sweeney, P.E. McHugh, A Review of Material Degradation Modelling for the Analysis and Design of Bioabsorbable Stents, Annals of Biomedical Engineering 44(2) (2016) 341-356.

[17] P.K. Bowen, E.R. Shearier, S. Zhao, R.J. Guillory, F. Zhao, J. Goldman, J.W. Drelich, Biodegradable Metals for Cardiovascular Stents: from Clinical Concerns to Recent Zn-Alloys, Advanced Healthcare Materials 5(10) (2016) 1121-1140.

[18] M. Santoro, S.R. Shah, J.L. Walker, A.G. Mikos, Poly (lactic acid) nanofibrous scaffolds for tissue engineering, Advanced drug delivery reviews 107 (2016) 206-212.

[19] S. Farah, D.G. Anderson, R. Langer, Physical and mechanical properties of PLA, and their functions in widespread applications—a comprehensive review, Advanced drug delivery reviews 107 (2016) 367-392.

[20] L.T. Sin, A.R. Rahmat, W.A.W.A. Rahman, 7 - Degradation and Stability of Poly(lactic Acid), Polylactic Acid, William Andrew Publishing, Oxford, 2013, pp. 247-299.

[21] S.A. Ashter, 5 - Types of Biodegradable Polymers, Introduction to Bioplastics Engineering, William Andrew Publishing, Oxford, 2016, pp. 81-151.

[22] L.T. Sin, A.R. Rahmat, W.A.W.A. Rahman, 5 - Mechanical Properties of Poly(lactic Acid), Polylactic Acid, William Andrew Publishing, Oxford, 2013, pp. 177-219.

[23] X. Zheng, J. Yan, V. Bhat, Biodegradable endoprostheses and methods for their fabrication, Google Patents, 2016.

[24] M. Cuiffo, J. Snyder, A. Elliott, N. Romero, S. Kannan, G. Halada, Impact of the Fused Deposition (FDM) Printing Process on Polylactic Acid (PLA) Chemistry and Structure, (2017).

[25] J. Krotký, J. Honzíková, P. Moc, Deformation of Print PLA Material Depending on the Temperature of Reheating Printing Pad, Ústí nad Labem (2016).

[26] X. Rong, M. Keif, A study of PLA printability with flexography.

[27] F.P.W. Melchels, J. Feijen, D.W. Grijpma, A poly(d,l-lactide) resin for the preparation of tissue engineering scaffolds by stereolithography, Biomaterials 30(23–24) (2009) 3801-3809.

[28] R.L. Flores, H. Liss, S. Raffaelli, A. Humayun, K.S. Khouri, P.G. Coelho, L. Witek, The technique for 3D printing patient-specific models for auricular reconstruction, Journal of Cranio-Maxillofacial Surgery.

[29] S.J. Hollister, Porous scaffold design for tissue engineering, Nat Mater 4(7) (2005) 518-524.

[30] C.X.F. Lam, X.M. Mo, S.H. Teoh, D.W. Hutmacher, Scaffold development using 3D printing with a starch-based polymer, Materials Science and Engineering: C 20(1–2) (2002) 49-56.

[31] T. Serra, J.A. Planell, M. Navarro, High-resolution PLA-based composite scaffolds via 3-D printing technology, Acta Biomaterialia 9(3) (2013) 5521-5530.

[32] C.-T. Kao, C.-C. Lin, Y.-W. Chen, C.-H. Yeh, H.-Y. Fang, M.-Y. Shie, Poly (dopamine) coating of 3D printed poly (lactic acid) scaffolds for bone tissue engineering, Materials Science and Engineering: C 56 (2015) 165-173.

[33] K.H. Tan, C.K. Chua, K.F. Leong, C.M. Cheah, W.S. Gui, W.S. Tan, F.E. Wiria, Selective laser sintering of biocompatible polymers for applications in tissue engineering, Bio-medical materials and engineering 15(1, 2) (2005) 113-124.

[34] E.N. Antonov, V.N. Bagratashvili, M.J. Whitaker, J.J.A. Barry, K.M. Shakesheff, A.N. Konovalov, V.K. Popov, S.M. Howdle, Three-Dimensional Bioactive and Biodegradable Scaffolds Fabricated by Surface-Selective Laser Sintering, Advanced Materials 17(3) (2005) 327-330.

[35] G. Ceccarelli, R. Presta, L. Benedetti, M.G. Cusella De Angelis, S.M. Lupi, R. Rodriguez y Baena, Emerging Perspectives in Scaffold for Tissue Engineering in Oral Surgery, Stem cells international 2017 (2017).

[36] O.T. David, C. Szuhanek, R.A. Tuce, A.P. David, M. Leretter, Polylactic Acid 3D Printed Drill Guide for Dental Implants Using CBCT, Revista de chimie 68(2) (2017) 341-342.

[37] T.R. Tiersch, W.T. Monroe, Three-dimensional printing with polylactic acid (PLA) thermoplastic offers new opportunities for cryobiology, Cryobiology 73(3) (2016) 396-398.

[38] J.-H. Shim, T.-S. Moon, M.-J. Yun, Y.-C. Jeon, C.-M. Jeong, D.-W. Cho, J.-B. Huh, Stimulation of healing within a rabbit calvarial defect by a PCL/PLGA scaffold blended with TCP using solid freeform fabrication technology, Journal of Materials Science: Materials in Medicine 23(12) (2012) 2993-3002.

[39] J. Korpela, A. Kokkari, H. Korhonen, M. Malin, T. Närhi, J. Seppälä, Biodegradable and bioactive porous scaffold structures prepared using fused deposition modeling, Journal of Biomedical Materials Research Part B: Applied Biomaterials 101(4) (2013) 610-619.

[40] E.Y. Teo, S.-Y. Ong, M.S.K. Chong, Z. Zhang, J. Lu, S. Moochhala, B. Ho, S.-H. Teoh, Polycaprolactone-based fused deposition modeled mesh for delivery of antibacterial agents to infected wounds, Biomaterials 32(1) (2011) 279-287.

[41] S.-W. Kang, J.-H. Bae, S.-A. Park, W.-D. Kim, M.-S. Park, Y.-J. Ko, H.-S. Jang, J.-H. Park, Combination therapy with BMP-2 and BMSCs enhances bone healing efficacy of PCL scaffold fabricated using the 3D plotting system in a large segmental defect model, Biotechnology letters 34(7) (2012) 1375-1384.

[42] S.A. Park, S.H. Lee, W.D. Kim, Fabrication of porous polycaprolactone/hydroxyapatite (PCL/HA) blend scaffolds using a 3D plotting system for bone tissue engineering, Bioprocess and Biosystems Engineering 34(4) (2011) 505-513.

[43] S. Park, G. Kim, Y.C. Jeon, Y. Koh, W. Kim, 3D polycaprolactone scaffolds with controlled pore structure using a rapid prototyping system, Journal of Materials Science: Materials in Medicine 20(1) (2009) 229-234.

[44] L. Jung-Seob, H. Jung Min, J. Jin Woo, S. Jin-Hyung, O. Jeong-Hoon, C. Dong-Woo, 3D printing of composite tissue with complex shape applied to ear regeneration, Biofabrication 6(2) (2014) 024103.

[45] S.H. Park, B.G. Yun, J.Y. Won, W.S. Yun, J.H. Shim, M.H. Lim, D.H. Kim, S.A. Baek, Y.D. Alahmari, J.H. Jeun, S.H. Hwang, S.W. Kim, New application of three-dimensional printing biomaterial in nasal reconstruction, The Laryngoscope 127(5) (2017) 1036-1043.

[46] Z.M. Hassan, A. Goyanes, V. Clark, A.W. Basit, S.T. Hilton, S. Gaisford, Patient-Specific 3D Scanned and 3D Printed Antimicrobial Polycaprolactone Wound Dressings, International Journal of Pharmaceutics (2017).

[47] W. Kempin, C. Franz, L.-C. Koster, F. Schneider, M. Bogdahn, W. Weitschies, A. Seidlitz, Assessment of different polymers and drug loads for fused deposition modeling of drug loaded implants, European Journal of Pharmaceutics and Biopharmaceutics 115 (2017) 84-93.

[48] L. Elomaa, S. Teixeira, R. Hakala, H. Korhonen, D.W. Grijpma, J.V. Seppälä, Preparation of poly(ε-caprolactone)-based tissue engineering scaffolds by stereolithography, Acta Biomaterialia 7(11) (2011) 3850-3856.

[49] H.F. Shieh, R.W. Jennings, Three-dimensional printing of external airway splints for tracheomalacia, Journal of Thoracic Disease 9(3) (2017) 414-416.

[50] J.M. Williams, A. Adewunmi, R.M. Schek, C.L. Flanagan, P.H. Krebsbach, S.E. Feinberg, S.J. Hollister, S. Das, Bone tissue engineering using polycaprolactone scaffolds fabricated via selective laser sintering, Biomaterials 26(23) (2005) 4817-4827.

[51] E. Saito, B. Partee, S. Das, S.J. Hollister, Engineered wavy fibered polycaprolactone soft tissue scaffolds: design, fabrication and mechanical testing, 2005, p. 1794.

[52] I. Gibson, D. Rosen, B. Stucker, Additive manufacturing technologies: 3D printing, rapid prototyping, and direct digital manufacturing, Springer2014.

[53] S.A. Park, S.J. Lee, K.S. Lim, I.H. Bae, J.H. Lee, W.D. Kim, M.H. Jeong, J.-K. Park, In vivo evaluation and characterization of a bio-absorbable drug-coated stent fabricated using a 3D-printing system, Materials Letters 141 (2015) 355-358.

[54] S.K. Misra, F. Ostadhossein, R. Babu, J. Kus, D. Tankasala, A. Sutrisno, K.A. Walsh, C.R. Bromfield, D. Pan, 3D-Printed Multidrug-Eluting Stent from Graphene-Nanoplatelet-Doped Biodegradable Polymer Composite, Advanced Healthcare Materials (2017) 1700008-n/a.

[55] R. van Lith, E. Baker, H. Ware, J. Yang, A.C. Farsheed, C. Sun, G. Ameer, 3D-Printing Strong High-Resolution Antioxidant Bioresorbable Vascular Stents, Advanced Materials Technologies 1(9) (2016) 1600138-n/a.

[56] K.D. Triantafyllou, S. Frangoulis, T.M. Kolettis, Coronary endarterectomy and stent removal with off-pump coronary artery bypass surgery, Heart 92(7) (2006) 885-885.

[57] FormLabs, Clear. Photoreactive resin for Form 1, Form 1+, Form 2, Safety Data Sheet - GHS Formal, USA, 2016.

[58] P.S. Poh, M.P. Chhaya, F.M. Wunner, E.M. De-Juan-Pardo, A.F. Schilling, J.T. Schantz, M. van Griensven, D.W. Hutmacher, Polylactides in additive biomanufacturing, Adv Drug Deliv Rev 107 (2016) 228-246.

[59] Arburg, ARBURG Plastic Freeforming, ARBURG (2017).

[60] FormLabs, 3D Printing Technology Comparison: SLA vs. DLP, FormLabs, 2016.

[61] G. Medical, Mechanical Properties of Nitinol Stents and Stent-Grafts, in: I. W.L. Gore & Associates (Ed.) 2011.

[62] H. Yu, N. Huang, C. Wang, Z. Tang, Modeling of poly (L-lactide) thermal degradation: Theoretical prediction of molecular weight and polydispersity index, Journal of applied polymer science 88(11) (2003) 2557-2562.

[63] R.J.C. Brown, R.F.C. Brown, Melting point and molecular symmetry, J. Chem. Educ 77(6) (2000) 724.

[64] N.D.N. Affandi, M.R. Ahmad, A. Baharudin, N.A.A. Shukry, Effect of crosslinking on the solubility and morphological structures of the PVA nanofibres, IEEE, 2014

, pp. 458-462.

[65] B.C. Smith, Infrared spectral interpretation: a systematic approach, CRC press1998.

[66] M. Simionescu, A.V. Sima, Morphology of Atherosclerotic Lesions, in: G. Wick, C. Grundtman (Eds.), Inflammation and Atherosclerosis, Springer Vienna, Vienna, 2012, pp. 19-37.

[67] Stratasys, Fused Deposition Modeling: Desing Guideline, in: Stratasys (Ed.) 2017.

[68] A.K. Sood, A. Equbal, V. Toppo, R.K. Ohdar, S.S. Mahapatra, An investigation on sliding wear of FDM built parts, CIRP Journal of Manufacturing Science and Technology 5(1) (2012) 48-54.

[69] A.H. Peng, Z.M. Wang, Researches into influence of process parameters on FDM parts precision, Trans Tech Publ, 2010, pp. 338-343.

[70] A. Tsouknidas, Friction induced wear of rapid prototyping generated materials: a review, Advances in Tribology 2011 (2011).

[71] A.T. Gaynor, J.K. Guest, Topology optimization for additive manufacturing: considering maximum overhang constraint, pp. 16-20.

[72] K.-L.G. Ho, A.L. Pometto, P.N. Hinz, Effects of temperature and relative humidity on polylactic acid plastic degradation, Journal of Polymers and the Environment 7(2) (1999) 83-92.

[73] M. Halidi, S.N. Amalina, J. Abdullah, Moisture and humidity effects on the abs used in fused deposition modeling machine, Trans Tech Publ, 2012

, pp. 641-644.

[74] A.A. Gill, F. Claeyssens, 3D structuring of biocompatible and biodegradable polymers via stereolithography, 3D Cell Culture: Methods and Protocols (2011) 309-321.

[75] J.-Y. Jeng, A.N. Konovalov, V.K. Popov, Y.-L. Cheng, R. Shafikova, Projection stereolithography of biocompatible polymer structures, Inorganic Materials: Applied Research 7(5) (2016) 745-749.

[76] F. ILT, Biocompatible photoresin for stereolithography, in: F.I.f.L. Technology (Ed.) Annual Report, 2014, p. 136.

[77] S. Tanodekaew, S. Channasanon, P. Uppanan, Preparation and degradation study of photocurable oligolactide-HA composite: A potential resin for stereolithography application, Journal of Biomedical Materials Research Part B: Applied Biomaterials 102(3) (2014) 604-611.

[78] J. Stampfl, M. Schuster, S. Baudis, H. Lichtenegger, R. Liska, C. Turecek, F. Varga, Biodegradable stereolithography resins with defined mechanical properties, Virtual and Rapid Manufacturing, Proceedings of VRAP, Leira, Portugal (2007) 283-288.

[79] J.F. LaDisa, L.E. Olson, I. Guler, D.A. Hettrick, S.H. Audi, J.R. Kersten, D.C. Warltier, P.S. Pagel, Stent design properties and deployment ratio influence indexes of wall shear stress: a three-dimensional computational fluid dynamics investigation within a normal artery, Journal of Applied Physiology 97(1) (2004) 424-430.

[80] Abbott, Absorb GT1 Bioresorbable Vascular Scaffold system in: A.C. Meeting (Ed.) 2016.

[81] J.S. Sharp, J.A. Forrest, R.A.L. Jones, Swelling of poly (DL-lactide) and polylactide-co-glycolide in humid environments, Macromolecules 34(25) (2001) 8752-8760.

[82] S.L. Milovanović, R.M. Kuska, M.L. Škorić-Lučić, M.T. Kalagasidis-Krušić, S. Frerich, I.T. Žižović, J.Z. Ivanović, Swelling kinetics and impregnation of PLA with thymol under supercritical CO2 conditions, Tehnika 71(1) (2016) 16-20.

[83] N.L. Thomas, A.H. Windle, A theory of case II diffusion, Polymer 23(4) (1982) 529-542.

[84] H. Tsuji, Hydrolytic Degradation, Poly(Lactic Acid), John Wiley & Sons, Inc.2010, pp. 343-381.

[85] K.A.a.B.N. Bhati P, Radial strength comparison of the PLA/PCL blends tubes manufactured by different fabrication processes. , in: F.B. Biotechnol (Ed.) Conference Abstract: 10th World Biomaterials Congress, 2016.

[86] G.L. Siparsky, Degradation kinetics of poly (hydroxy) acids: PLA and PCL, ACS Publications2000.

[87] K.M. Nampoothiri, N.R. Nair, R.P. John, An overview of the recent developments in polylactide (PLA) research, Bioresource technology 101(22) (2010) 8493-8501.

[88] Z. Wang, Y. Wang, Y. Ito, P. Zhang, X. Chen, A comparative study on the in vivo degradation of poly (L-lactide) based composite implants for bone fracture fixation, Scientific reports 6 (2016).

[89] H. Sun, L. Mei, C. Song, X. Cui, P. Wang, The in vivo degradation, absorption and excretion of PCL-based implant, Biomaterials 27(9) (2006) 1735-1740.

[90] L.M. Orozco-Castellanos, A. Marcos-Fernández, A. Martínez-Richa, Hydrolytic degradation of poly (ε-caprolactone) with different end groups and poly (ε-caprolactone-co-γ-butyrolactone): characterization and kinetics of hydrocortisone delivery, Polymers for Advanced Technologies 22(4) (2011) 430-436.

[91] A.B. Strong, Fundamentals of composites manufacturing: materials, methods and applications, Society of Manufacturing Engineers2008.

[92] M. Demjanenko, K. Dusek, Statistics of Degradation and Cross-Linking of Polymer Chains with the Use of the Theory of Branching Processes, Macromolecules 13(3) (1980) 571-579.

[93] H. Shih, C.-C. Lin, Crosslinking and degradation of step-growth hydrogels formed by thiol-ene photo-click chemistry, Biomacromolecules 13(7) (2012) 2003-2012.

[94] C.L. Beyler, M.M. Hirschler, Thermal decomposition of polymers, SFPE handbook of fire protection engineering 2 (2002) 111-131.

[95] H. Nishida, Thermal Degradation, Poly(Lactic Acid), John Wiley & Sons, Inc.2010, pp. 401-412.

[96] S.L. Malhotra, L. Minh, L.P. Blanchard, Thermal Decomposition and Glass Transition Temperature of Poly(ethyl Methacrylate) and Poly(n-butyl Methacrylate), Journal of Macromolecular Science: Part A - Chemistry 19(4) (1983) 559-578.

[97] C.M. Agrawal, D. Huang, J.P. Schmitz, K.A. Athanasiou, Elevated temperature degradation of a 50: 50 copolymer of PLA-PGA, Tissue engineering 3(4) (1997) 345-352.

[98] R.G. Sousa, W.F. Magalhães, R.F.S. Freitas, Glass transition and thermal stability of poly (N-isopropylacrylamide) gels and some of their copolymers with acrylamide, Polymer degradation and stability 61(2) (1998) 275-281.

[99] K. Wondraczek, J. Adams, J. Fuhrmann, Effect of Thermal Degradation on Glass Transition Temperature of PMMA, Macromolecular Chemistry and Physics 205(14) (2004) 1858-1862.

[100] V.S. Silverajah, N.A. Ibrahim, N. Zainuddin, W.M.Z.W. Yunus, H.A. Hassan, Mechanical, thermal and morphological properties of poly (lactic acid)/epoxidized palm olein blend, Molecules 17(10) (2012) 11729-11747.

[101] S.D. Pandita, L. Wang, R.S. Mahendran, V.R. Machavaram, M.S. Irfan, D. Harris, G.F. Fernando, Simultaneous DSC-FTIR spectroscopy: Comparison of cross-linking kinetics of an epoxy/amine resin system, Thermochimica Acta 543 (2012) 9-17.

[102] G. Nikolic, S. Zlatkovic, M. Cakic, S. Cakic, C. Lacnjevac, Z. Rajic, Fast Fourier Transform IR Characterization of Epoxy GY Systems Crosslinked with Aliphatic and Cycloaliphatic EH Polyamine Adducts, Sensors (Basel, Switzerland) 10(1) (2010) 684-696.

[103] C.S. Proikakis, N.J. Mamouzelos, P.A. Tarantili, A.G. Andreopoulos, Swelling and hydrolytic degradation of poly(d,l-lactic acid) in aqueous solutions, Polymer Degradation and Stability 91(3) (2006) 614-619.
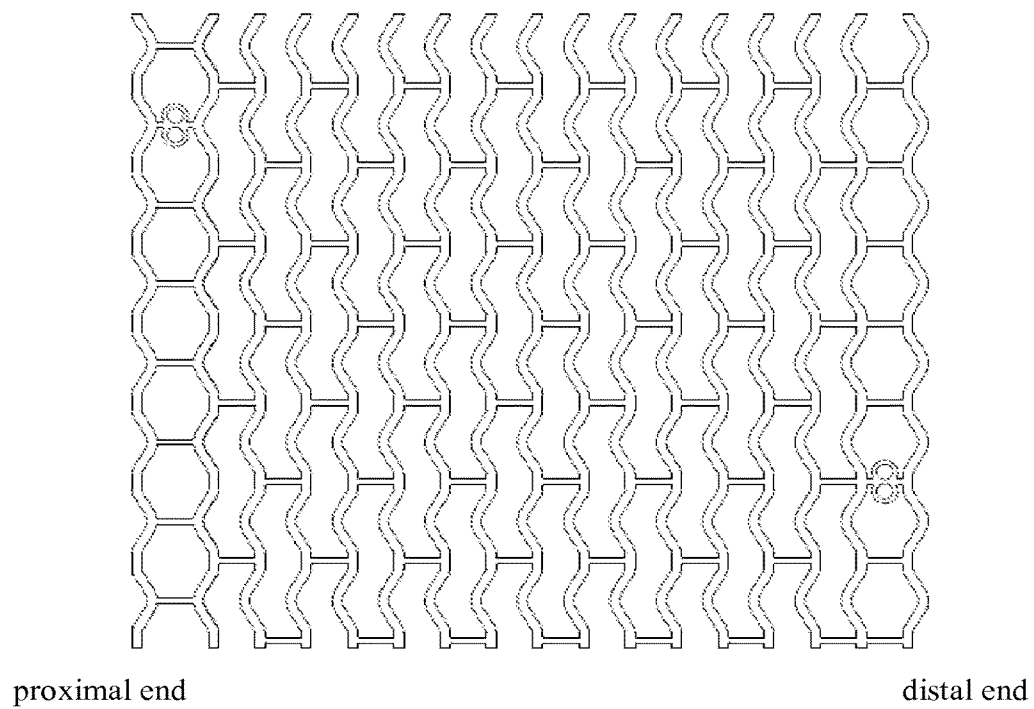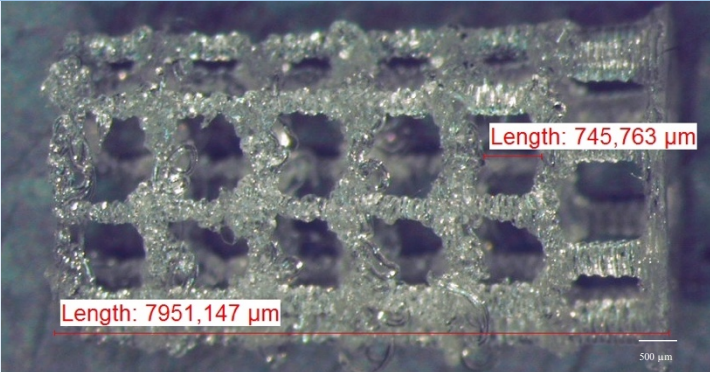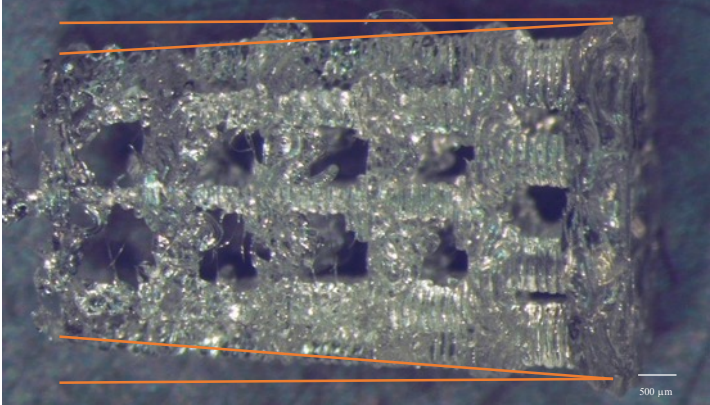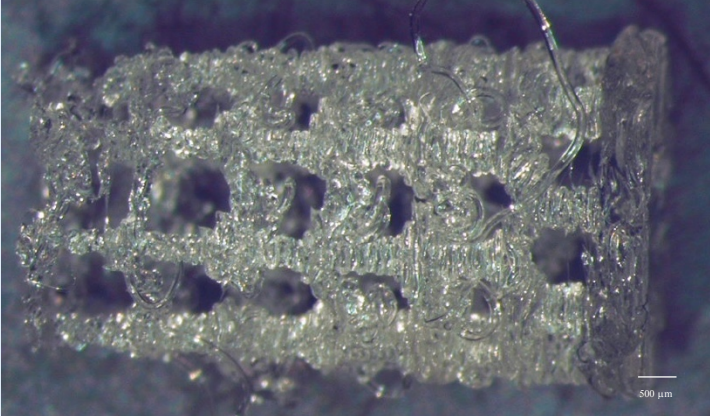
Appendix A

proximal end   distal end
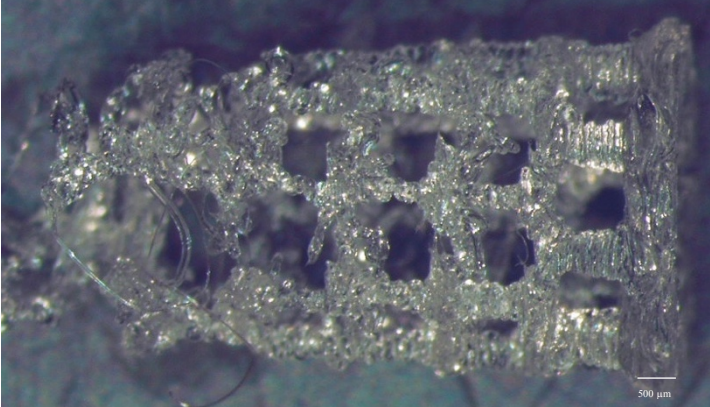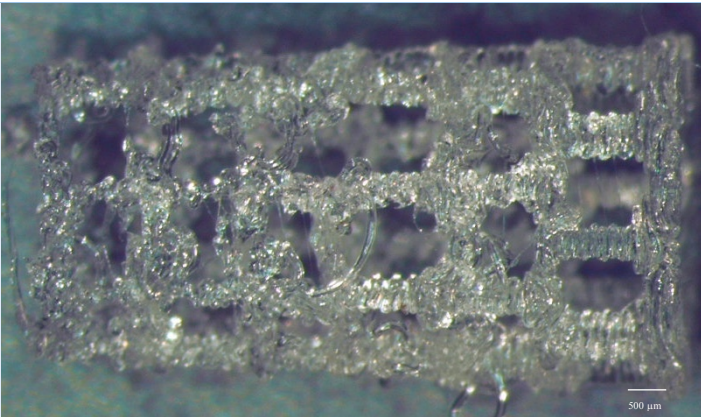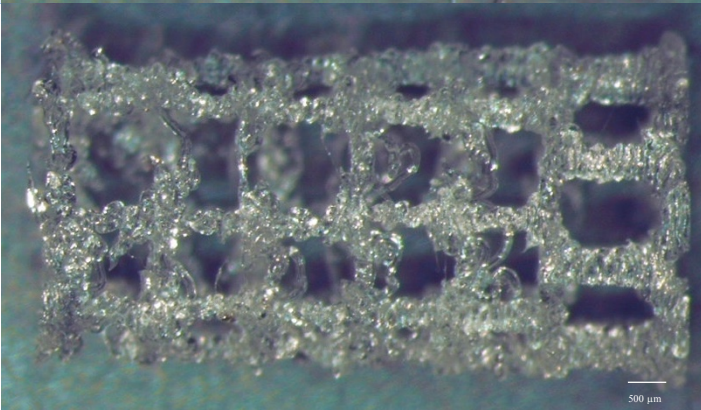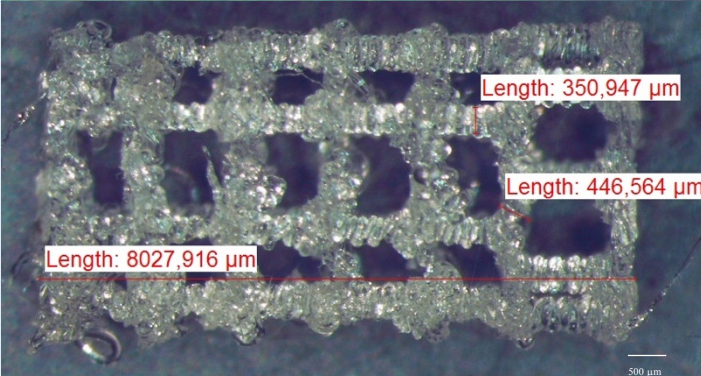
Figure 29 - DeSolve stent design used for the final stent design [23].

Appendix B

Table 2 - Effects of changing various printing parameters when printing a cardiovascular stent. NC-PLA material with an Ultimaker 2+ was used for testing.

Parameters	Sample	Notes
Diameter: 5 mm Extrusion width: 0.09 mm Printing speed: 2500 mm/min X/Y speed: 6000 mm/min Nozzle T°: 205 °C Retraction: 4 mm	 Length: 745,763 µm Length: 7951,147 µm	Printing time: 10 min Struts with overhangs difficult to print due to the lack of support material.
Diameter: 4 mm **Extrusion width: 0.06 mm** Printing speed: 2500 mm/min X/Y speed: 6000 mm/min Nozzle T°: 205 °C Retraction: 4 mm		Printing time: 8 min Decrease in dimensions calls for a decrease in extrusion width for correct interpretation in the software.
Diameter: 4 mm Extrusion width: 0.06 mm **Printing speed: 2000 mm/min** X/Y speed: 6000 mm/min Nozzle T°: 205 °C Retraction: 4 mm		Printing time: 8 min Decrease in printing speed resulted in less precision in between struts and more material deposition.
Diameter: 4 mm Extrusion width: 0.06 mm **Printing speed: 2000 mm/min** **X/Y speed: 4000 mm/min** Nozzle T°: 205 °C Retraction: 4 mm		Printing time: 8 min Decrease in both printing speed and X/Y speed results in lower precision and loose of connections.

Diameter: 4 mm Extrusion width: 0.06 mm Printing speed: 2500 mm/min **X/Y speed:** **4000 mm/min** Nozzle T°: 205 °C Retraction: 4 mm		Printing time: 8 min Decrease in X/Y speed results in a higher quality when compared to reduction in printing speed.
Diameter: 4 mm Extrusion width: 0.06 mm **Printing speed:** **3000 mm/min** **X/Y speed:** **5000 mm/min** Nozzle T°: 205 °C Retraction: 4 mm		Printing time: 8 min Increase in printing speed and reduction in X/Y speed allowed for less material deposition and therefore finer structures.
Diameter: 4 mm Extrusion width: 0.06 mm **Printing speed:** **3200 mm/min** X/Y speed: 5000 mm/min Nozzle T°: 205 °C Retraction: 4 mm		Printing time: 8 min Further increases in printing speed, allow for better precision on material deposition.

Appendix C
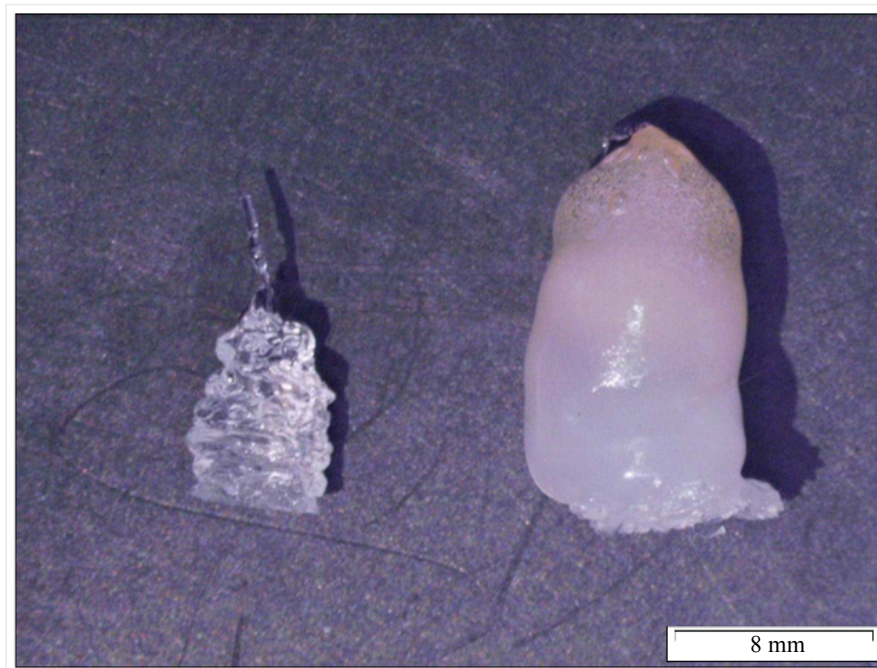
Figure 30 - Freeformer test print at 4 mm and 8 mm. The constant heat from the upper plate, in addition to the nozzle diameter hinder correct printing of the stent structures and dimensions.
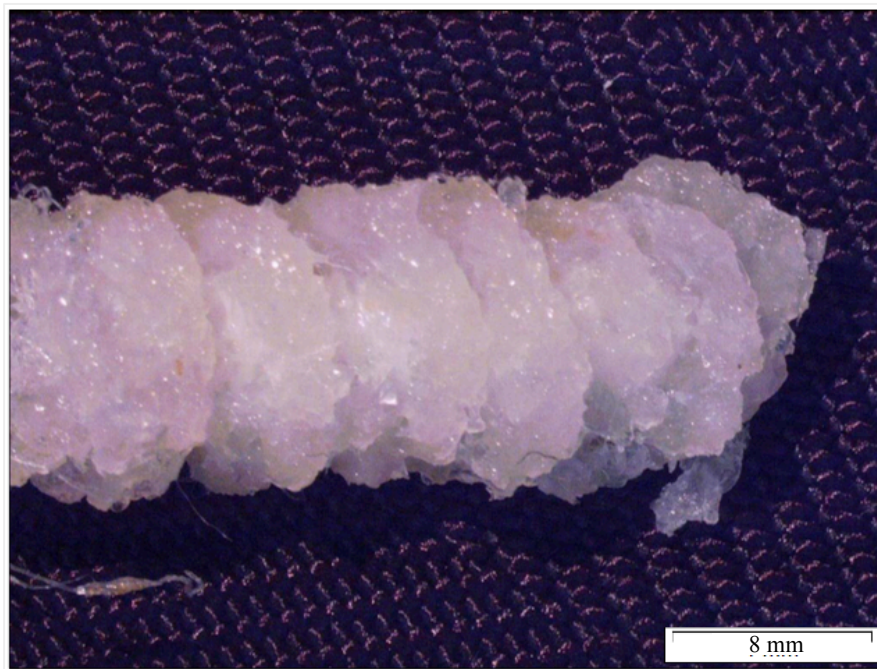

Figure 31 - Constant heat makes the support material spread through the whole print in between layers affecting correct adhesion between layers.
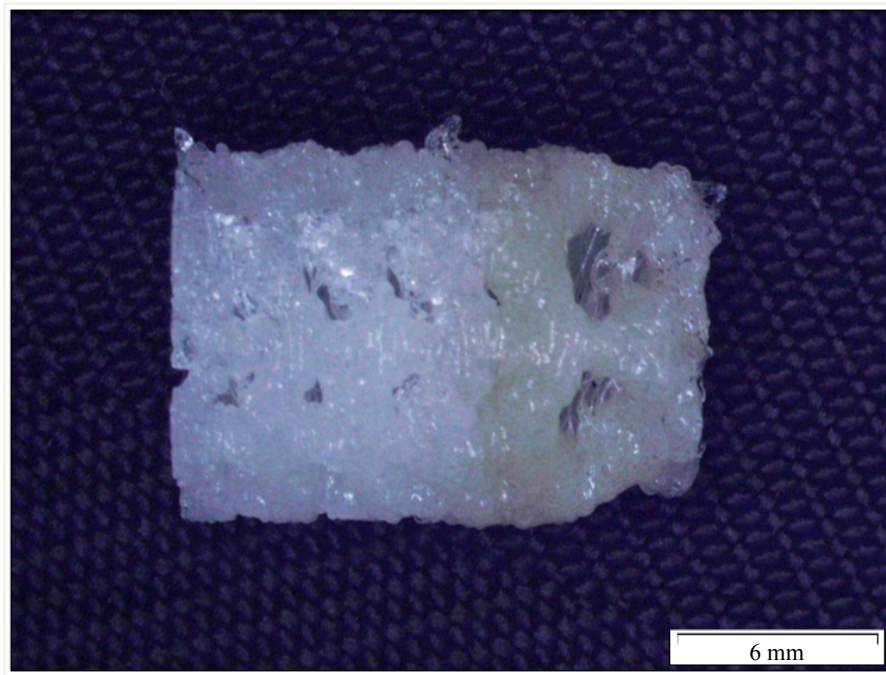
Figure 32 - Test print of a 1 cm diameter stent. The distal portion of the stent shows change in color from white to cream as a cause of material degradation.

Appendix D
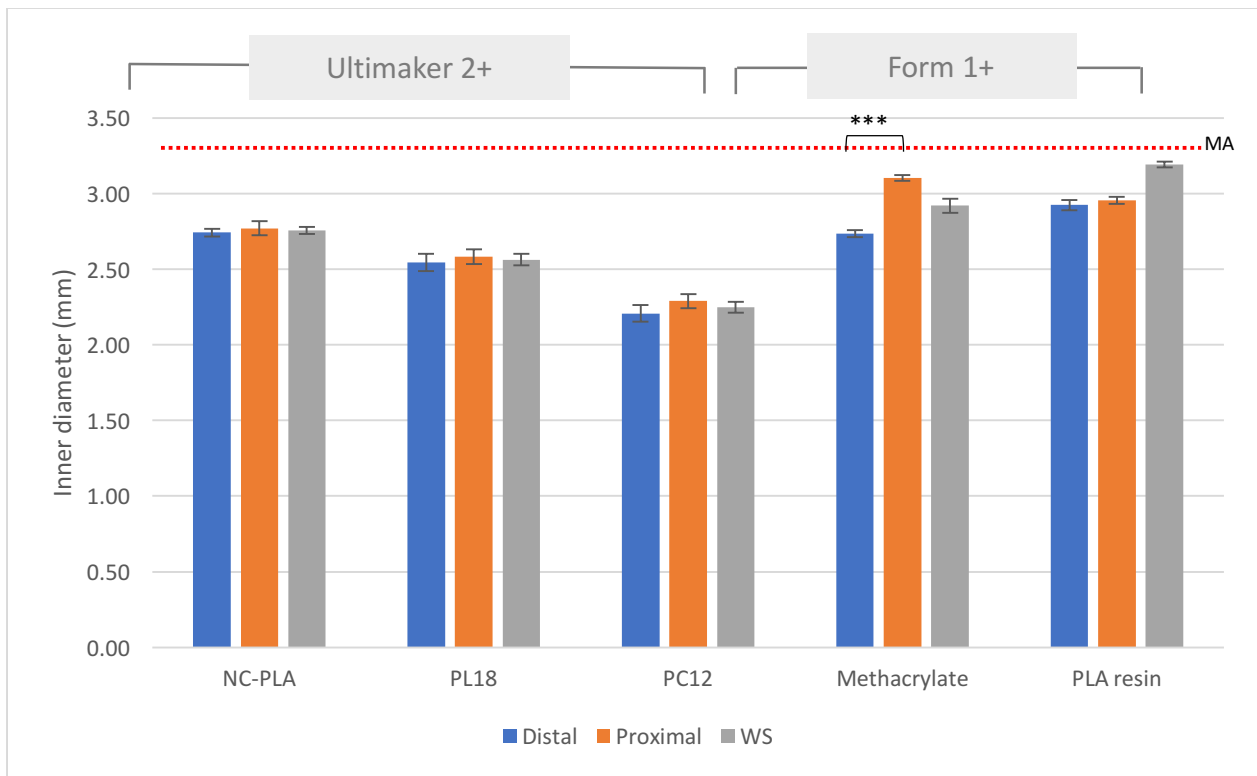
Figure 33 - Total average of the inner diameter in various materials before post processing, at both the distal and proximal edges of the stent. WS corresponds to the total average of the distal and proximal area. Dotted line corresponds to the market-available stent average (MA). NC PLA, PL18, PC12 stents were printed with an Ultimaker 2+. Methacrylate and PLA resin stents were printed with a Form 1+. Three printed stents were used per material. Error bars correspond to standard deviation. Statistical significance with $P < 0.05$ (*), $P < 0.01$ (**) and $P < 0.001$ (***) is presented.
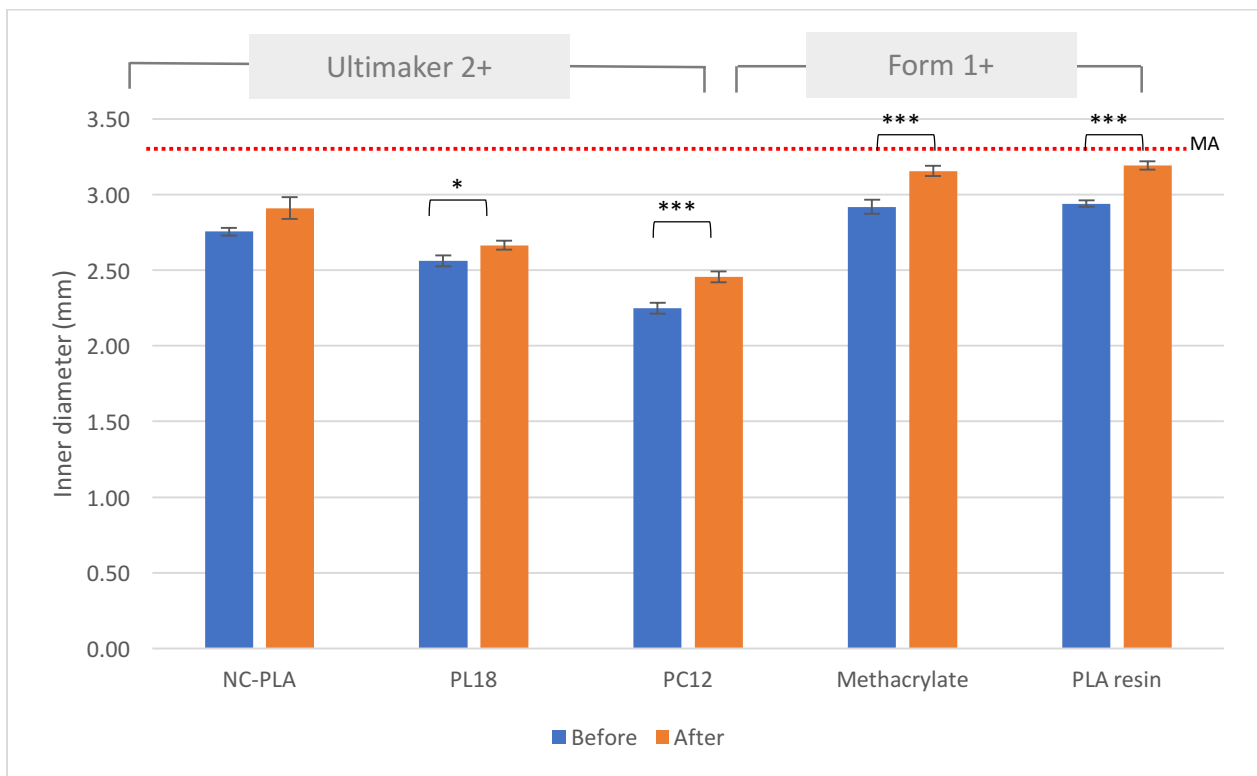

Figure 34 - Comparison of the inner diameter in the stent before and after post processing. Dotted line corresponds to the market-available stent average (MA). NC PLA, PL18, PC12 stents were printed with an Ultimaker 2+. Methacrylate and PLA resin stents were printed with a Form 1+. Three printed stents were used per material. Error bars correspond to standard deviation. Statistical significance with $P < 0.05$ (*), $P < 0.01$ (**) and $P < 0.001$ (***) is presented.
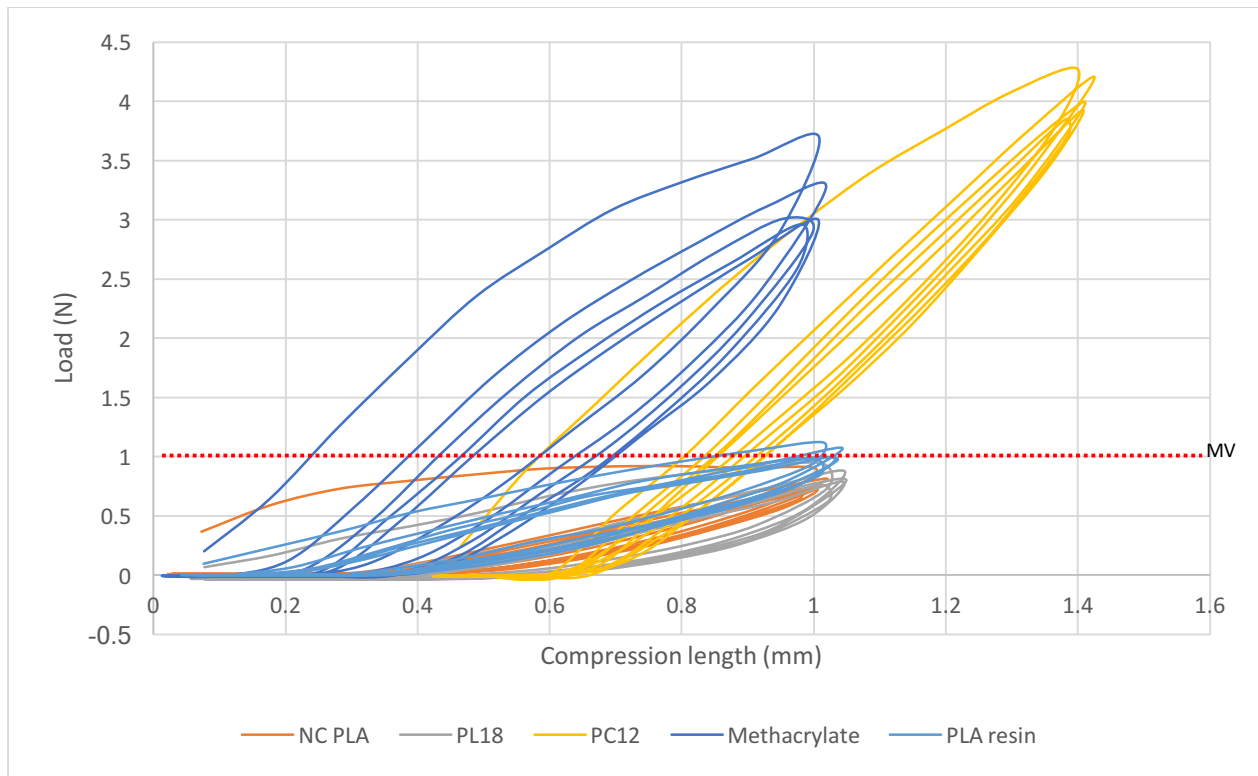
Appendix E

Figure 35 - Radial strength and recovery behavior up to a 25% compression of the initial diameter. Radial strength is correlated to a horizontal compression force. The compression test was recorded for a total of five cycles to investigate recovery of the stent after compression. Minimal value (MV) considered as a standard is represented by the dotted line. Three stents per material were measured.

Appendix F

Table 3 - Changes in the weight-average molecular weight (Mw), number-average molecular weight (Mn) and polydispersity (PDI) of NC-PLA, PL18 and PC12, as a result of printing with an Ultimaker 2+ and Freeformer.

| Material	Printer	Mw (g/mol)	Mn (g/mol)	PDI	σ Mw (g/mol)	σ Mn (g/mol)	PDI
NC-PLA filament		215,133	103,260	2.09	2281	6011	0.10
NC-PLA printed	Ultimaker 2+	133,033	70,433	1.89	4477	2863	0.05
PL18 pellet		182,000	159,000	1.14	0	0	0.00
PL18 filament		166,333	143,000	1.16	577	1000	0.01
PL18 printed	Ultimaker 2+	164,333	139,667	1.18	1155	577	0.00
	Freeformer 0.15mm	121,333	82,600	1.47	6110	5575	0.02
	Freeformer 0.25mm	86,967	57,100	1.52	3044	1852	0.00
PC12 pellet		124,000	83,000	1.49	0	0	0.00
PC12 filament		120,000	83,567	1.44	1000	551	0.01
PC12 printed	Ultimaker 2+	122,333	84,700	1.44	1155	608	0.00

Appendix G
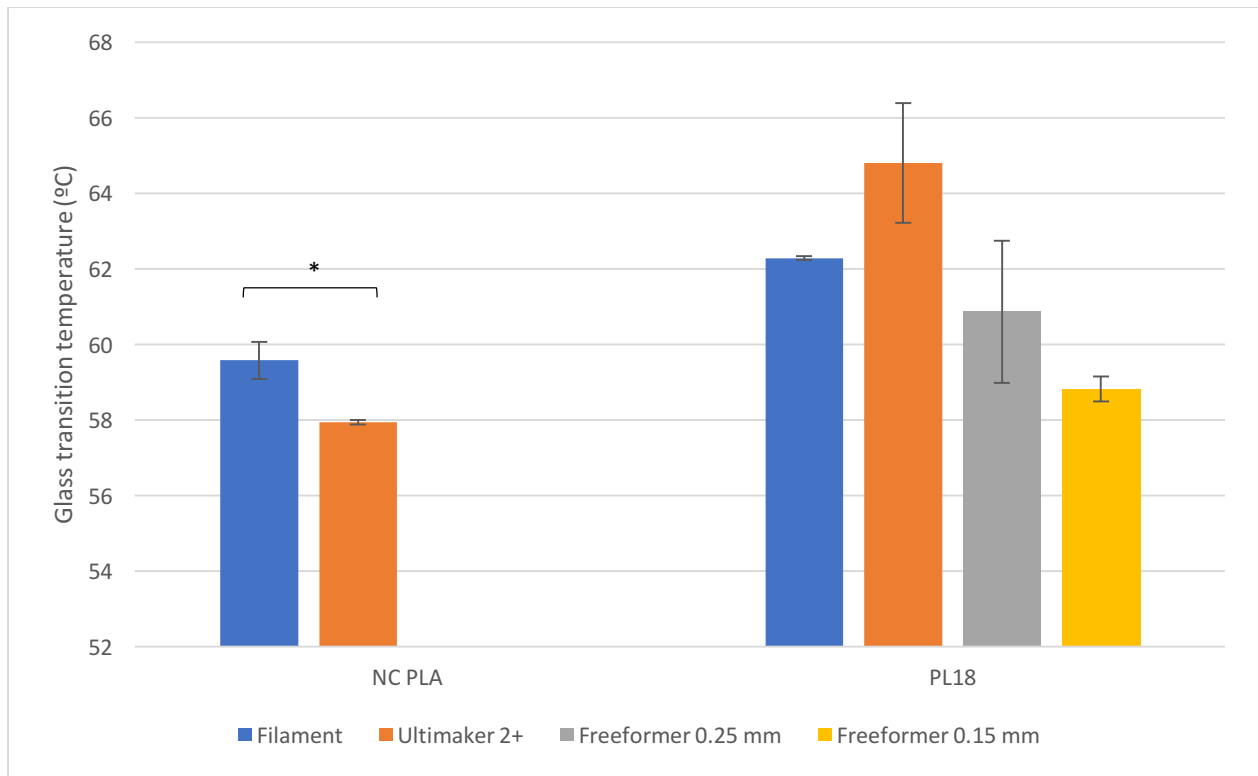
Figure 36 - Changes experienced on NC PLA and PL18 in the glass transition temperature after every heat cycle, PC12 was not evaluated as its glass transition temperature lies at -60 ℃. Three printed stents were used per material. Error bars correspond to standard deviation. Statistical significance with P < 0.05 (*), P < 0.01 (**) and P < 0.001 (***) is presented.
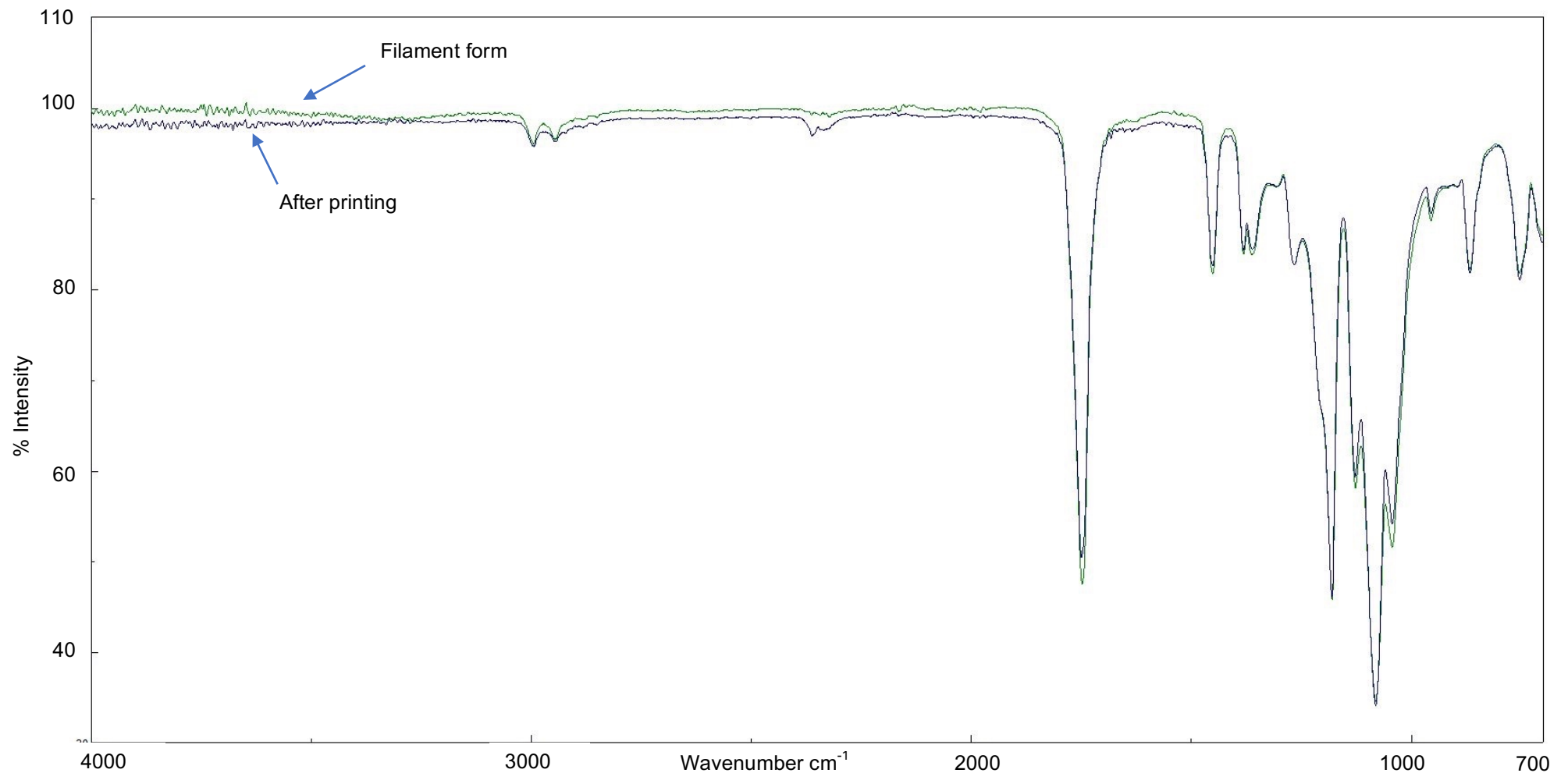
Appendix H

Figure 37 - FTIR Analysis of NC PLA in filament form (green) and after printing with Ultimaker 2+ (blue).
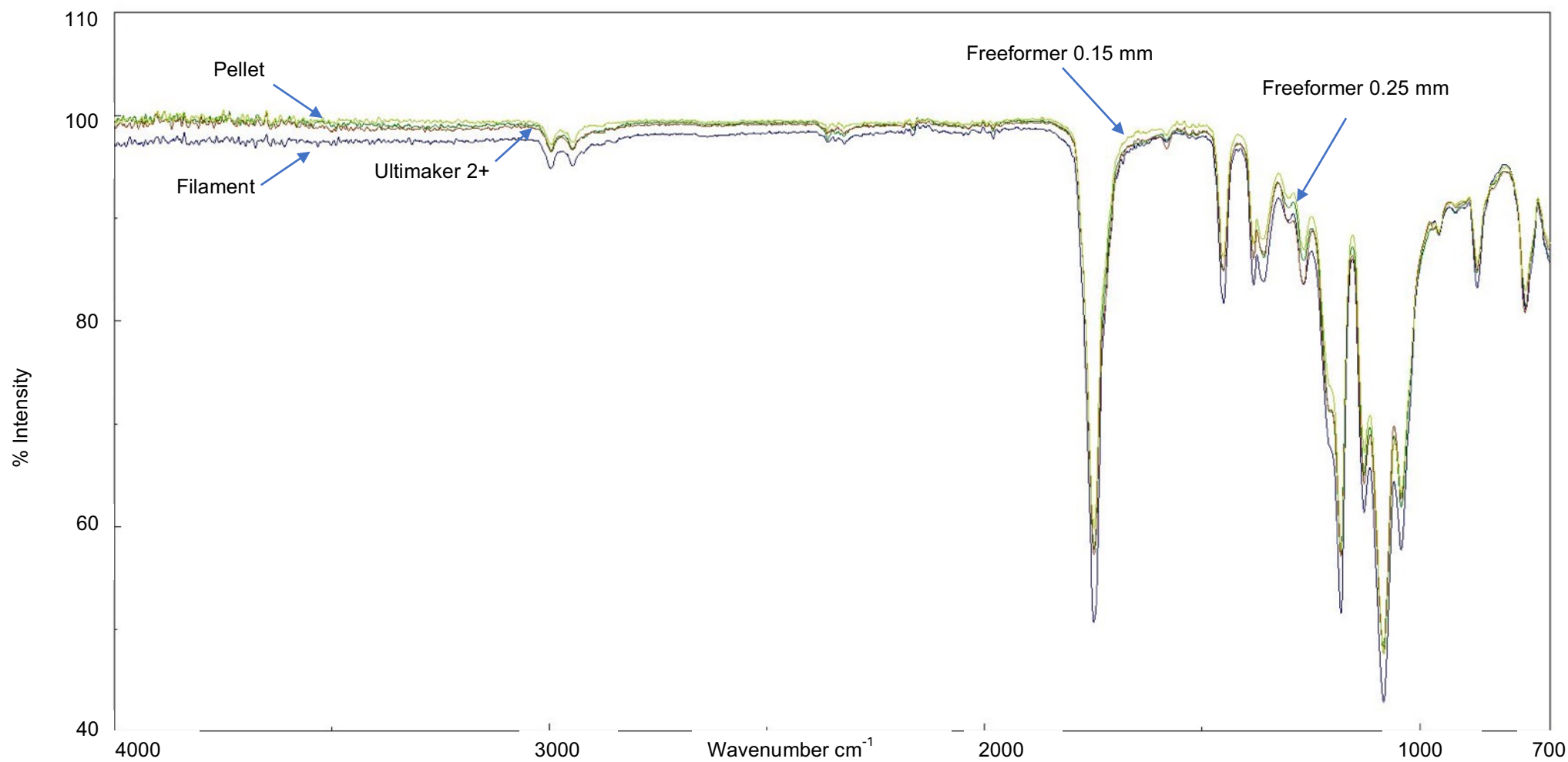
Figure 38 - FTIR analysis of PL18 in pellet form (green), filament form (blue), and after printing with Ultimaker 2+ (brown), Freeformer 0.15mm (yellow), Freeformer 0.25mm (dark green).
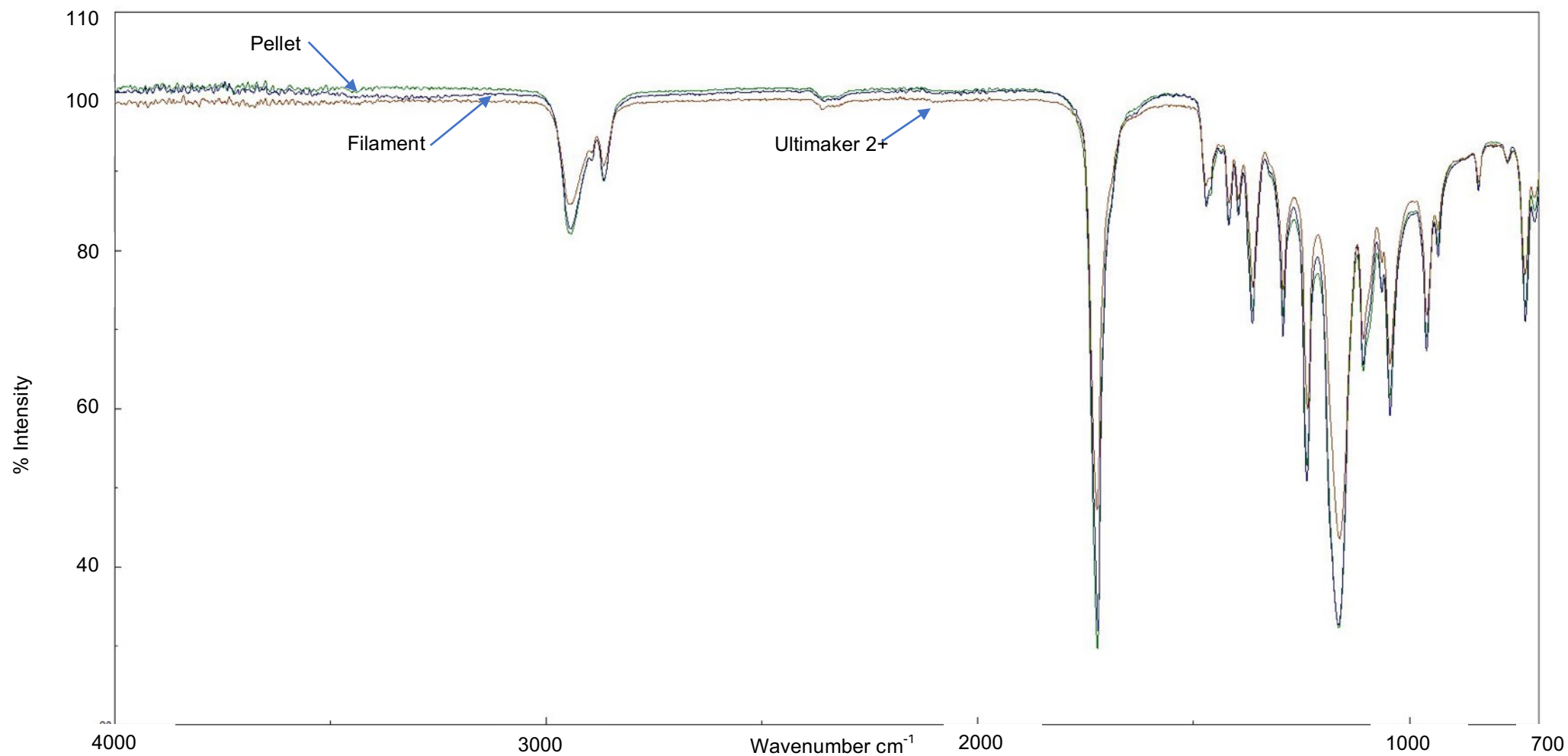
Figure 39 - FTIR analysis of PC12 in pellet form (green), filament form (blue) and after printing with Ultimaker 2+ (brown).
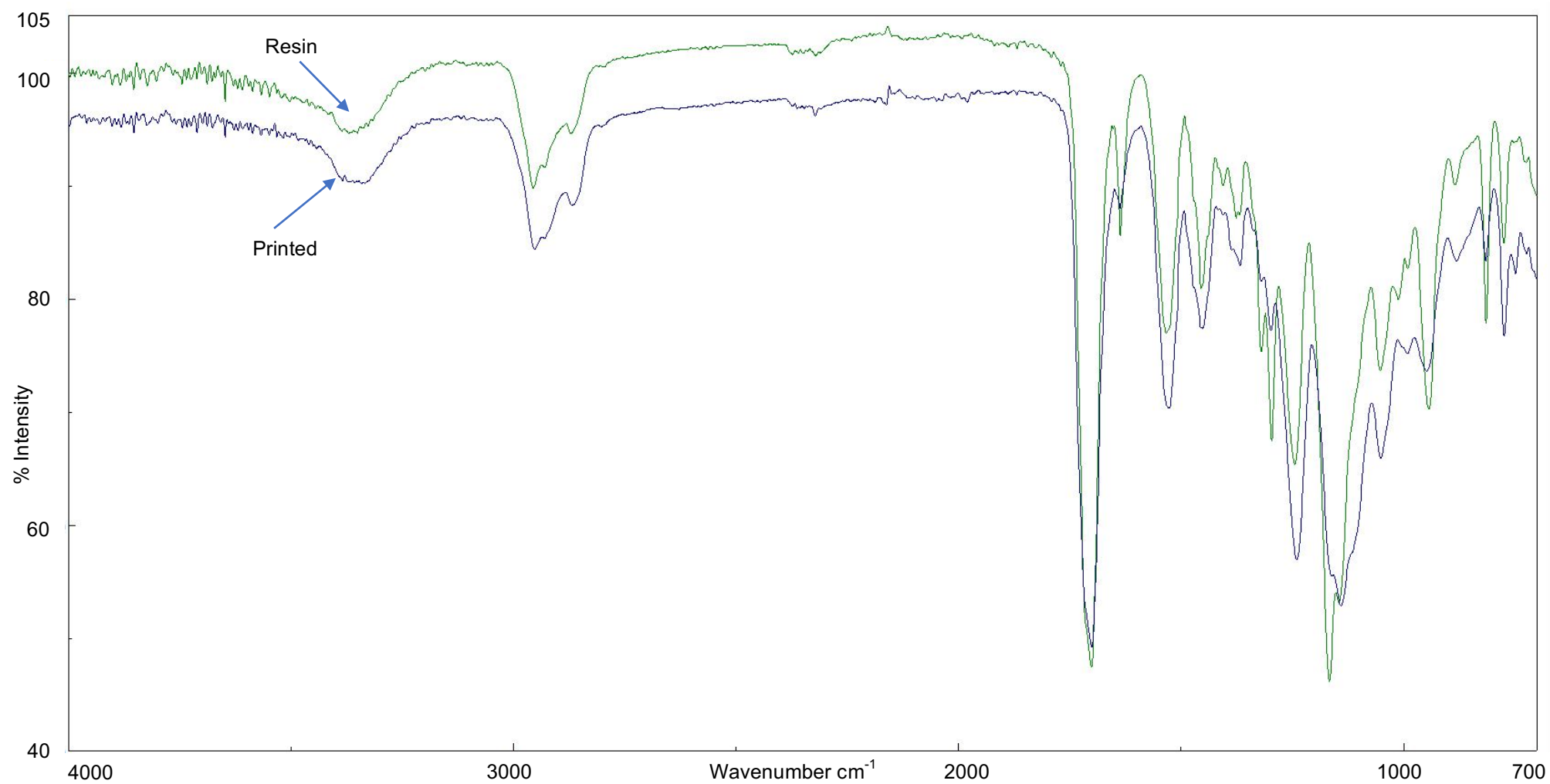
Figure 40 - FTIR analysis of methacrylate in resin form (green] and after printing with Form 1+ (blue).